THESIS FOR THE DEGREE OF DOCTOR OF PHILOSOPHY

Method Development for Signatures in Nuclear Material for Nuclear Forensic Purposes

ANNA VESTERLUND

Department of Chemistry and Chemical Engineering

CHALMERS UNIVERSITY OF TECHNOLOGY

Gothenburg, Sweden, 2019

Method Development for Signatures in Nuclear Material for Nuclear Forensic Purposes
ANNA VESTERLUND
ISBN 978-91-7905-197-6

Doktorsavhandlingar vid Chalmers tekniska högskola
Ny serie nr 4664
ISSN 0346-718X

Department of Chemistry and Chemical Engineering
Chalmers University of Technology
SE-412 96 Gothenburg
Sweden
Telephone + 46 (0)31-772 1000

Cover: A piece of uranium metal used in the nuclear forensic exercise CMX-6.
Photo by Ellinor Algin, Swedish National Forensic Centre (NFC)

Chalmers Reproservice
Gothenburg, Sweden, 2019

METHOD DEVELOPMENT FOR SIGNATURES IN NUCLEAR MATERIAL FOR NUCLEAR FORENSIC PURPOSES

ANNA VESTERLUND

Nuclear Chemistry
Department of Chemistry and Chemical Engineering
CHALMERS UNIVERSITY OF TECHNOLOGY

CBRN Defence and Security
SWEDISH DEFENCE RESEARCH AGENCY

Abstract

Nuclear forensics is a scientific discipline where signatures in nuclear and other radioactive material are investigated and evaluated in order to aid in criminal investigations concerning these materials. Examples of signatures that may be useful is the age and isotopic composition of the nuclear material and trace elements in the material. In order for evidence to hold up in court, the information extracted from forensic investigations need to be accurate and precise.

This work shows some possibilities and limitations of using two common techniques for measurements of nuclear material and other radioactive material: gamma spectrometry and inductively coupled plasma - mass spectrometry. One part of this work is dedicated to the applicability of hand-held instruments. The categorization of uranium using low-resolution gamma spectrometry and possibility of using signatures in high activity ^{241}Am sealed sources that can be obtained by HPGe were explored. In the other part, methods for high confidence measurements of lanthanides using ICP-MS were developed and problems arising when performing these analyses with as small uncertainties as possible were investigated.

The results show that nuclear forensic analyses require deep understanding in the measurement process in order to provide accurate results. Low-resolution instruments in the current configuration have been shown to be a poor choice for categorization of uranium. On the other hand, there are a number of interesting signatures in ^{241}Am-sources that can be provided by high-resolution gamma spectrometry. By using chemical separations or desolvating sample introduction systems in combination with careful data evaluation, it is possible to measure the lanthanide series without spectral interferences and with low uncertainties. By investing meticulous work to the analyses, it is possible to achieve measurements with high confidence.

Keywords: Nuclear forensics, Uranium, Lanthanide patterns, ^{241}Am, ICP-MS, gamma spectrometry

If a model is simple, it likely will be wrong, if it is complex, it surely is impractical.

- Unknown

LIST OF PUBLICATIONS

This thesis is based on the work contained in the following papers:

Paper I

Vesterlund, A., Ulvsand, T., Lidström, K., Skarnemark, G., Ekberg, C., Ramebäck, H.,
On the categorization of uranium materials using low-resolution gamma ray spectrometry,
Appl. Radiat. Isot., 72 (2013) 54–57.

Contribution: Main author, evaluation of experimental data.

Paper II

Vesterlund, A., Chernikova, D., Cartemo, P., Axell, K., Nordlund, A., Skarnemark, G., Ekberg, C., Ramebäck, H., Characterization of strong ^{241}Am sources, Appl. Radiat. Isot., 99 (2015) 162–167.

Contribution: Main author, evaluation of experimental data.

Paper III

Vesterlund A., Ramebäck H., Avoiding polyatomic interferences in measurements of lanthanides in uranium material for nuclear forensic purposes, J Radioanal. Nucl. Chem., 321 (2019) 723-731.

Contribution: Main author, all experimental work, all evaluation of experimental data.

Paper IV

Vesterlund A., Ramebäck H., Achieving confidence in trace element analysis for nuclear forensic purposes: ICP-MS measurements using external calibration. Accepted for publication in Journal of Radiochemical and Nuclear Chemistry.

Contribution: Main author, all experimental work, all evaluation of experimental data.

TABLE OF CONTENTS

1 INTRODUCTION

Nuclear material has been under strong worldwide regulation for over 60 years. Ever since the first military use of fission was realised as a result of the Manhattan project, the implications of such a weapon have been feared. The safeguards organization under the International Atomic Energy Agency (IAEA) has the main responsibility to ensure that member states maintain accountability of nuclear material kept within their borders. Even so, there have been incidents where nuclear material has been found out of regulatory control [Wallenius et al., 2006; Wallenius et al., 2007; Keegan et al., 2014]. Between 1993 and early 2019, the IAEA Incident and Trafficking Data Base (ITDB) has reported 3387 incidents involving nuclear material or other radioactive material out of regulatory control. Of these incidents, 759 have been associated with criminal activity and 16 of the criminal events have involved nuclear material usable for nuclear weapons (highly enriched uranium or plutonium) [ITDB, 2019].

Whereas the safeguards organization is meant to prevent incidents involving nuclear material, there is also a need for bringing actors who have handled nuclear material illegally to justice [UNSCR 1540, 2004]. The purpose of legal proceedings may be twofold: deterrence and retribution. The deterrence is directed against both non-state actors as well as against states. Since production of nuclear material is both resource demanding and a complex process, state involvement and a state's knowledge of the presence of nuclear material production is considered unavoidable. A confiscation of nuclear material found out of regulatory control would imply that a state has failed to follow international resolutions and agreements such as UNSCR 1540 [2004] concerning nuclear material. This concern would reinforce a state's will to control nuclear material and thereby deter from both negligence and proliferation. To help in these legal proceedings there has been a need for forensic science that focuses on the information that can be provided from the nuclear material itself, to complement traditional forensic evidence.

Nuclear forensic science is a scientific discipline that has been developing for the last 25 years, following the surge of cases of illicit trafficking of nuclear material after the dissolution of the Soviet Union. The aim of nuclear forensics is to aid criminal investigations concerning nuclear- or other radioactive material to find the origin and intended use of the seized material, i.e. the attribution. Commonly, the investigated material is nuclear material such as uranium and plutonium, but also radioactive sources may be the subject of investigation. Furthermore, there are other radionuclides, such as ^{241}Am, that are fissionable and hence sometimes referred to as alternative nuclear material [IAEA, 2002].

1.1 OBJECTIVES

The objective of the work presented in this thesis has been to investigate and develop signatures that may be useful in the field of nuclear forensics using gamma spectrometry and mass spectrometry as measurement techniques. For nuclear material, both techniques can be used. Gamma spectrometry is a robust, fairly quick, non-destructive technique but requires macroscopic amounts of material to be useful. Mass spectrometry, on the other hand, provides accurate and precise results with very small amounts of material, but is a destructive technique that often requires extensive sample preparation such as dissolution of the material followed by chemical separations. For solid-sample mass spectrometric techniques, such as laser ablation and SIMS, the sample preparation is minimal. However, a practical requirement for measuring radionuclides using mass spectrometry is that the

nuclides have sufficiently long half-lives. Another advantage of mass spectrometry is, of course, that non-radioactive elements, such as certain trace elements, also can be measured.

The first two papers concern measurements of radioactive material using hand-held gamma spectrometry. These gamma detectors are commonly used by first-responders or customs, or in early stages of a nuclear forensic investigation, i.e. in the detection and identification as well as in a basic characterization of the material at e.g. the site of incident. **Paper I** shows some of the difficulties when attempting to categorize uranium using low-resolution gamma spectrometry and intends to explain why categorizations may be erroneous. Furthermore, the risk of making erroneous decisions based on low-resolution measurements is highlighted. **Paper II** shows what kind of characteristics can be extracted from a simple high-resolution gamma spectrometric measurement of a strong radioactive source containing the alpha-emitter ^{241}Am. These characteristics could be included in a National Nuclear Forensics Library (NNFL) to help identify a radioactive source found out of regulatory control.

The last two papers deal with measurements of stable elements in uranium material using ICP-MS that can be used for either origin attribution or for comparison between different materials. In **Paper III,** a comparison is made between interfered and interference-free measurements. The paper shows two methods to produce precise and interference-free lanthanide patterns using ICP-MS for uranium attribution. **Paper IV** shows that by decreasing the measurement uncertainty in trace element measurements to be able to compare small differences in analyte concentration of stable elements for nuclear forensic purposes, it can be shown that certified reference materials may have underestimated uncertainties and/or a concentration bias. The paper also shows the difference between using ordinary least squares regression, which is frequently applied to external calibration in the literature, and weighted least squares regression, which is the correct statistical approach for evaluation.

2 BACKGROUND

2.1 THE POLITICAL HISTORY OF NUCLEAR EVENTS

In 1938 Otto Hahn and Fritz Strassmann irradiated uranium with neutrons and discovered that one resulting entity from the irradiations was barium, but they could not explain how this was possible [Hahn and Strassmann, 1939]. Shortly after, Lise Meitner and her nephew Otto Frisch devised the theoretical explanation that the neutron irradiation splits the uranium atom into two nuclei of roughly equal size, which would explain the presence of barium observed by Hahn and Strassmann. They also explained that energy is released in the process [Meitner and Frisch, 1939]. By this, fission was discovered and shortly after, it was found that the neutrons produced in the fission could cause a chain reaction [Zinn and Szilard, 1939]. In the Frisch-Peierls memorandum, written in 1940, Rudolf Peierls and Otto Frisch presented the first technical description of the possibility of utilizing the fission chain reaction in a bomb construction using uranium enriched in ^{235}U [Arnold, 2003], and July 16 1945, the first nuclear test, the "Trinity" test, was conducted in New Mexico, U.S. The test was followed by the atomic bombs over Hiroshima and Nagasaki shortly after. Soon, technical details on the construction of the atomic bomb leaked to the Soviet Union, and when the Soviet Union had implemented the nuclear weapons technology in 1949, when the first Soviet test was conducted, the nuclear arms race became a part of the Cold War.

The IAEA was established in 1957 after the "Atoms for Peace" initiative by the U.S. president Dwight D. Eisenhower to promote peaceful use of nuclear energy and to prevent nuclear material to be used for military purposes [Fischer, 1997]. The original idea was that the IAEA would serve as a bank for nuclear material. A safeguards organization was created to ensure that nuclear material was not used for military purposes. However, the Cold War prevented the implementation of the IAEA as a nuclear material protector. Instead, while the nuclear technology intended for peaceful purposes spread across the world, so did the nuclear weapons technology. For example, the plutonium used for the Indian nuclear weapons programme was produced in a research reactor supplied by Canada [Fischer, 1997]. By 1968, five countries around the world had nuclear weapons technology and, furthermore, conducted nuclear weapons tests. It became clear that the spread of this knowledge and technology had to be stopped. In 1970, the Nuclear Non-Proliferation Treaty (NPT) entered into force.

2.2 NUCLEAR SECURITY

The NPT can be described as having three pillars: non-proliferation, disarmament, and peaceful use of nuclear technology. The first part, non-proliferation, obligates the nuclear weapons states not to share nuclear weapons or technology related to nuclear weapons with states that do not have nuclear weapons. Furthermore, non-nuclear weapons states are obligated not to receive or develop nuclear weapons technology. In addition, non-nuclear weapons states are obligated to accept IAEA safeguards to verify that the nuclear technology within the state is used for peaceful purposes. The safeguards organization maintains credible assurance that nuclear material under safeguards is used for peaceful aims and is not converted into nuclear weapons [NPT/CONF.2015/13, 2015]. The second pillar, disarmament, implies that the nuclear weapons states are obligated to pursue the complete disarmament of nuclear weapons, and the third pillar gives the states the right to develop and use nuclear technology for peaceful purposes, e.g. nuclear energy [Reed and Stillman, 2009]. Despite the NPT, a few states have developed and tested nuclear weapons after the implementation of the treaty. After the disintegration of the Soviet Union, there were suddenly three new nuclear weapons states,

Belarus, Kazakhstan and Ukraine. However, these three states soon transferred their stock of nuclear weapons to the Russian Federation [Reed and Stillman, 2009]. In the aftermath of the breakup of the Soviet Union, seizures of illicit radiological and nuclear material at borders started to increase rapidly. Concerns that a black market for nuclear material was developing, resulted in the growing interest to be able to identify the origin of seized material, i.e. a forensic science focussed on nuclear and other radioactive materials [Mayer and Glaser, 2015].

After the 9/11 attacks, concerns were raised about the possibility for terrorists to use nuclear or other radioactive material for their objectives. Three ways for terrorist groups to obtain nuclear material have been proposed [Litwak, 2016]. One option, indigenous production, is that the terrorist group, without the aid of a state, could build a nuclear weapon. This option is considered unlikely due to the complexity and the technical skill needed to construct a nuclear weapon. Somewhat more likely is the event that a terrorist group obtains weapons grade nuclear material and weaponizes the material without the involvement of a state. The second option, transfer, is that a terrorist group acquires a functioning nuclear weapon, by the aid of a state. A third way for terrorists to acquire nuclear weapons is by "unintended leakage" such as theft and insider operations. A perhaps more likely event is the antagonistic use of radioactive sources in combination with explosives, so called Radiological Dispersion Devices (RDD), or more colloquially "dirty bombs", where the explosives are used to disperse radioactive material in a selected location. These events may not be as disastrous as a nuclear weapon detonation but on a psychological level, it has been suggested that the fear spread by such a device may be as serious as that caused by a nuclear device [Litwak, 2016].

While terrorist groups may not be deterred from using nuclear weapons by threat of retaliation from the international community, the proliferation of nuclear weapons may be prevented by deterring states from, by either neglect or intention, conveying nuclear weapons or nuclear weapons material to terrorist organisations. Under the threat of the possibility to attribute nuclear material, found out of regulatory control, to a certain state, states will be forced to comply with international agreements by maintaining nuclear security to avoid retaliation from either the international community or another state [Litwak, 2016].

A number of initiatives have been realised to highlight the importance of nuclear security. The Global Initiative to Combat Nuclear Terrorism (GICNT) was initiated in 2006 as a joint effort between Russia and the United States. The aim of GICNT is to strengthen the global capability to prevent, detect and respond to nuclear terrorism. The organization is open to any state that is committed to implementing the eight principles in the Statement of principles [GICNT, 2018]. As of early 2019, 88 nations and 6 organizations were members.

To handle events with nuclear material and other radioactive material out of regulatory control, the IAEA has established a nuclear security programme. This programme focuses on prevention and detection of and response to criminal or other unauthorized acts involving nuclear or other radioactive material [IAEA, 2011]. The IAEA recommends each state to implement a nuclear security infrastructure to protect nuclear and radioactive material within its borders. The state should also have the ability to "prevent, detect and respond to nuclear security events" [IAEA, 2015]. The preventive measures involve deterrence, ensuring information security and trustworthiness of personnel by the implementation of a "nuclear security culture". The detection measures should involve detection by instruments as well as information alerts. The response measures involve the actions that follow a detected nuclear security event and includes notification and activation of all relevant authorities including the initiation of investigations concerning the event. For the purpose of both deterrence and response, nuclear forensics plays an important part.

2.3 NUCLEAR FORENSICS

The aim of nuclear forensics is to find the attribution of unknown nuclear and other radioactive material. The attribution assessment is used to determine the origin of the material, the intended use and the responsible individuals connected to the material [Hutcheon et al., 2013]. Methodology in nuclear forensics includes measurements of radioactive nuclides as well as stable elements that can be used to link a material to another material, facility or even a geographical location. Many methods in nuclear forensics are based on methods used in other disciplines such as age dating and lanthanide analysis, both commonly employed in geology [Cheong et al., 2015; Lobato et al., 2015]. However, a major difference between nuclear forensics and, for instance, geology is the need for quality assurance to meet the high legal and scientific scrutiny [Leggitt et al., 2009]. Therefore, a considerable amount of the conducted research focuses on improving the measurement accuracy and minimizing uncertainties [Williams et al., 2014]. Nuclear forensics often combines laboratory methods used for ordinary analysis of nuclear and other radioactive material and interpretation of the analysis results to provide technical conclusions about, for example, seized illicit nuclear or radioactive materials [Kristo and Tumey, 2013].

A nuclear forensic investigation can be divided into three parts [IAEA, 2006]:

- Categorization

The IAEA report "Nuclear Forensics Support" [2006] states that "*categorization is used to address the threat posed by a specific incident*". The aim of the categorization is to identify the safety risk to first responders and to the public, as well as to evaluate whether the incident is part of criminal activity and/or a threat to national security. One example of need for categorization may be the interception of uranium at a border control. The categorization done at this stage could include gamma spectrometric measurements of the material. Measuring the enrichment of the uranium would provide information on how to proceed with confiscation or even if a crime has been committed.

- Characterization

Characterization handles the determination of specific characteristics of the material. Table 1 lists some useful techniques and methods and gives a recommended sequencing of analysis to give the most valuable information early in an investigation without limiting the possibility of subsequent analyses [IAEA, 2015]. The table is a recommendation from the Nuclear Forensics International Technical Working Group (ITWG), which is an association of nuclear forensics practitioners. Important nuclear forensic characteristics include isotopic and elemental composition and physical characteristics.

The isotopic composition analysis can be performed using gamma or alpha spectrometry or any of the mass spectrometric techniques depending on sample size [Ramebäck et al., 2012]. The isotopic composition provides information about the intended use of the nuclear material but can also reveal if e.g. a uranium material is reprocessed [Zsigrai et al., 2015]. Elemental composition, or impurity measurements, is the measurement of remaining elemental impurities and can be used to explain the production process of the nuclear material or the geographical origin of the source material [Healy and Button, 2013; Varga et al., 2010a]. Physical characterization is used to tell the grain size or the chemical phase of a material and is mainly performed using surface characterization techniques such as scanning electron microscopy (SEM) and x-ray diffraction (XRD) but also other, more basic techniques, such as dimensions, mass determination and density measurements [Holmgren Rondahl et al., 2018; Sweet et al., 2013]. Another useful characteristic is the age of a material, i.e. the time that has passed since the last separation. The idea of age dating is to investigate the relation between a mother nuclide and the ingrowth of a daughter nuclide [Eppich et al., 2013; Gehrke and East, 2000; Nygren et al., 2007; Ramebäck et al., 2008; Varga et al., 2011]. The principles of age dating are explained in Chapter 3.

Table 1 Suggested priorities for common characterization methods [IAEA, 2015].

Techniques/Methods	24 h	One week	Two months
Radiological	Dose rate		
	Surface contamination		
	Radiography		
Physical	Visual inspection	SEM	TEM
	Photography	XRD	
	Mass determination		
	Dimensions		
	Optical microscopy		
	Density		
Traditional forensics	Collection of evidence		Analysis and interpretation
Isotope analysis	Gamma spectrometry	TIMS	SIMS
		ICP-MS	Radiometric techniques
Radiochronometry	Gamma spectrometry (for Pu)	TIMS	Gamma spectrometry (for U)
		ICP-MS	Alpha spectrometry
Elemental/chemical analysis	XRF	ICP-MS	GC-MS
		IDMS	
		FTIR	
		Assay (Titration, IDMS)	
		SEM/X ray spectrometry	

- Nuclear Forensic Interpretation

The results acquired in the characterization are used in the nuclear forensic interpretation where possible connections between materials and events are evaluated. Nuclear forensic analysis can be divided into two groups: comparative and predictive analysis [Hutcheon et al., 2013]. A measurement technique or a measurand can be used both for comparative and predictive analysis, depending on the question. The comparative analyses can be used to answer questions such as "Do these materials have the same origin?" or "Does this material correspond to any material in the database or any material we have knowledge about?" The predictive analyses, on the other hand, can be used to explain the origin of the material, processes the material has undergone and intended use of the material. For example, the isotopic composition can be used to compare different samples to see whether it is likely that they are originating from the same batch, but the composition can also be used to explain the intended use of the material and possibly the production process. Thus, the nuclear forensic interpretation is used for both linking materials and events to each other, and for the determination of the intention of the nuclear security event. The nuclear forensic interpretation requires highly skilled experts, so called subject matter experts (SME), who can interpret the analysis results and assess the significance of the findings [Mayer and Glaser, 2015].

2.3.1 National Nuclear Forensics Libraries

The IAEA encourages its member states to implement a national system for identification of nuclear and other radioactive material found out of regulatory control, to support nuclear security and non-proliferation [IAEA, 2018]. To determine whether a seized material originates from a state, a register of the nuclear material and other radioactive material held within a country can be helpful. This register is often referred to as a National Nuclear Forensics Library (NNFL) and may consist of reference information regarding nuclear material and radioactive sources. Ideally, this compilation of data would be available to the international community, but due to the sensitive nature of the information, the aim is to keep the libraries at a national level. The IAEA, however, encourages information sharing between countries when needed, either by direct contact between states or by using an international organization as the intermediary [IAEA, 2018; Mayer and Glaser, 2015].

The library may contain information that can be used to compare with data from analyses in nuclear forensic investigations, as well as with information from manufacturers. It is also possible to include archive samples of different sources in the library to facilitate ad hoc comparisons of characteristics of an investigated material and samples in the archive [Wacker and Curry, 2011]. Another crucial part in an NNFL is subject matter expertise to aid in the determination of what information to include and how it should be interpreted [Borgardt et al, 2017]. The aim of the NNFL is to ensure that nuclear material and radioactive sources are identifiable and traceable, or when this is not feasible, ensure that there are alternative processes for identifying and tracing sources [IAEA, 2004; IAEA, 2015]. The complexity of the NNFL may depend on a state's nuclear and radioactive material holdings. The signatures could be used to compare with the NNFL in order to determine whether a seized material is consistent with material that has been produced, used or stored within a state.

3 THEORY

3.1 NUCLEAR FORENSIC SIGNATURES

3.1.1 Isotopic ratios

In categorization of nuclear material, isotopic ratio measurements provide the enrichment of e.g. uranium, which will reveal the intended use of the material. In characterization, the isotopic ratio measurements will provide means for the comparison of different materials and, in addition, reveal whether the material has been reprocessed or not. Isotopic ratio measurements can be performed with either radiometric or mass-spectrometric techniques depending on the nuclides in question.

3.1.2 Radiochronometry

Radiochronometry is an important tool for nuclear forensics as, unlike many other signatures, it is a predictive signature that does not necessarily need a comparison to other materials to be useful [Mayer and Glaser, 2015].

The time that has passed since the last chemical separation is referred to as the age of a nuclear or other radioactive material. The age can be assessed by measuring the relation between the mother nuclide and its progeny. The rationale is that, at the time of separation, only the mother nuclide is present, e.g. uranium nuclides or ^{241}Am while all daughter products have been completely removed in the separation process. With time, the daughter nuclides will grow in and by measuring the ratio between the mother and daughter nuclide, the age of the material can be calculated. When performing radiochronometry, a few assumptions have to be made. The first assumption is that, at the time of separation (t=0), all of the daughter nuclides are removed. The second assumption is that the material is contained in a closed system, i.e. as the daughter nuclides grow in they remain in the material and is not removed by any process [Sturm et al., 2014]. Since these assumptions may be difficult to confirm, the measured age, also called the model age may not be the same as the actual age, i.e. the sample age. Another requirement for radiochronometry is that the mother and daughter nuclide are in radioactive disequilibrium. This means that not all mother/daughter-pairs are useful for radiochronology.

Radioactive decay can be described according to:

$$\mathrm{X}_1 \overset{\lambda_1}{\rightarrow} \mathrm{X}_2 \overset{\lambda_2}{\rightarrow} \mathrm{X}_3 \overset{\lambda_3}{\rightarrow}_{\ldots} \tag{1}$$

where λ_i is the decay constant for radionuclide X_i. The age of a material, t, can, in the case of two successive decays, be calculated according to

$$t = \frac{1}{\lambda_1 - \lambda_2} \cdot \ln\left(1 - \left(1 - \frac{\lambda_1}{\lambda_2}\right)\frac{A_2}{A_1}\right) \tag{2}$$

where A_i is the activity of radionuclide X_i. The corresponding expression of the age performed by atom counting (mass spectrometry) is analogous to Eq. 2.

In cases where the half-life of the daughter X_3 is substantially shorter than the half-life of X_2, the X_3 activity will rapidly grow into secular equilibrium and equal that of X_2. This means that X_3 will decay with the half-life of X_2. In this case, it is possible to use the A_3/A_1 activity ratio together with the decay constant of X_2 in Eq. 2 to calculate the age of the material. This may be convenient in cases where the

gamma photon yield of radionuclide X_2 is too small to be detected with gamma spectrometry within reasonable measurement time. One such example is given in **Paper II**. The age determination of ^{241}Am was performed by using the granddaughter ^{233}Pa to ^{241}Am instead of its daughter ^{237}Np, since the photon emission probability of ^{237}Np are too small to be visible in a high activity ^{241}Am spectrum. The half-lives of ^{241}Am, ^{237}Np and ^{233}Pa are 432.6 y, $2.144 \cdot 10^6$ y and 26.98 d, respectively [DDEP, 2018].

3.1.3 Trace elemental impurities

Trace elemental impurities are elements found in a material that have not been deliberately added to the material [Lützenkirchen et al., 2019]. One common example in the field of nuclear forensics is trace elements found in uranium material. These impurities can either originate from the geological deposit and remain in the uranium ore concentrate (UOC) after milling, or from the various processes the material undergo. Therefore, the trace elements can be used both to compare materials to each other and to estimate the type of processes the material has passed [Varga et al., 2017]. Elements that have been added intentionally in the material and that are relevant for the properties of the material are called additives and are, in general, substantially more abundant than trace elements.

3.1.3.1 Lanthanide patterns

Lanthanide patterns have been considered a good predictor of geographical origin of uranium material for some time [Mercadier et al, 2011]. The lanthanide series comprises 15 elements, whereof 14 are naturally occurring. The 15th, promethium, does not have any stable isotopes and is therefore omitted from the lanthanide patterns. The composition of the lanthanides depends on the geological processes that the material have undergone. Examples of different lanthanide patterns are shown in Figure 1. The lanthanide patterns originate from different types of uranium ore formations. Due to environmental conditions, such as temperature and salinity during the ore formation process, the lanthanides will fractionate [Mercadier et al, 2011]. The reason why the lanthanide series is a good indicator for geographical origin is that all the lanthanides are trivalent under normal conditions and have similar characteristics. Therefore, the relative abundance of the lanthanides in a material remain, on a relatively short time scale, even though the material undergo various processes. The exceptions are cerium and europium that, additionally to the trivalent state, may be tetravalent and divalent, respectively.

The measured concentrations of lanthanides in a sample is often normalised to chondrite to allow for an easier interpretation of geological processes. The normalised values are then plotted in increasing atomic number to receive the lanthanide pattern. Chondrite is a meteoritic material that is assumed to represent the average concentrations of elements in the solar system, and the assumption is that the composition of the lanthanides on earth as a whole is the same as that of the chondrite meteorites. Due to various processes during the history of Earth, the lanthanides have fractionated [White, 2013; Prohaska et al., 1999]. By normalizing the lanthanides measured in a sample to chondrite values, geologists can use the information given by the pattern to explain the history and source of a rock [White, 2013]. Another reason for presenting the lanthanides as chondrite normalised abundances rather than absolute concentrations is that all odd-numbered elements, with only a few exceptions, are less abundant than their even-numbered neighbours, resulting in a saw tooth-shaped lanthanide pattern. The normalisation produces a smooth pattern that is more easily interpretable [White, 2013].

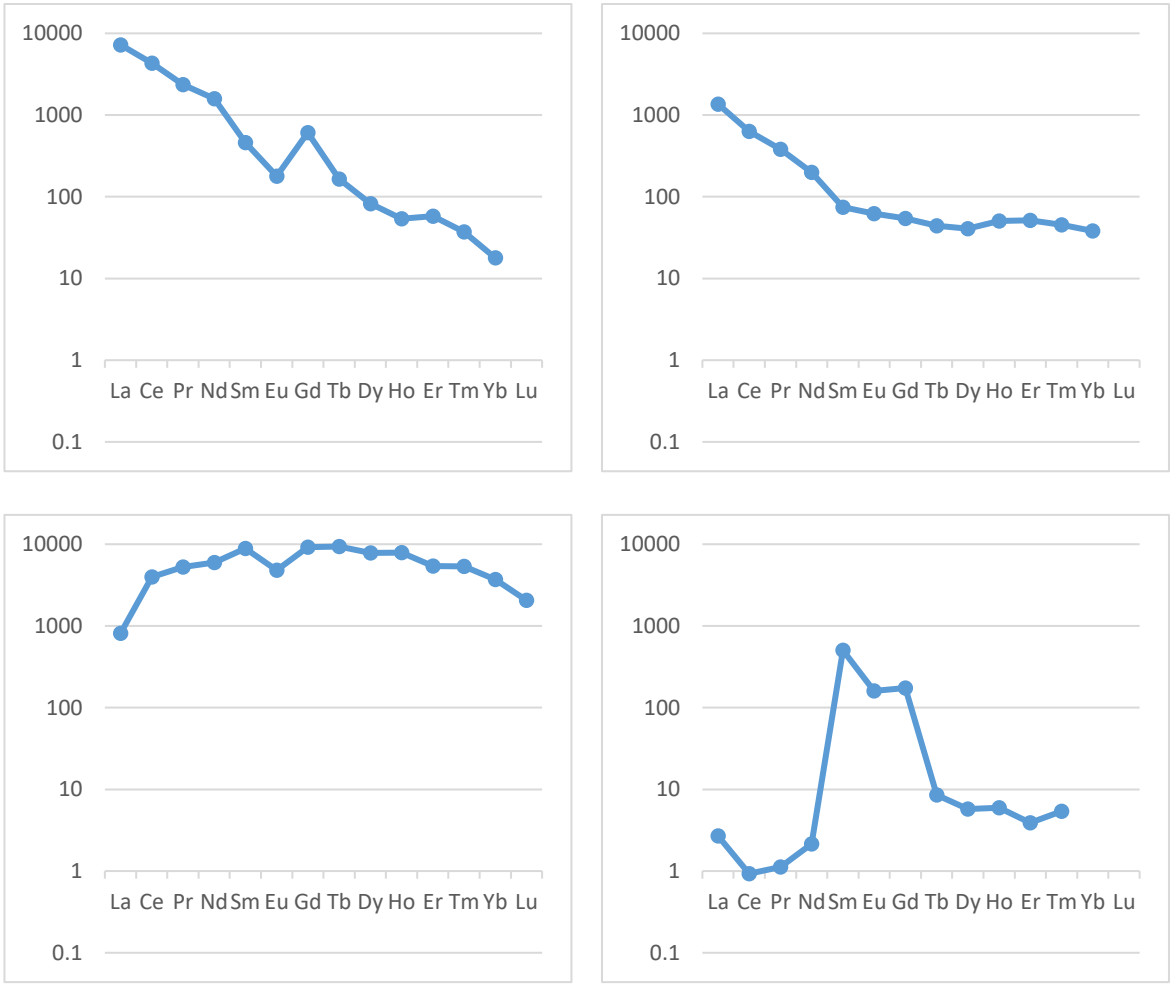

Figure 1 Examples of chondrite normalized lanthanide patterns from four different geographical origins. Top left: Vein-type from Commanderie, France, Top right: Roll-front from Kazakhstan, Bottom left: Synmetamorphic from Mistamisk and Bottom right: Volcanic-related from Streltsovskoye. Data from Mercadier [2011].

Uranium is commonly found as an oxide in nature. Due to their similar ionic radii, the elements in the lanthanide series are often found together with uranium in non-negligible amounts. Therefore, many papers have suggested lanthanide patterns as a good indicator of geographical origin of uranium [Frimmel et al., 2014; Fryer and Taylor, 1987; Mercadier et al., 2011; Spano et al., 2017; Varga et al., 2010a].

3.1.3.2 Measurements of lanthanides in uranium material

Due to the generally low abundance of lanthanides in uranium materials, lanthanide measurements require a measurement technique with low detection limits. Mass spectrometry is such a technique, even though there are some difficulties in measuring lanthanide concentrations using ICP-MS [Vaughan and Horlick, 1990; Dulski, 1994]. The heavy uranium matrix may cause matrix effects with a following decrease in measurement sensitivity and signal stability [Tan and Horlick, 1987; Beauchemin et al., 1987]. This will in turn increase the detection limits. The high amount of uranium introduced into the instrument may also cause memory effects, i.e. high uranium backgrounds that may be difficult to eliminate. To solve this problem Varga et al. proposed a method for group separation of the lanthanide series to remove uranium and barium from the samples using a resin based on CMPO/TBP (TRU resin) [2010b].

Many of the lanthanides have many isotopes and therefore there is a number of isobars among the lanthanides. There is, however, at least one isotope of each lanthanide free of isobars. Another problem with measuring lanthanides using ICP-MS is the presence of polyatomic interferences such as oxides and hydrides. Especially lighter lanthanides, such as cerium and praseodymium are prone to oxide formation. These oxides will interfere with the heavier lanthanides [Dulski, 1994; Longerich et al., 1987]. One such example is $^{141}Pr^{16}O^{+}$ that interferes with $^{157}Gd^{+}$. This may cause a problem since the lighter lanthanides often are more abundant than the heavier ones in uranium bearing material. The interference may then be a substantial part of the measured signal of the heavier elements. The lanthanides and their most prominent interferences can be seen in Figure 2. Each isotope is coloured in green, yellow or red to illustrate that quantification using the isotopes is suitable, suitable with caution and unsuitable, respectively. To be able to use the isotopes marked in yellow for accurate quantification, the interferences should be addressed [Vesterlund et al, 2014].

m/z	Ba	La	Ce	Pr	Nd	Sm	Eu	Gd	Tb	Dy	Ho	Er	Tm	Yb	Lu
130	0.11														
131															
132	0.1														
133															
134	2.42														
135	6.59														
136	7.85		0.19												
137	11.23														
138	71.7	0.089	0.25												
139	^{138}BaH	99.911													
140		^{139}LaH	88.45												
141			^{140}CeH	100											
142			11.11	^{141}PrH	27.2										
143			^{142}CeH		12.2										
144					23.8	3.1									
145					8.3										
146	^{130}BaO				17.2										
147	^{130}BaOH				^{146}NdH	15									
148	^{132}BaO				5.8	11.3									
149	^{132}BaOH				^{148}NdH	13.8									
150	^{134}BaO				5.6	7.4									
151	^{135}BaO				^{150}NdH	^{150}SmH	48								
152	^{136}BaO		^{136}CeO			26.7	^{151}EuH	0.2							
153	^{137}BaO					^{152}SmH	52								
154	^{138}BaO		^{138}CeO			22.7	^{153}EuH	2.18							
155	^{138}BaOH	^{139}LaO				^{154}SmH		14.8							
156		^{139}LaOH	^{140}CeO					20.47		0.056					
157			^{140}CeOH	^{141}PrO				15.65							
158			^{142}CeO	^{141}PrOH	^{142}NdO			24.84		0.095					
159			^{142}CeOH		^{143}NdO			^{158}GdH	100						
160					^{144}NdO	^{144}SmO		21.86	^{159}TbH	2.329					
161					^{145}NdO	^{144}SmOH		^{160}GdH		18.889					
162					^{146}NdO					25.475		0.14			
163					^{146}NdOH	^{147}SmO				24.896					
164					^{148}NdO	^{148}SmO				28.26		1.6			
165					^{148}NdOH	^{149}SmO				^{164}DyH	100				
166					^{150}NdO	^{150}SmO					^{165}HoH	33.5			
167					^{150}NdOH	^{150}SmOH	^{151}EuO					22.87			
168						^{152}SmO	^{151}EuOH	^{152}GdO				26.98		0.12	
169						^{152}SmOH	^{153}EuO					^{168}ErH	100		
170						^{154}SmO	^{153}EuOH	^{154}GdO				14.91	^{169}TmH	2.98	
171						^{154}SmOH		^{155}GdO				^{170}ErH		14.09	
172								^{156}GdO		^{156}DyO				21.69	
173								^{157}GdO		^{164}DyOH				16.1	
174								^{158}GdO		^{158}DyO				32.03	
175								^{158}GdOH	^{159}TbO	^{164}DyOH				^{174}YbH	97.4
176								^{160}GdO	^{159}TbOH	^{160}DyO				13	2.6

Figure 2 Isotopes of the lanthanides with abundances [Meija et al, 2016] and their most prominent hydride, oxide and hydroxide interferences in ICP-MS, based on water and nitric acid chemistry. The green marked isotopes are not interfered or only slightly interfered and can be used for quantitative determination. The red marked isotopes should be avoided for quantitative measurements. The yellow marked isotopes are the best choices for the interfered elements and may be used for determination. Barium is included to show the importance of considering this element when measuring the lanthanides. All oxides in the chart refer to $^{16}O^{+}$.

Many ways of avoiding the impact of polyatomic interferences have been proposed. Neutron activation analysis (NAA) is a non-mass spectrometric technique that provides relatively low detection limits but requires access to a research reactor [Bulska et al., 2012; Dampare et al., 2005]. Funderberg et al. [2017] has presented a method for measuring the lanthanide series using medium-resolution LA-ICP-MS (laser ablation ICP-MS) which allows for peak separation of the polyatomic interferences from the analytes. However, the method did not resolve the interference of e.g. $^{143}Nd^{16}O^{+}$ on $^{159}Tb^{+}$. The resolution needed to resolve these peaks is approximately 7700. Using higher resolution also

decreases the sensitivity that may be required to measure low concentrations with good accuracy and precision [Nelms, 2005]. Attempts have been made to correct for these interferences mathematically [Raut et al., 2003; Vaughan and Horlick, 1990] but this approach may lead to large measurement uncertainties if the correction is large compared to the analyte in question and may require extensive measurements each day of analysis [Simitchiev et al., 2008]. Groopman et al. [2017] has presented the SIMS-SSAMS (secondary ion mass spectrometry-single stage accelerator mass spectrometry) as an excellent technique for providing interference free lanthanide patterns at low concentrations. However, this technique is rare and therefore there is a need for more available mass spectrometric techniques. Inductively coupled plasma-mass spectrometry (ICP-MS) is a widespread, multi-elemental technique that is suitable for the purpose due to low detection limits for these elements.

Many papers have put forward the possibility of performing chemical separations for at least some of the elements in the lanthanide series to remove interfering lanthanide oxides. Pin and Zalduegui [1997] used a combination of TRU resin (CMPO/TBP) and Ln resin (HDEHP) to separate thorium and uranium and light rare earth elements, LREE, respectively for measurement of neodymium isotope ratios and concentrations of uranium, thorium, neodymium and samarium. Another example is Yang et al [2010] who presented a separation method using Ln resin for measuring both Sm-Nd and Lu-Hf isotope systems used for geochronological dating.

3.2 MEASUREMENT TECHNIQUES

3.2.1 Gamma spectrometry

Gamma spectrometry is a non-destructive measurement method for gamma emitting radionuclides. The instruments used for gamma spectrometry can be divided into low- and high-resolution instruments. Low-resolution instruments such as NaI(Tl) scintillation detectors [Knoll, 2000] are commonly used as first-responder or customs instruments, but the ability of these instruments to identify radionuclides has been shown to be unsatisfactory [Blackadar et al. 2003; Nelson et al., 2011; Pibida et al., 2004]. This is mainly due to the low-resolution characteristics. A number of publications have put forward different identification algorithms but the problem seems to remain [Estep et al., 1998; Hofstetter et al., 2008; Sprinkle Jr et al., 1997]. The instrument is not able to separate peaks that are close in energy, which makes the instrument a blunt tool for identification and requires highly qualified users in many cases. However, this is not always enough since the resolution often prohibits even manual identification. The instrument used in **Paper I** does have the ability to automatically evaluate both measured nuclides as well as the category regarding uranium. High-resolution instruments, high purity germanium detectors (HPGe) [Knoll, 2000], do not have this problem.

An advantage of low-resolution instruments is that they operate at room temperature as opposed to HPGe detectors that require cooling. The need for cooling in HPGe detectors somewhat limits its flexibility. Another advantage of the low-resolution detectors is that the acquisition is fast due to the high measurement efficiency since e.g. NaI(Tl) detectors can be produced with a much larger volume compared to HPGe detectors.

3.2.1.1 Absolute and relative efficiency calibrations

As the measurement efficiency of a gamma spectrometric system is energy dependent, the detectors need carefully executed efficiency calibrations in order to make accurate activity and activity ratio measurements. This is normally done by using a calibration solution containing a number of radionuclides with known, certified activities and with energies covering the energy region in question.

The radioactivity of isotope x, A_x, evaluated from a gamma spectrometric measurement is given by

$$A_{\mathrm{x}} = \frac{C_{\mathrm{x},\gamma}}{t \cdot I_{\mathrm{x},\gamma} \cdot \Psi_{\gamma}} \tag{3}$$

where $c_{x,\gamma}$ and $I_{x,\gamma}$ are the number of counts and photon emission probability of isotope x at energy E_γ, respectively, t is the measurement time and Ψ_γ is the measurement efficiency at energy E_γ. The measurement efficiency is given by rearranging Eq. 3:

$$\Psi_{\gamma} = \frac{C_{\mathrm{x},\gamma}}{t \cdot I_{\mathrm{x},\gamma} \cdot A_{\mathrm{x}}} \tag{4}$$

Hence, the calibration spectra and the certificate information for each energy can be used to fit a response function by using an empirical equation. In this work the 5-term equation previously published by Ramebäck et al. [2010] where c_1,…, c_5 are constants and E is the energy, has been used:

$$\Psi(E) = e^{c_1 + {c_2}/{E^2} + c_3 \cdot (\ln(E))^2 + c_4 (\ln(E))^3 + {c_5}/{E}} \tag{5}$$

In special cases, where the absolute activity is unimportant, such as in activity or isotope ratio determinations, it is possible to construct a relative calibration if there is a radionuclide in the sample with a number of gamma lines covering the energy region of interest. As the activity is equal for all calibration points, Eq. 4 can be simplified and the relative measurement efficiency for a certain gamma line is then given by

$$\Psi_{\mathrm{rel},\,\gamma} = \frac{C_{\mathrm{x},\gamma}}{I_{\mathrm{x},\gamma}} \tag{6}$$

The calculated $\Psi_{rel,\gamma}$ can be used to fit Eq. 5 in the same manner. The advantage of using inherent calibrations is that the sample geometry including absorbing materials between the sample and the detector as well as sample composition is unimportant as opposed to absolute calibrations. The peaks used for the construction of an intrinsic response function for uranium abundance calculations in high-resolution spectra are peaks in the low energy region for ^{235}U and peaks in the high-energy region for ^{234m}Pa. The condition for fitting the function is that the ^{234m}Pa peak at 258 keV is visible. This peak connects the low energy ^{235}U peaks with the high-energy ^{234m}Pa peaks and enables a fit of a function over the whole energy region, from 144 keV to 1001 keV. For high-resolution instruments, this vital peak is visible in almost all uranium spectra except possibly spectra of very highly enriched uranium. In the case of very highly enriched uranium in the high-resolution case, it would be possible to use ^{228}Th daughters to establish the response function if the material contains reprocessed uranium (^{232}U) [Ramebäck et al., 2010]. However, for low-resolution instruments, this peak is not discernible and, furthermore, the low resolution reduces the number of distinct peaks for the fitting of the response function from eight to two or possibly three peaks. Hence, the construction of an intrinsic response function of a low-resolution spectrum is not possible. Instead, the instrument must be calibrated for absolute efficiency for a certain measurement setup.

3.2.1.2 Categorization of uranium by gamma spectrometry

Uranium can be categorized by evaluating the fraction of ^{235}U of the total amount of uranium. Using gamma spectrometry, this can be done by using the 185.7 keV peak from ^{235}U and the 1001 keV peak from ^{234m}Pa in the gamma spectrum, assuming radioactive equilibrium between ^{234m}Pa and ^{238}U. Four months after separation, the activity difference between ^{234m}Pa and ^{238}U is within the uncertainty of the gamma spectrometric measurement. Hence, radioactive equilibrium can be assumed after this period of time. The abundance of ^{235}U, f_{235}, is, if the abundance of minor uranium isotopes is neglected, given by

$$f_{235} = \frac{N_{235}}{N_{235}+N_{238}} \tag{7}$$

where N_x is the number of atoms of uranium isotope x. When the enrichment of ^{235}U approaches 90%, the ^{234}U abundance is around 1% depending on the history of the material [Nguyen and Zsigrai, 2006]. Therefore, the amount of ^{234}U, N_{234}, is, in this case, considered negligible. Furthermore, the 185.7 keV peak is assumed not to be interfered by ^{226}Ra. This assumption is made on the basis that there are no significant amounts of ^{226}Ra in a processed anthropogenic uranium material due to the relatively young age. Moreover, the ^{226}Ra originating from the background may be subtracted from the spectrum.

Using the well-known relation

$$A_{\mathrm{x}} = \frac{N_{\mathrm{x}} \cdot \ln(2)}{t_{½,\mathrm{x}}} \tag{8}$$

where $t_{½,x}$ is the half-life of isotope x in combination with Eq. 6-7, the abundance of ^{235}U can be written as:

$$f_{235} = \frac{c_{235,185\mathrm{keV}} \cdot t_{½,235} \Big/ I_{235,185\mathrm{keV}} \cdot \Psi_{185\mathrm{keV}}}{c_{235,185\mathrm{keV}} \cdot t_{½,235} \Big/ I_{235,185\mathrm{keV}} \cdot \Psi_{185\mathrm{keV}} + c_{238,1001\mathrm{keV}} \cdot t_{½,238} \Big/ I_{238,1001\mathrm{keV}} \cdot \Psi_{1001\mathrm{keV}}} \tag{9}$$

3.2.2 ICP-MS

The mass spectrometer used in this work is a double focusing sector field ICP-MS, Element 2 (Thermo Scientific, Bremen, Germany). Double focusing means the ions are separated by both mass in a magnetic sector and by energy in an electrostatic analyser (ESA). The ESA may be placed either before or after the magnet sector (Nier-Johnson and reversed Nier-Johnson geometry, respectively). The instrument used in this work has the reversed Nier-Johnson geometry, which improves abundance sensitivity and reduces noise since the mass analyser reduces the high ion currents from the ion source and the only ions that reach the ESA are ions with the correct mass [Jakubowski et al., 1998].

3.2.2.1 Interferences

Interferences in mass spectrometry can be divided into two groups, spectral and non-spectral interferences.

3.2.2.1.1 Polyatomic interferences

Common spectral interferences in mass spectrometry are the polyatomic interferences. These interferences are the result of two or more atoms in the matrix, solvent or plasma gas, forming a molecular species. The formation rate and type of molecule is largely dependent on the presence of isotopes and the plasma conditions [Nelms, 2005]. Common polyatomic species are argides, nitrides, oxides and hydrides due to the abundance of these elements in the plasma and the solvent [Jakubowski et al., 2011]. Due to the dependence on sample composition and plasma conditions, the

amount and type of polyatomic interferences may be difficult to predict, making mathematical interference corrections difficult to perform. One way to remove the interferences is to increase the resolution, but this measure may not be sufficient to remove all interferences [Funderberg et al., 2017].

3.2.2.1.2 Isobars

Many of the isotopes measurable with ICP-MS have isobars, i.e. isotopes of another element but with the same mass, such as $^{241}Pu^{+}$ and $^{241}Am^{+}$. This type of interference requires very high resolution for peak separation (up to 10^{7} [Nelms, 2005]). Therefore, the options when measuring these isotopes are to either correct for the interference or remove the elements with interfering isotopes using chemical separations. Since the isobars in many cases are predictable it is possible to mathematically subtract the portion of the peak coming from the interfering isotope, assuming that the elements have a natural composition [Jakubowski et al., 2011].

3.2.2.1.3 Multiply charged ions

Multiply charged ions arise when the atom loses more than one electron in the plasma. The detection of the formed ion will be at mass m/Z where Z is the charge of the ion. The probability of the formation of multiply charged ions is low since the second ionisation energy is substantially higher than the first ionisation energy but can cause interference problems if the interfering element is abundant in the measured samples. One such example is the measurement of trace lanthanides in a uranium matrix where ^{139}La may be interfered by $^{238}U^{40}Ar^{++}$ [Boulyga et al., 2017].

3.2.2.1.4 Abundance sensitivity

A fourth kind of spectral interference is the tailing of isotopes on neighbouring masses. Due to scattering of ions in the beam, the energy spread of the ions increases, resulting in higher abundance sensitivity [Becker, 2007]. A typical abundance sensitivity is between 10^{-7}-10^{-6} [Nelms, 2005]. Therefore, the abundance sensitivity does not affect the measurement unless the ratio between the tailing isotope and the neighbouring isotope is >100000 [Nelms, 2005].

3.2.2.1.5 Non-spectral interferences

Non-spectral interferences, or matrix effects, are effects that are not limited to a certain mass but cause an overall change in the analyte signal independent of the mass [Evans and Giglio, 1993; Nelms, 2005]. The signal changes are caused by for example sample transport, ionization in the plasma and ion extraction. Another reason for signal suppression may be build-up of salts on the cones causing the orifices to clog [Evans and Giglio, 1993]. The level of the matrix effect depends on the concentration and nature of the matrix. A heavy matrix often leads to signal suppression and can be resolved by dilution or, to some extent, the use of an internal standard. Another way to minimize matrix effects is to chemically separate the analytes from matrix elements.

Corrections for non-spectral interferences can be done by the use of an internal standard. The internal standard should be an element absent in the sample and show the same behaviour as the analyte in the plasma. It has been suggested that elements suitable as internal standards have mass and ionization potential close to the analyte [Thompson and Houk, 1987]. According to Vanhaecke et al. [1992], only the mass needs to be a close match for the internal standard to be appropriate. In this study, the impact of ionization potential was regarded as insignificant.

3.2.2.2 Quantification

For quantification, different approaches such as isotope dilution, standard addition and external calibration, can be used.

3.2.2.2.1 Isotope dilution

The approach that usually provides the lowest measurement uncertainties is isotope dilution, where a spike with a different isotopic composition than the isotopic composition of the analyte in the sample, is added to the measured sample [Trešel et al., 2003]. Another possibility is to use an isotope, which is not naturally occurring, i.e. long-lived radioactive isotopes. One such example is the use of ^{233}U for quantification of uranium [Kristo et al., 2015, Nelwamondo et al., 2018]. By knowing the isotopic compositions of the spike and the sample as well as the amount of added spike, the concentration of the sample can be determined. A limitation to this method is the lack of reference materials that are isotopically enriched to be useful for isotope dilution. Another limitation is that some elements, such as aluminium and yttrium, have only one stable isotope, which makes isotope dilution impossible.

3.2.2.2.2 Standard addition

In standard addition, increasing and known amounts of the analyte is added to the sample and by measuring the sample with an increasing amount of analyte spike, it is possible to calculate the amount of the analyte in the sample when no spike is added as the relation between signal intensity and the concentration is linear [Harris, 2003]. Standard addition limits the impact of matrix effects but may require tedious work, as every measured sample requires a number of measurements with different amounts of analyte spike.

3.2.2.2.3 External calibration

Due to the lack of isotopic spikes and the work effort of standard addition, the most commonly used method for quantitative measurements by ICP-MS is done using external calibration where calibration samples with a known amount of analyte are measured to establish a calibration with instrument signal as a function of concentration [Nelms, 2005]. In this way, unknown samples can be measured and the signal from the sample can be used to calculate the concentration. External calibrations using pure standard solutions do not take any matrix effects into account. Depending on the matrix, analyte concentrations in the sample can be over- or underestimated. Therefore, the calibration samples often need to be matrix-matched when the samples have a high matrix content, in order to provide a calibration that corresponds to the samples [Nelms, 2005].

3.3 SEPARATION CHEMISTRY

3.3.1 Solvent extraction

The purpose of solvent extraction may be to preconcentrate the analyte(s), eliminate matrix interferences or to differentiate chemical species, and is a method to separate compounds depending on differentiating solubility in two immiscible phases, normally an aqueous phase and an organic phase. The distribution ratio, *D*, of a compound between the organic phase and the water phase can be expressed by:

$$D = \frac{[M]_{org}}{[M]_{aq}} \tag{10}$$

where $[M]_{org}$ and $[M]_{aq}$ is the total concentration, i.e. the concentration of all species of M, in the organic and aqueous phase, respectively [Nash, 2000]. The organic phase consists of an extractant that has the ability to extract the desired compound from the aqueous phase into the organic phase, i.e. making it more soluble in the organic phase. Sometimes a diluent is added to enhance the performance of the extractant. The goal of the extraction is to form an uncharged hydrophobic molecule that includes the wanted species, which can be dissolved in the organic phase.

The extractants can be divided into different groups depending on the extraction mechanism [Rydberg, 1992]. Some examples of extractants and their mechanisms are acidic extractants, basic or ion pair forming extractants and solvating or neutral extractants. The overall mechanism for acidic extractants, where the metal cation reacts with a suitable anion, the extractant, to form a neutral complex, can be written as

$$M^{n+} + \overline{nHA} \rightleftharpoons \overline{MA_n} + nH^+ \tag{11}$$

The ion pair forming extractant mechanism where the metal cation forms an ion pair with the extractant can be summarized as

$$MX_p^{(n-p)-} + \overline{(n-p)R_3NH^+X^-} \rightleftharpoons \overline{R_3NH_{(n-p)}MX_p} + (n-p)X^- \tag{12}$$

Correspondingly, the mechanism of solvating extractants where the coordinated water molecules are replaced by an organic solvating reagent can be written as

$$MY_q + \overline{rB} \rightleftharpoons \overline{MY_qB_r} + xH_2O \tag{13}$$

The species in reactions 11-13 with a line on top are species in the organic phase. In this work, commercial resins, Ln resin (Triskem, Bruz, France) based on di-2 ethylhexyl orthophosphoric acid (HDEHP) have been used.

3.3.2 Extraction using HDEHP

HDEHP, see Figure 3, has for a long time been used for the separation of lanthanides and other trivalent elements and the properties of the HDEHP extractant system has been thoroughly investigated [Qureshi et al., 1969; Alstad et al., 1974; Peppard et al., 1957].

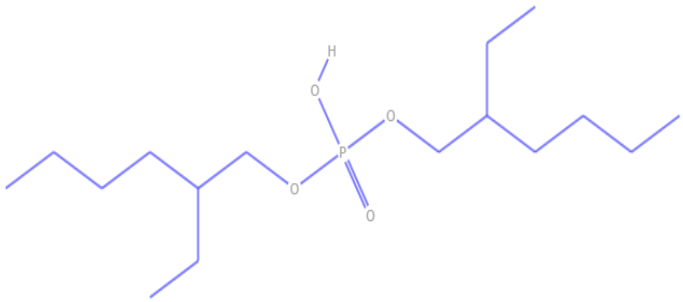

Figure 3. Structural formula of HDEHP.

The overall reaction is assumed to be:

$$M^{3+} + \overline{3(HDEHP)_2} \rightleftharpoons \overline{M(H(DEHP)_2)_3} + 3H^+ \quad (14)$$

where M^{3+} is the lanthanide ion [Alstad et al, 1974]. Peppard et al. [1957] showed that the extraction of the lanthanides show an inverse third-power dependence on the acid concentration which agrees with Eq. 14, and if the acid concentration increases, the extraction decreases, allowing for stripping of the extracted species. However, Alstad et al. [1974] showed that this dependence becomes directly proportional at nitric acid concentrations above approximately 5 M. Qureshi et al. [1969] proposed two possible mechanisms for this increased extraction:

$$M^{3+} + 3X^- + \overline{(HDEHP)_2} \rightleftharpoons \overline{MX_3(HDEHP)_2} \quad (15)$$

$$H^+ + X^- + \overline{(HDEHP)_2} \rightleftharpoons \overline{HX(HDEHP)_2} \quad (16)$$

where X^- represents the anion of the acid. The proposed reaction in Eq. 15 indicates that increasing the amount of acid anion drives the extraction of the lanthanide to an HDEHP complex together with the anion, while Eq. 16 indicates that acid ions are removed from the aqueous phase that in turn leads to increased extraction of lanthanide ions according to Eq. 14.

3.4 LINEAR REGRESSION

Using external calibration in ICP-MS measurements involves the procedure of fitting a straight line to a number of calibration points with the analytical signal, *y*, as a function of concentration, *x*:

$$y = a + bx \quad (17)$$

where *a* and *b* are the estimates of intercept and slope of the line, respectively. The common method to evaluate this line is to use ordinary least squares regression (OLS) where the distance between the data points and the line along the *y*-axis is minimized [Miller and Miller, 2010]. The slope, *b*, is calculated according to Eq. 18.

$$b = \frac{\sum_i [(x_i - \bar{x})(y_i - \bar{y})]}{\sum_i (x_i - \bar{x})^2} \quad (18)$$

where y_i and x_i are the signal intensity and the concentration of calibration point i, respectively, and $\bar{y}$ and $\bar{x}$ are the corresponding mean values of all calibration points. The intercept can then be calculated by Eq. 19:

$$a = \bar{y} - b\bar{x} \quad (19)$$

However, in order for the OLS to be a valid method for establishing this line, a number of requirements need to be fulfilled [Raposo, 2016; Hubaux and Vos, 1970]:

- A linear relationship between x and y.
- The uncertainty of the concentrations on the x-axis is negligible.
- The variance in y is homoscedastic.
- Normally distributed variance in y.

If at least one of these requirements are not fulfilled, the OLS will not provide the best estimate of the calibration line. Whereas the first and last point frequently are fulfilled in mass spectrometric measurements, the second point at least needs to be evaluated to check the validity of the OLS. However, the third point is almost exclusively invalid in mass spectrometry [Ketkar and Bzik, 2000]. In the case of mass spectrometry, the data points have heteroscedastic variance; the relative variance is the same with the exception of low measurement intensities where the relative variance is higher. Therefore, OLS is not a valid method for fitting a line to mass spectrometric calibration data. In OLS, each data point is given the same importance in the regression, which infers that, even though data points on the far right side of the calibration have higher absolute uncertainties, these data points have unreasonably large impact on the fitted line. This means that at low concentrations, the line does not represent the data points very well.

To fit a line to heteroscedastic data another regression type such as weighted linear regression (WLS) should be used [Sayago, 2004]. In WLS, each data point is weighted with a suitable parameter, or weight factor, to give data points with low absolute variance higher importance in the regression. The classical approach is to use $1/s_y^2$ as weight factor, where s_y is the uncertainty in y [Deming, 1964] but also other weight factors such as $1/y$ or $1/x$ can be used if there is only one data point for each x [Almeida, 2002]. In WLS the slope, b, is calculated as

$$b = \frac{\sum_i w_i [(x_i - \bar{x}_w)(y_i - \bar{y}_w)]}{\sum_i w_i (x_i - \bar{x}_w)^2} \quad (20)$$

where w_i is the weight factor at calibration point i and $\bar{y}_w$ and $\bar{x}_w$ are the weighted mean values of all y_i and x_i. The intercept, a, can be calculated in a corresponding manner to Eq. 19 with the exception that the weighted means of all calibration points are used rather than the means of x and y [Sayago and Asuero, 2004]:

$$a = \bar{y}_w - b\bar{x}_w \quad (21)$$

The detection limit, L_D, used for external calibrations in this thesis is

$$L_D = a + 3u_a \quad (22)$$

where u_a is the uncertainty of the intercept [Miller and Miller, 2010].

4 EXPERIMENTAL

4.1 MEASUREMENT UNCERTAINTY

The measurement uncertainties presented in this work were evaluated according to ISO: Guide to the Expression of Uncertainty in Measurement, ISO/GUM [2008]. The results were calculated using GUM Workbench 2.4 (Metrodata GmbH, Grenzach-Wyhlen, Germany) and are presented with a coverage factor *k*=2, unless otherwise stated which corresponds to an approximate 95% confidence interval.

4.2 LOW-RESOLUTION GAMMA SPECTROMETRY FOR URANIUM CATEGORIZATION

4.2.1 Measurements

Spectra were acquired of the following materials using the hand-held NaI(Tl) scintillation detector identiFINDER (ICx, FLIR Systems Inc., Wilsonville, USA):

- Natural uranium as UO_2
- Low-enriched uranium with an approximately 4% enrichment as UO_2
- Depleted uranium as UO_2
- Natural uranium in an aqueous solution (IRMM-184, Geel, Belgium)

Data was collected for 60 s at a distance of 10 cm from the source. The data from the certified reference material IRMM-184 was collected during 600 s due to low uranium content. The instrument reported the uranium category after the measurement using the automatic evaluation algorithm. The spectrum data was also downloaded for off-line evaluations according to Eq. 5 and Eq. 9.

4.2.2 Simulations

The following setups were simulated using the Monte Carlo based simulation software VGSL (Visual Gamma Spectroscopy Laboratory:

- Water matrix, ρ = 1 g/cm^3
- UO_2 matrix, ρ = 11 g/cm^3
- Uranium metal matrix, ρ = 19 g/cm^3
- Water matrix with a 1 mm lead shielding, ρ_{Pb} = 11 g/cm^3
- Water matrix with a 5 mm steel shielding, ρ_{Steel} = 7.5 g/cm^3

VGSL uses a modified version of MCNPX as particle transport simulation engine [Plenteda, 2002; Waters, 2002]. The detector was simulated to correspond to the identiFINDER. Therefore, the crystal dimensions and density were set to 35 x 51 mm^2 and 3.7 g/cm^3, respectively. Eq. 5 was fitted to each set of efficiency data retrieved from the simulations and the abundance of ^{235}U according to Eq. 9 was calculated for each spectrum, with different response functions, from the peak areas at 185.7 keV and 1001 keV.

4.3 SIGNATURES IN ^{241}AM SOURCES

Five sources were studied for investigation of possible signatures:

- Source 1: ^{241}Am sealed source contained in a lead shield during the gamma spectrometric measurement. Nominal activity 185 GBq.
- Source 2: ^{241}Am sealed source contained in a lead shield during the gamma spectrometric measurement. Nominal activity 185 GBq.
- Source 3: ^{241}Am sealed source measured with 1.1 mm Cd shielding.
- Source 4: Electroplated ^{241}Am source. Nominal activity 3.7 GBq.
- Source 5: Ionising smoke detector containing an ^{241}Am source.

Source 1 and 2 were visually similar. Sources 1-4 were measured overnight, at a distance of about 30 cm using a p-type coaxial high purity germanium detector (Detective-EX, EG&G Ortec, Oak Ridge, TN, USA) which has a relative efficiency of about 15% and a resolution of 2.5 keV at 1332 keV. The smoke detector, Source 5, was measured in a lead shield setup, using a p-type coaxial HPGe detector (EG&G Ortec, Oak Ridge, TN, USA) with a relative efficiency of 50% and a resolution of 2.0 keV at 1332 keV. The measurement time for Source 5 was approximately 1 week due to low activity of its daughter radionuclides.

An intrinsic response function was established for each spectrum using ^{241}Am lines between 59.5 and 801.9 keV, see Table 2, and Eq.5. Using the response function, the activity of ^{233}Pa relative to ^{241}Am could be calculated and the ages of the sources could then be determined using Eq.2. The gamma lines used for the calculation was the 322.6 keV ^{241}Am line and 311.9 keV ^{233}Pa line. Furthermore, the relative activities of the impurity elements could be determined.

Table 2 Gamma energies with corresponding photon emission probabilities used for the intrinsic calibration and the age determination. Data are taken from Decay Data Evaluation Project [2018].

	E_γ [keV]	I_γ [%]
^{241}Am	59.5	35.92
^{241}Am	103.0	0.0195
^{241}Am	125.3	0.0041
^{241}Am	208.0	0.000786
^{233}Pa	300.1	6.6
^{233}Pa	311.9	38.3
^{241}Am	322.6	0.000151
^{233}Pa	340.5	4.47
^{241}Am	376.7	0.000137
^{241}Am	383.8	0.0000281
^{233}Pa	398.5	1.408
^{241}Am	619.0	0.000060
^{241}Am	662.4	0.000367
^{241}Am	722.0	0.000196
^{241}Am	801.9	0.0000012

4.4 LANTHANIDE PATTERN MEASUREMENTS

Two reference materials were used for the study, REE-2 and CUP-2 (both CanmetMINING, Ottawa, Canada). REE-2 is certified for most lanthanides and has provisional values for the lanthanides that are not certified (includes gadolinium, ytterbium and lutetium). CUP-2 is a UOC and is not certified for lanthanides but is often used as a working reference material for lanthanide pattern measurements. The materials were dissolved by microwave digestion and lithium borate fusion, respectively. The samples were measured directly, after an appropriate dilution, using both a standard sample introduction system and a desolvating sample introduction system to study the difference in oxide formation and impact on polyatomic interferences on the elements in the lanthanide series. The samples were also measured after chemical separation where the samples were separated into three different fractions as a measure to avoid interferences.

4.4.1 Oxide formation measurements

To study the lanthanide oxide formation rate, single element standard solutions of each element in the lanthanide series, were diluted to 1 ng g^{-1}, 10 ng $g^{-1}$and 100 ng g^{-1}. Each solution was measured with respect to all masses between 137 and 192 using an ElementXR (Thermo Fischer Scientific, Bremen, Germany) in triple detection mode (counting mode, analog mode and Faraday cup). The sample introduction consisted of a Twinnabar spray chamber and a Micromist nebulizer (both from GlassExpansion, Port Melbourne, Australia). The measurement data was corrected for dead time and blank subtracted. The ratios for each oxide, hydride and hydroxide was calculated.

4.4.2 Sample dissolution

CUP-2 was dissolved by microwave digestion (Mars5, CEM Corporation, Matthews, U.S). 0.2 g of the material was mixed with 9 mL concentrated HNO3 + 0.09 M HF and 1 mL of ultra-pure water (Milli-Q, Merck KGaA, Darmstadt, Germany) in a Teflon tube. The temperature was ramped to 180°C during 20 minutes and that temperature was held for 15 minutes. The samples were thereafter diluted to a concentration of approximately 10 mg U g^{-1}.

The reason for using lithium borate fusion for the REE-2 material was due to incomplete digestion when using the microwave oven. 1 g of the material was placed in a graphite crucible together with 3 g of $LiBO_2$ (Ultrapure, Claisse, Quebec, Canada). The sample was pre-oxidized for 2 h in 650°C. Thereafter, the temperature was increased to 1050°C and the sample was fused for 15 minutes. After cooling, the resulting glass bead was dissolved in 100 mL 1.4 M HNO_3 while heating and stirring. After dissolution, 0.4 g of polyethylene glycol (PEG-2000, Alfa Aesar, Karlsruhe, Germany) was added to flocculate silica. The solution was evaporated to approximately 50 mL and left overnight to let the slow flocculation proceed. The solution was filtered through a OOM filter paper (Munktell, Alstrom Munksjö, Helsinki, Finland) and diluted in 1 M HNO_3. Blanks were prepared in the same manner as the samples for each of the methods above.

4.4.3 Chemical separations

An aliquot was taken from the dissolved reference materials and either diluted to 0.05 M HNO_3 or evaporated to almost dryness and dissolved in 2 mL 0.05 M HNO_3. For the yield determination, two samples were prepared for each replicate whereof one was spiked with a known amount of lanthanide standard solution. Due to the low amount of uranium in the REE-2 reference material, 1 mg of uranium was added to these samples to mimic a high uranium content. The in-house prepared 2 mL Ln resin columns (resin and columns both from Triskem International, Bruz, France) were conditioned with 1 mL 0.05 M HNO_3. Thereafter, the samples were added to the column. The samples tubes were rinsed with 2x1 ml 0.05 M HNO_3 and the rinse solutions were also added to the columns. Next, La-Nd was eluted into 25 mL Teflon beakers using 6 mL 0.4 M HCl. The beakers were changed and Sm-Gd was eluted with 10 mL 0.75 mL HCl. The change of beakers was repeated and Tb-Lu was eluted using 20 ml 10 M HNO_3. All solutions were evaporated to near dryness and dissolved in 2% nitric acid.

4.4.4 Measurements

The unseparated samples as well as the separated samples were diluted to a concentration between 6 pg g^{-1} and 2 ng g^{-1} using 2% HNO_3. Indium, rhodium and rhenium was added as internal standard to a concentration of 1 ng g^{-1}. The choice of internal standard element depended on lanthanide.

The measurements were performed on an Element2 (Thermo Fischer Scientific, Bremen, Germany). The standard sample introduction consisted of a cyclonic Twister spray chamber and a 1 mL min^{-1} concentric Conikal nebulizer (both from GlassExpansion, Port Melbourne, Australia). The desolvating sample introduction system consisted of a Cetac Aridus II and a 100 µL min^{-1} C-flow nebulizer (both from Teledyne Cetac Technologies, Omaha, Nebraska, US). The instrumental settings and measurement parameters can be found in Table 3. The instrument was tuned with a 1 ng g^{-1} cerium standard solution to minimize the cerium oxide formation rate and maximizing the sensitivity.

Table 3 Instrumental settings for the two sample introduction systems measurement parameters.

	Standard sample introduction	**Desolvating sample introduction**
	Twister spray chamber	**Aridus II**
Nebulizer	Conikal	C-flow PFA
Forward power [W]	1250	1200
Cool gas flow [L min^{-1}]	16	16
Auxiliary gas flow [L min^{-1}]	0.7	0.7
Nebulizer gas flow [L min^{-1}]	1.1	0.9
Ar Sweep gas [L min^{-1}]	N/A	3.2
Nitrogen [mL min^{-1}]	N/A	10
Resolution	300	
Mass window	5%	
Samples per peak	100	
Runs and passes	100 x 1	
Scan type	E-scan	
Measured analyte isotopes	^{137}Ba, ^{139}La, ^{140}Ce, ^{141}Pr, ^{146}Nd, ^{147}Sm, ^{153}Eu, ^{157}Gd, ^{159}Tb, ^{163}Dy, ^{165}Ho, ^{167}Er, ^{169}Tm, ^{174}Yb, ^{175}Lu	
Measured internal standard isotopes	^{103}Rh, ^{115}In, ^{185}Re	

The quantification was performed with a calibration curve based on five points using standard solutions certified by mass. For the direct measurements, a multi-element solution containing all lanthanides (Sigma Aldrich, Buchs, Switzerland) was used. For the separated samples, three different certified standard solutions containing La-Nd, Sm-Gd and Tb-Lu, respectively (Spectrascan, Inorganic Ventures, Christiansburg, USA) were used. For quality assurance, a control sample consisting of a dilution of a certified standard solution of different origin than the calibration standard solution was used (CPAchem Ltd, Stara Zagora, Bulgaria). For the direct measurements, the control sample standard solution was purchased from Sigma Aldrich (Buchs, Switzerland) and for the separated samples, the standard solutions were purchased from CPAchem Ltd (Stara Zagora, Bulgaria).

The dead time was evaluated according to Appelblad and Baxter [2000] using a Lu standard solution. All data reduction and calculations were performed off-line. The external calibrations, using weighted linear regression with the standard uncertainty in *y* as weight, were carried out according to Sayago and Asuero [2004] and the calculations as well as the measurement uncertainties were evaluated using a Monte Carlo method in the same manner as Ramebäck and Lindgren [2018] using Microsoft Excel. The measurement results were normalized with respect to Chondrite values, see Figure 10-11 and 13-14 [Anders and Grevesse, 1989].

4.5 EXTERNAL CALIBRATION FOR TRACE ELEMENT ANALYSIS

4.5.1 Sample preparation

Three different certified reference materials (CRM) were chosen for the study: Periodic Table Mix 3 for ICP (Sigma Aldrich, Buchs, Switzerland), Spectrascan (Spectrascan, Inorganic Ventures, Christiansburg, USA) and CPAchem (CPAchem Ltd, Stara Zagora, Bulgaria). All reference materials were certified by mass and traceable to NIST. The certified uncertainty varied between 0.2% and 0.8% depending on analyte and supplier. One of the CRMs was used as a calibration standard and was diluted to 500 pg g^{-1}, 1000 pg g^{-1}, 1500 pg g^{-1}, 2000 pg g^{-1} and 2500 pg g^{-1}. The other two CRMs were used as quality control samples and diluted to 100 pg g^{-1} and 1000 pg g^{-1}. The dilutions were performed using in-house sub-boiled nitric acid and ultra-pure water. All measurement samples contained 2% HNO_3. 1 ng g^{-1} rhodium was added to each sample as internal standard. Blank samples were prepared together with the samples. The sample preparation was performed gravimetrically in order to reduce uncertainties compared to volumetric additions. However, uncertainty modelling was also done in order to compare volumetric and gravimetric additions from an uncertainty perspective. The analytical balance used in this work was a Mettler Toledo AX204 (Columbus, Ohio, US) with an uncertainty of 0.3 mg, *k*=2.

4.5.2 Measurements

The measurements were performed using an Element 2 (Thermo Scientific, Bremen, Germany) with a concentric nebulizer and a cyclonic spray chamber (both GlassExpansion, Melbourne, Australia). The conditions for the measurement setup can be found in Table 3. Also in this case, the instrument was tuned with a 1 ng g^{-1} cerium solution to maximize the signal of cerium while keeping the formation of CeO low. The magnitude of the CeO formation was 2.5% during all measurements.

4.5.3 Data evaluation

All measurement raw data from calibration and quality control samples were extracted from the instrument software and evaluated offline. For each sample, the mean intensity and standard deviation of the mean were calculated from the 500 data points resulting from samples per peak and 100 sweeps, for each isotope. The intensities were corrected for dead time and thereafter corrected for internal standard. The internal standard intensities were corrected for the added amount of internal standard according to Eq. 23 to improve the internal standard correction:

$$I_{corr,i,j} = \frac{I_{i,j}}{\frac{I_{IS,i}}{m_{IS,i}}} * \frac{I_{IS,blk}}{m_{IS,blk}} \quad (23)$$

where $I_{corr,i,j}$ is the intensity for isotope *j* in sample *i* corrected for internal standard, $I_{i,j}$ is the dead-time corrected intensity of isotope *j* in sample *i*, $I_{IS,i}$ and $I_{IS,blk}$ are the dead-time corrected intensities of the internal standard in sample *i* and the blank sample and $m_{IS,i}$ and $m_{IS,blk}$ are the mass of the added internal standard in sample *i* and the blank sample, respectively. Calibration functions were calculated using two methods, OLS and WLS with the standard uncertainty in *y* as weight, see Eqs. 18-19 and Eqs. 20-21, respectively. OLS was performed using the LINEST() function in Microsoft Excel 2016. In the OLS regression, additional regression statistics was retrieved and used as uncertainties. Using WLS, two different regressions were calculated using uncertainties from sample preparations performed gravimetrically as well as volumetrically to compare the differences in the results depending on choice of sample preparation. For each type of linear regression, the slope and intercept together with uncertainties of respective parameter were estimated.

The calibration functions were used to calculate the detection limits according to Eq. 22 and to evaluate the concentrations of the quality control samples of the two CRMs here named Standard solution 1 and 2. The calculated concentrations were compared to the certified value using the zeta score (ζ) [ISO 13528:2015]:

$$\zeta = \frac{c_{measured} - c_{reference}}{\sqrt{u^2(c_{measured}) - u^2(c_{reference})}} \quad (24)$$

where $c_{measured}$ is the measured and calculated concentration and $c_{reference}$ is the certified concentration and $u(c_{measured})$ and $u(c_{reference})$ are their respective uncertainties. If $|\zeta| \leq 2$ the measured value is consistent with the certified value within their respective uncertainties at a 95% confidence level.

5 RESULTS AND DISCUSSION

5.1 LOW-RESOLUTION GAMMA SPECTROMETRY FOR URANIUM CATEGORIZATION

The fitted simulated response functions can be seen in Figure 4. It is obvious that the response of a very dense material such as uranium metal is very different from the response of a matrix containing water. This effect is seen in both the low as well as the high-energy region but is more prominent in the low energy region. The efficiency at 185.7 keV is approximately 40 times higher in the water matrix than in the uranium metal matrix. At 1001 keV, the difference is a factor 2.9. It is evident that the enrichment calculation of a water sample using a response function for a uranium metal matrix will overestimate the enrichment.

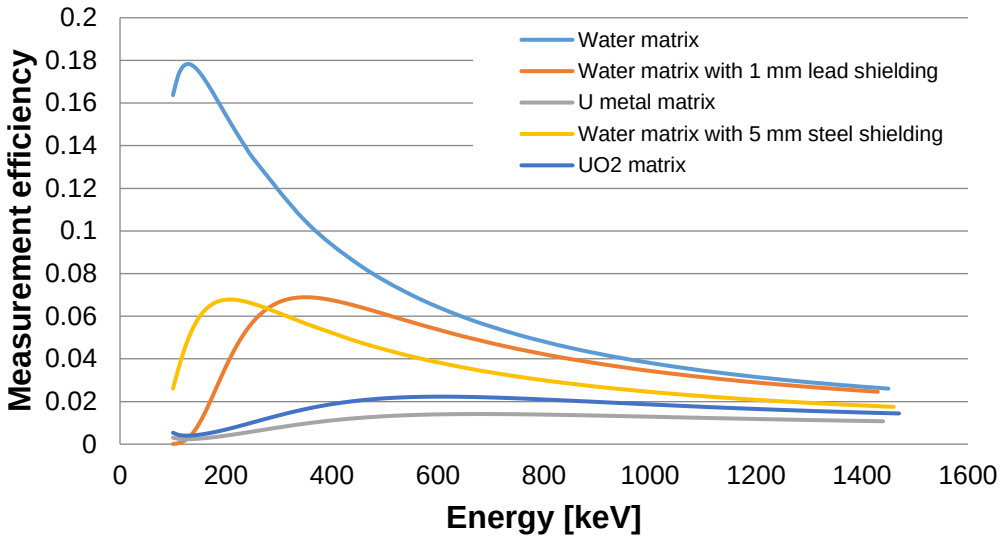

Figure 4 Simulated response functions for the investigated matrices and shielding.

The results of the categorizations done by the Identifinder can be found in Table 4. The table shows that UO_2 is categorized as depleted uranium (DU) independent of the enrichment for the measured materials. On the other hand, the natural uranium (NU) water sample is categorized as low-enriched uranium (LEU). This implies that the response function used in the instrument is based on neither UO2 nor a water matrix.

Table 4 Results of the automatic instrument categorization.

Uranium type	Sample matrix	Instrument categorization
NU	UO_2	DU
LEU	UO_2	DU
DU	UO_2	DU
NU	Aqueous	LEU

The American National Standard Performance Criteria for Hand-Held Instruments for the Detection and Identification of Radionuclides states that an instrument should be able to identify radionuclides shielded by 5 mm of steel [ANSI N42.34-2006]. The results of the evaluated enrichment of all collected spectra using all response functions can be seen in Table 5. The results show that when the correct

response functions are used, i.e. the UO_2 matrix response function for the UO_2 samples and the water matrix response function for the aqueous sample, the enrichments agree with the materials.

Table 5 Results from enrichment calculations using all simulated response functions, respectively.

Sample		**Evaluated abundance of ^{235}U, f_{235}, with respective response function**				
Uranium type	**Real matrix**	**Water matrix**	**Water matrix + 5 mm steel shielding**	**Water matrix + 1 mm lead shielding**	**UO2 matrix**	**U metal matrix**
NU	UO_2	0.000681(51)	0.001052(79)	0.00348(26)	0.00882(66)	0.01041(78)
LEU	UO_2	0.00166(20)	0.00257(30)	0.0085(10)	0.0213(25)	0.0251(30)
DU	UO_2	0.0000449(63)	0.000069(10)	0.000230(32)	0.000587(82)	0.00069(10)
NU	Aqueous	0.0106(16)	0.0163(24)	0.0520(77)	0.123(18)	0.142(21)

On the other hand, the instrument categorization results agree well with the results obtained using the water matrix + 5 mm steel shielding response function. This implies that the inherent response function of the instrument could be based on a water matrix with a 5 mm steel shielding, or something similar.

The results show that it is evident that a correct categorization requires knowledge of the investigated material. If the categorization algorithm is dependent of the nature of the uranium material, which seems to be the case with this instrument, the outcome of the instrument is unreliable. It is therefore necessary for the user to take the acquired spectrum off-line and perform enrichment calculations using response functions based on the knowledge of the material to make sure that the categorization is accurate.

To solve the problem with misclassifications, one option could be to provide the instrument with a range of response functions covering a variety of matrices. The user could then select the appropriate response function depending on the nature of the investigated material, when this is known. If the composition of the material is unknown, the evaluation could be performed with a number of response functions to provide a range of categories for initial decision-making.

5.2 SIGNATURES IN ^{241}AM SOURCES

The fitted response function using the ^{241}Am peaks for Source 1 can be seen in Figure 5.

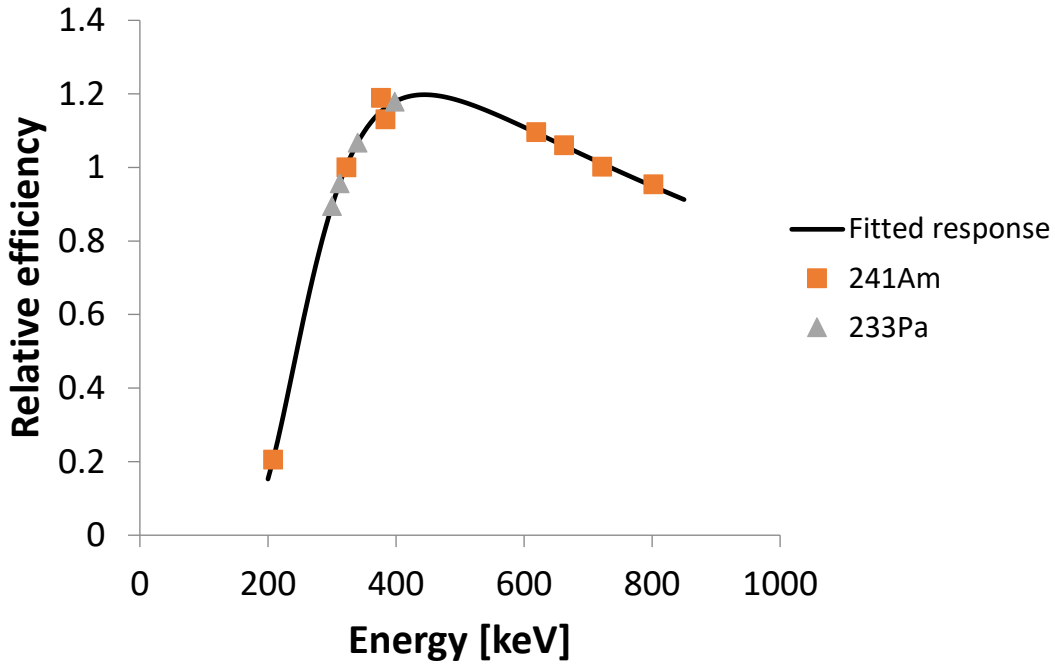

Figure 5 Efficiency response function of Source 1. The squares are the ^{241}Am gamma lines used for the response function construction and the triangles are calculated responses for ^{233}Pa peaks.

5.2.1 Age

The calculated ages at the time of measurement as well as the corresponding separation dates of all sources can be found in Table 6. The results show that Source 1 and Source 2, which are visually similar, have significantly different ages. The age of Source 4 was known, since the chemical separation and the electroplating was performed in 2001, which is in very good agreement with the calculated age.

Table 6 Results for the age determination of the different sources. The presented ages are the ages at the time of measurement. The separation dates are derived from the calculated ages at the time of measurement.

	Age [y]	U [y] *k*=2	Separation date
Source 1	31.4	2.0	1982-01-06
Source 2	40.8	2.6	1972-07-18
Source 3	43.9	3.6	1969-07-06
Source 4	12.2	2.3	2001-06-25
Source 5	21.5	6.9	1985-07-09

5.2.2 Impurities

Spectra from Source 1-3 show peaks at gamma lines that do not originate from ^{241}Am. Many of these peaks do not have a Gaussian shape. Instead, they seem to have two components, a narrow top and a broad base. The broad base is explained by Doppler broadening which occurs when an atom captures a particle and the formed nucleus de-excites while still in motion [Gilmore, 2008]. A comparison between a normal-shaped, Gaussian peak and a Doppler broadened peak can be seen in Figure 6.

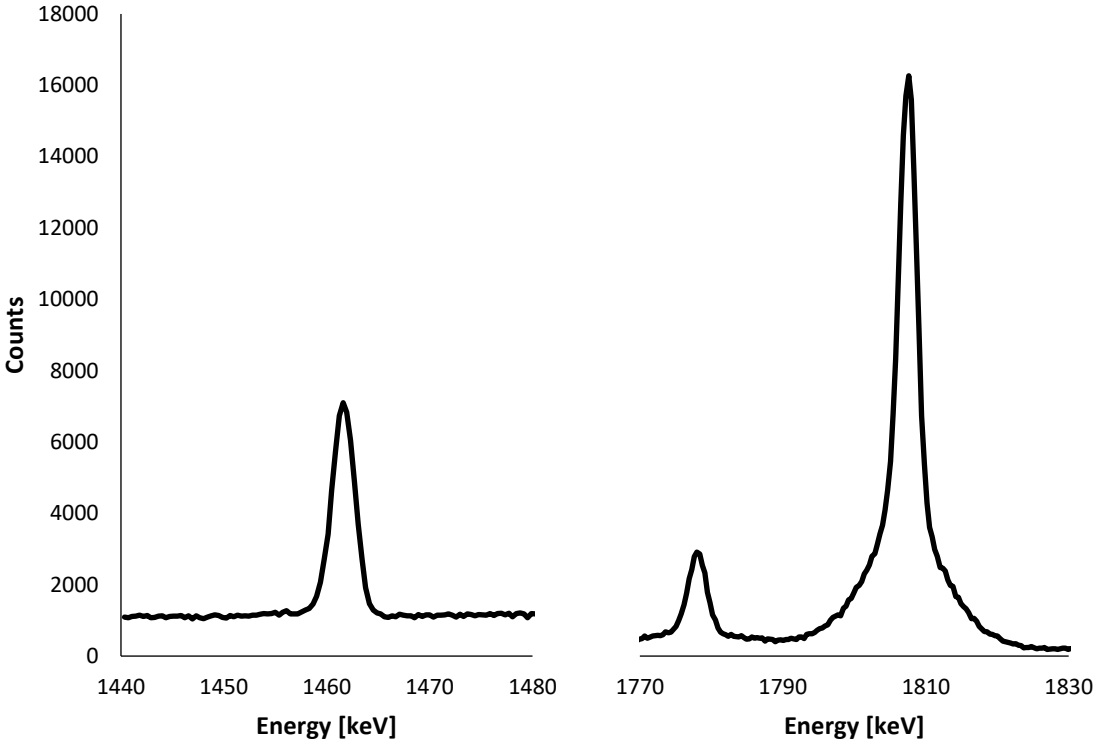

Figure 6 Left: Gaussian 1460 keV peak of ^{40}K, right: a peak, which is Doppler, broadened at the base.

This type of reactions (capture of alpha particles, neutrons or protons) requires that low-Z elements are present in the source to be more probable. Therefore, these peaks indicate that there are low-Z elements present in the sources and that nuclear reactions are taking place within the sources [Gehrke et al., 2003; Catz and Amiel, 1967]. Proposed reactions and their corresponding gamma peaks found in spectra from Source 1-3 can be seen in Figure 7. Source 4 and 5 are ^{241}Am electroplated on stainless steel. Therefore, there are no signs of low-Z elements in these spectra.

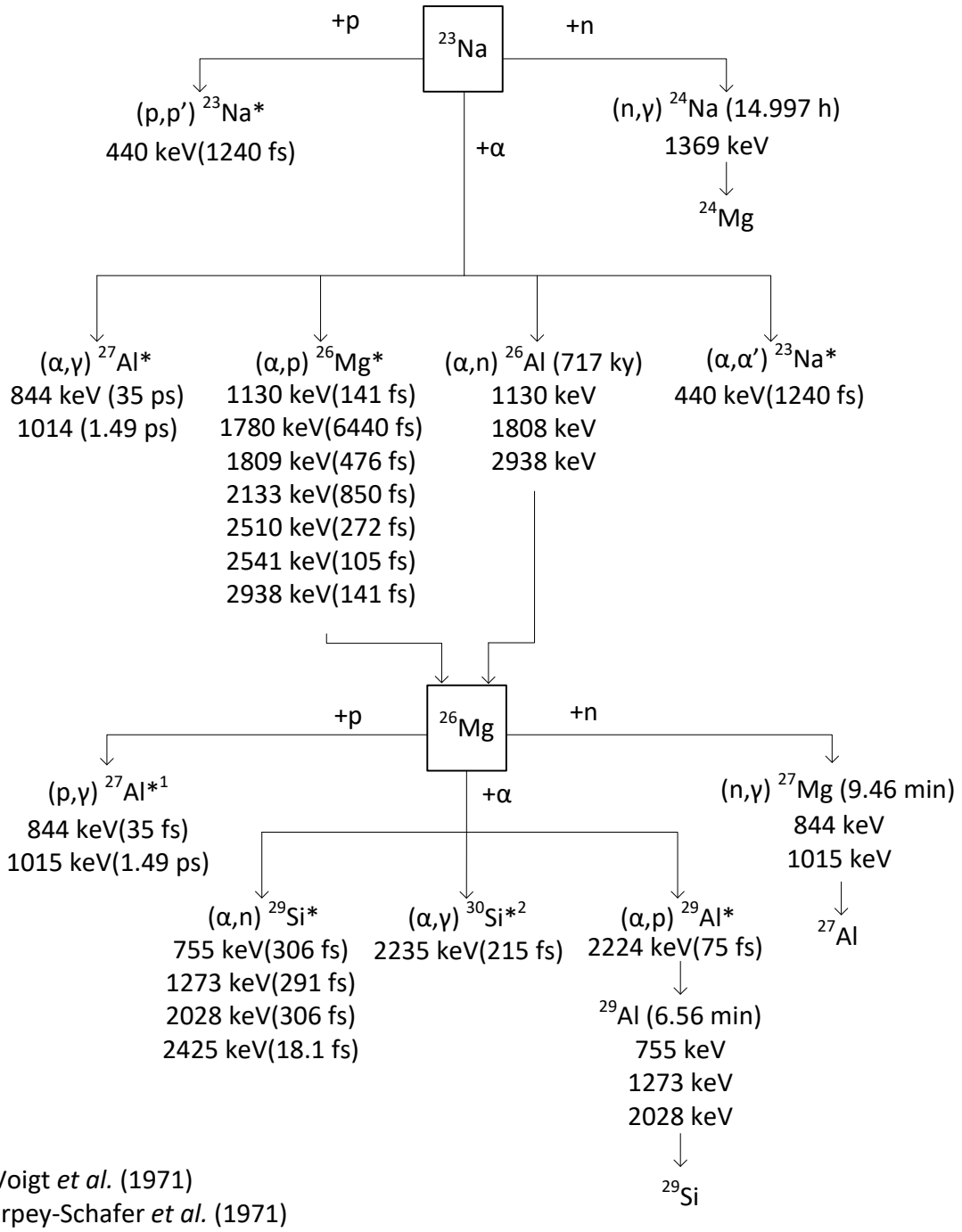

[1] DeVoigt *et al.* (1971)
[2] Sharpey-Schafer *et al.* (1971)

Figure 7 Identified gamma lines from nuclides other than ^{241}Am and its progeny, and suggested reactions based on impurities. The nuclides with an asterisk are emitting gamma rays due to de-excitation. The reference to the gamma lines and corresponding half-lives are taken from the Nudat 2.6 database (2014) unless otherwise stated.

Another kind of impurities are radioactive elements. The spectra of Source 1 and 2 are compared in Figure 8. The figure shows that Source 1 have peaks of ^{239}Np, while these are absent in Source 2. Since the half-life of ^{239}Np is 2.356 days [DDEP, 2018], it is clear that ^{243}Am is present in the source and that the daughter ^{239}Np is in secular equilibrium with ^{243}Am. Therefore, it is possible to calculate an ^{243}Am/^{241}Am-activity ratio. For source 1 and 3 the ratio was $1.444(48)\cdot10^{-6}$ and $2.09(11)\cdot10^{-7}$, respectively.

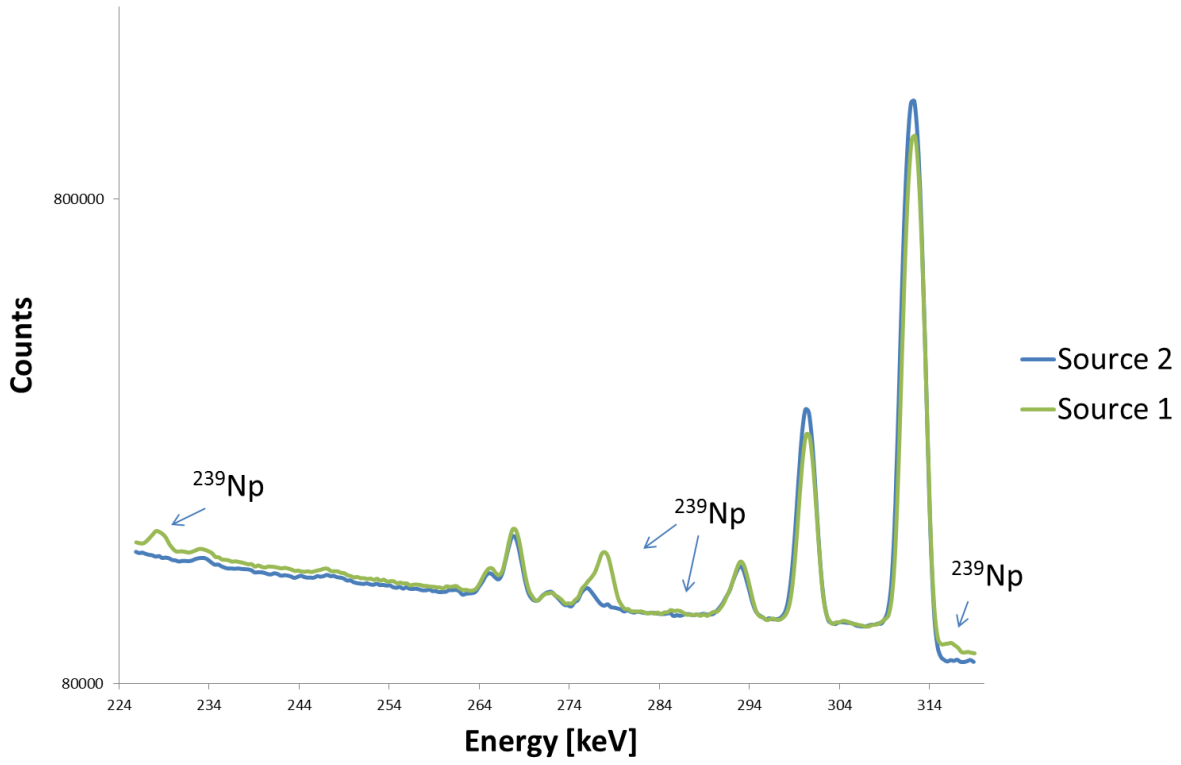

Figure 8 Excerpt of spectra of source 1 and 2.

This study shows that there are a number of potential signatures that can be used to distinguish different ^{241}Am sources. The ^{239}Np content alone was, in this case, enough to distinguish three different sources. Another potentially distinctive signature was the age. The ages of Source 1 and 2 were significantly different. This means that even though these two sources are visually very similar, they can be distinguished with one or two signatures obtained by gamma spectrometric measurements. It may therefore be possible to distinguish sources even though serial numbers are missing. This information could be added in an NNFL containing all indigenous ^{241}Am-sources to be able to investigate found orphan sources in an efficient manner.

5.3 LANTHANIDE PATTERN MEASUREMENTS

5.3.1 Oxide formation measurements

The oxide formation fraction of each of the lanthanides can be seen in Figure 9. The results show that the highest amount of oxides can be found for the lightest of the lanthanides with a decreasing pattern. The lowest oxides are formed for europium and ytterbium. The level of the oxide formation vs element in Figure 9 agrees well with results published by Dulski [1994]. Since the oxide formation is highly dependent on instrumental conditions [Vaughan and Horlick, 1986; Longerich et al, 1987], the variation of the oxide formation may change on a daily basis. However, the relation between oxides remain the same. The fraction of formed hydroxides and hydrides were, if detectable, in the low ppm range. Therefore, the interferences coming from hydroxides and hydrides are considered negligible.

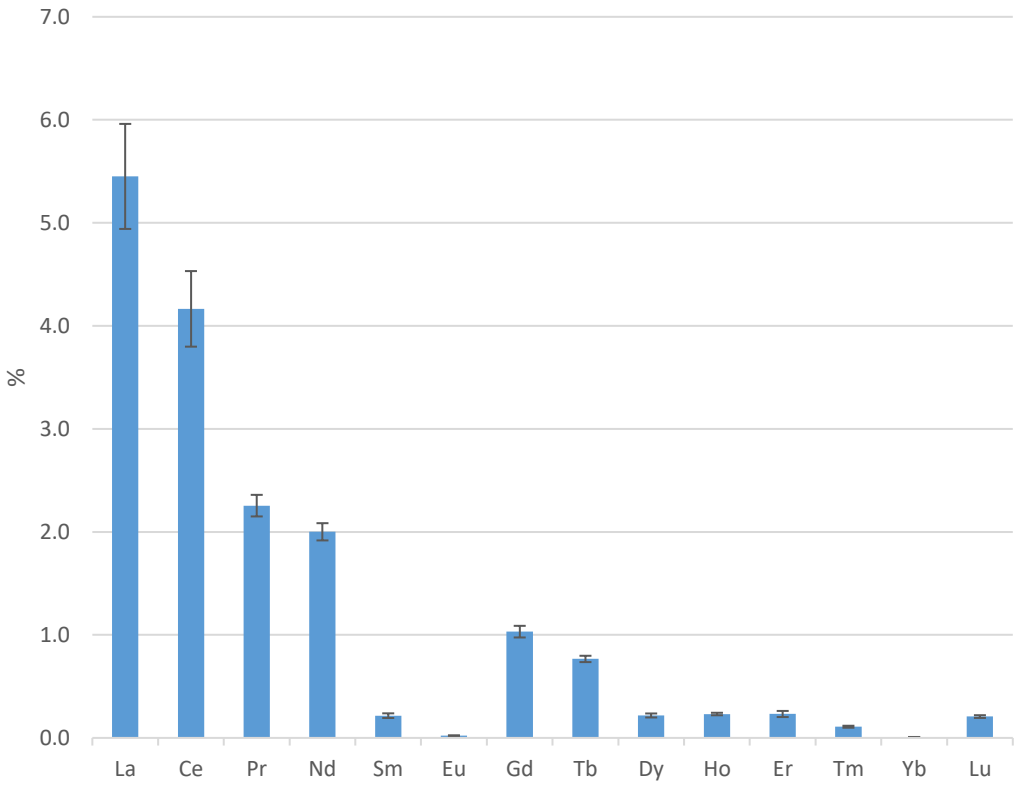

Figure 9 Fraction of oxide formation of the elements in the lanthanide series.

5.3.2 Interfered measurements

The results of the measurements of unseparated samples of REE-2 using the standard sample introduction system can be found in Figure 10. For most elements in the lanthanide series, the results correspond well with the certified values, but for gadolinium and terbium, the measurement results are overestimated. This is due to polyatomic interferences from the light lanthanides, where the oxides of praseodymium and neodymium, $^{141}Pr^{16}O^{+}$ and $^{143}Nd^{16}O^{+}$, end up in the same peak as ^{157}Gd and ^{159}Tb, respectively. The overestimation of these elements were in this case approximately 60% and 40%, respectively.

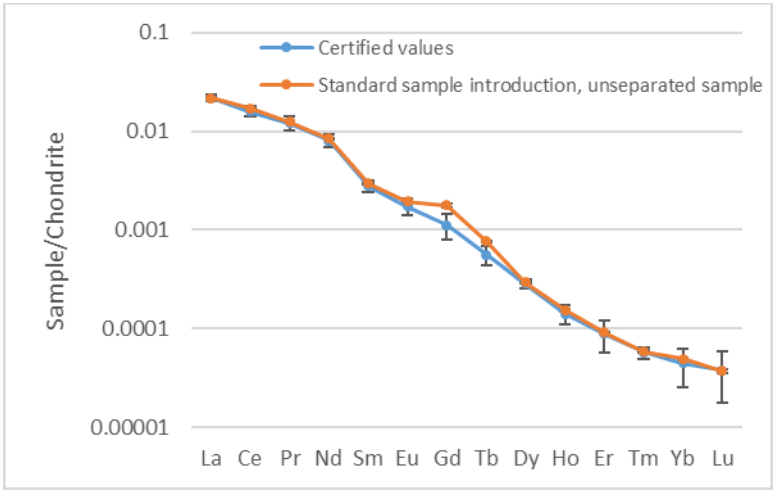

Figure 10 Comparison of the lanthanide pattern for REE-2 between certified values and results from direct measurement using a standard sample introduction system. The uncertainty bars are, in some cases, smaller than the bullets.

5.3.3 Interference-reduced measurements

The resulting lanthanide pattern of REE-2 of the measurements performed with a desolvating sample introduction system and on separated samples, using a standard sample introduction system can be found in Figure 11 and 13, respectively. The results correspond very well with the certified values, i.e. no significant deviations were observed.

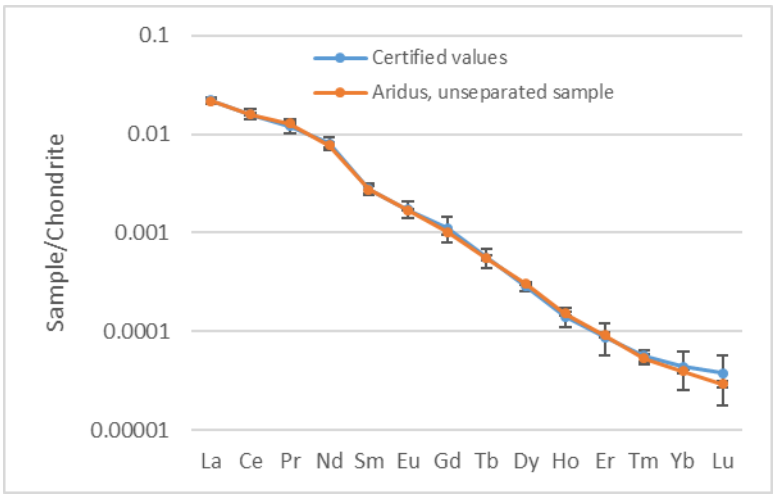

Figure 11 Comparison of the lanthanide pattern for REE-2 between certified values and measured results using a desolvating sample introduction system. The uncertainty bars are, in some cases, smaller than the bullets.

The chemical separation method divides the lanthanides into three fractions. By examining Figure 2, the most effective separation method to remove the most prominent polyatomic interferences would be to separate the lanthanide series into two fractions: La-Eu and Gd-Lu. However, to separate gadolinium from europium in a single separation step using HDEHP has been proven difficult to accomplish [Nash and Jensen, 2000; Morais and Ciminelli, 1998; Morais and Ciminelli, 2007].

A more easily achievable separation method that still solves the issue with interferences from light lanthanides from the heavy ones is to separate the series into three fractions rather than two: La-Nd, Sm-Gd and Tb-Lu. The method development was based on methods previously proposed by Pin and Zalduegui [1997] and Yang et al. [2010]. By increasing the acid concentration, the lanthanides will elute in groups. For the last elution, the acid was changed to nitric acid to avoid the elution of uranium, which will co-elute with the heavy lanthanides when high concentrations of hydrochloric acid is used [Shabana and Ruf, 1977; Kaminski and Nuñez, 2000].

The impact of interferences onto the elements in the lanthanide series after the samples have been separated into three fractions can be seen in Figure 12. The figure shows that, compared to Figure 2 most interferences are removed by the separation. It should be noted that the only element that still does not have any isotope that is free from oxide interferences is lutetium, where ^{175}Lu is interfered by $^{159}Tb^{16}O$. However, this should only be a problem if the amount of terbium is many orders higher than that of lutetium.

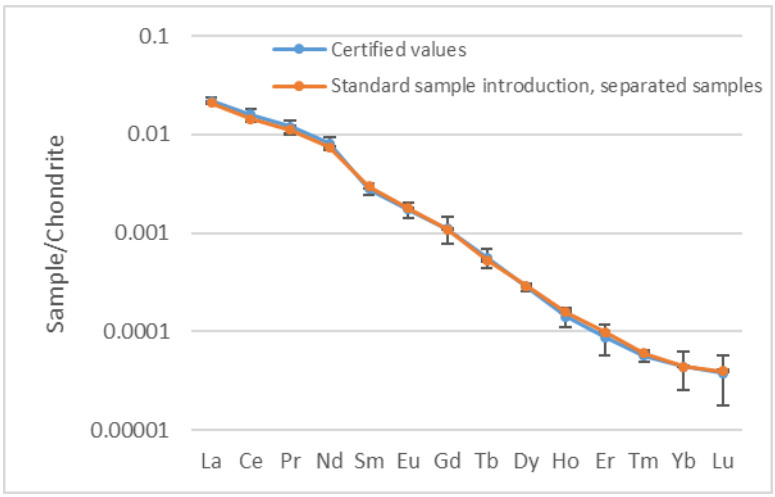

Figure 12 Comparison of the lanthanide pattern for REE-2 between certified values and measured values using a standard sample introduction system after a chemical separation. The uncertainty bars are smaller than the bullets in some cases.

m/z	Ba	La	Ce	Pr	Nd	Sm	Eu	Gd	Tb	Dy	Ho	Er	Tm	Yb	Lu
130	0.11														
131															
132	0.1														
133															
134	2.42														
135	6.59														
136	7.85		0.19												
137	11.23														
138	71.7	0.089	0.25												
139	^{138}BaH	99.911													
140		^{139}LaH	88.45												
141			^{140}CeH	100											
142			11.11	^{141}PrH	27.2										
143			^{142}CeH		12.2										
144					23.8	3.1									
145					8.3										
146	^{130}BaO				17.2										
147	^{130}BaOH				^{146}NdH	15									
148	^{132}BaO				5.8	11.3									
149	^{132}BaOH				^{148}NdH	13.8									
150	^{134}BaO				5.6	7.4									
151	^{135}BaO				^{150}NdH	^{150}SmH	48								
152	^{136}BaO		^{136}CeO			26.7	^{151}EuH	0.2							
153	^{137}BaO					^{152}SmH	52								
154	^{138}BaO		^{138}CeO			22.7	^{153}EuH	2.18							
155	^{138}BaOH	^{139}LaO				^{154}SmH		14.8							
156		^{139}LaOH	^{140}CeO					20.47		0.056					
157			^{140}CeOH	^{141}PrO				15.65							
158			^{142}CeO	^{141}PrOH	^{142}NdO			24.84		0.095					
159			^{142}CeOH		^{143}NdO			^{158}GdH	100						
160					^{144}NdO	^{144}SmO		21.86	^{159}TbH	2.329					
161					^{145}NdO	^{144}SmOH		^{160}GdH		18.889					
162					^{146}NdO					25.475		0.14			
163					^{146}NdOH	^{147}SmO				24.896					
164					^{148}NdO	^{148}SmO				28.26		1.6			
165					^{148}NdOH	^{149}SmO				^{164}DyH	100				
166					^{150}NdO	^{150}SmO					^{165}HoH	33.5			
167					^{150}NdOH	^{150}SmOH	^{151}EuO					22.87			
168						^{152}SmO	^{151}EuOH	^{152}GdO				26.98		0.12	
169						^{152}SmOH	^{153}EuO					^{168}ErH	100		
170						^{154}SmO	^{153}EuOH	^{154}GdO				14.91	^{169}TmH	2.98	
171						^{154}SmOH		^{155}GdO				^{170}ErH		14.09	
172								^{156}GdO		^{156}DyO				21.69	
173								^{157}GdO		^{164}DyOH				16.1	
174								^{158}GdO		^{158}DyO				32.03	
175								^{158}GdOH	^{159}TbO	^{164}DyOH				^{174}YbH	97.4
176								^{160}GdO	^{159}TbOH	^{160}DyO				13	2.6

Figure 13 Isotopes of the lanthanides with abundances [Meija et al, 2016] and their most prominent hydride, oxide and hydroxide interferences in ICP-MS, based on water and nitric acid chemistry. The colour scheme corresponds to separating the lanthanides into three fractions: La-Nd, Sm-Gd and Tb-Lu. The green marked isotopes are not interfered or only slightly interfered and can be used for quantitative determination. The red marked isotopes should be avoided for quantitative measurements. The yellow marked isotopes may be used for determination but are not completely free from interferences. All oxides in the chart refer to ^{16}O.

In the direct measurements, the uranium concentration was approximately 10 µg g^{-1}. This level of heavy matrix did not affect the measurements using the standard sample introduction to any extent. However, the measurements using the desolvating sample introduction suffered from an almost 50% signal suppression due to the high concentration of uranium in the samples. This could however, to some extent, be compensated by the higher sensitivity that can be achieved by the desolvating sample introduction system.

5.3.4 CUP-2

The lanthanide patterns for all three types of measurements, based on the CUP-2 reference material can be seen in Figure 14. The pattern is similar to previously published results [Balboni et al, 2017]. In this case, all three methods provide similar results. This means that for this kind of material, it is possible to use a standard sample introduction system with unseparated samples and still obtain an unaltered lanthanide pattern. However, the amounts of lanthanides in the CUP-2 material are rather low which means that higher concentrations of uranium has to be used in order to have measurable amounts of lanthanides. Since too high concentrations of a heavy matrix such as a uranium matrix causes both signal instability and memory effects, a separation to remove the uranium may be necessary even though the polyatomic interferences are negligible.

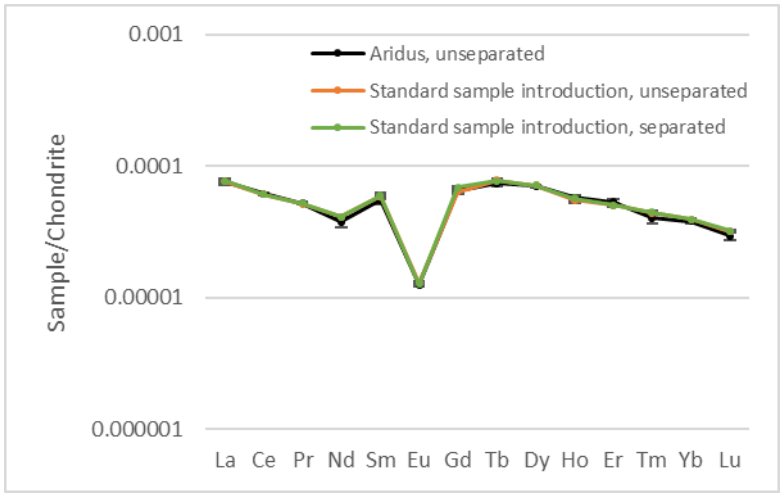

Figure 14 Comparison of the lanthanide pattern for CUP-2 between measurements using all three methods. The uncertainty bars are smaller than the bullets in some cases.

5.3.5 Measurement uncertainties

The lowest measurement uncertainties can be achieved with direct measurement using a standard sample introduction system. Using a desolvating sample introduction system would, in theory, result in just as low uncertainties, but the signal stability is, in general, lower for this kind of sample introduction, which increases the measurement uncertainty slightly. The highest uncertainty was found for the separated samples. This is due to the uncertainties in the yield determination. Even though a standard sample introduction system is used, the combined uncertainty is significantly higher. The measurement uncertainties for the separated samples were on average around 3% with a few exceptions where the combined uncertainty was higher.

5.4 EXTERNAL CALIBRATION FOR TRACE ELEMENT ANALYSIS

5.4.1 OLS vs WLS

The effect of an OLS compared to a WLS regression can be seen in Figure 15. On closer inspection, the calibration function based on OLS regression is strongly overestimating the intercept of the line. This, together with high uncertainty of the intercept, will cause the detection limit to be very high in the case of OLS. The WLS regression, on the other hand, provides a calibration function that corresponds well at concentrations close to zero. The OLS detection limit in the case of Figure 15 was 10 pg g^{-1} while the corresponding detection limit for WLS was 14 fg g^{-1}.

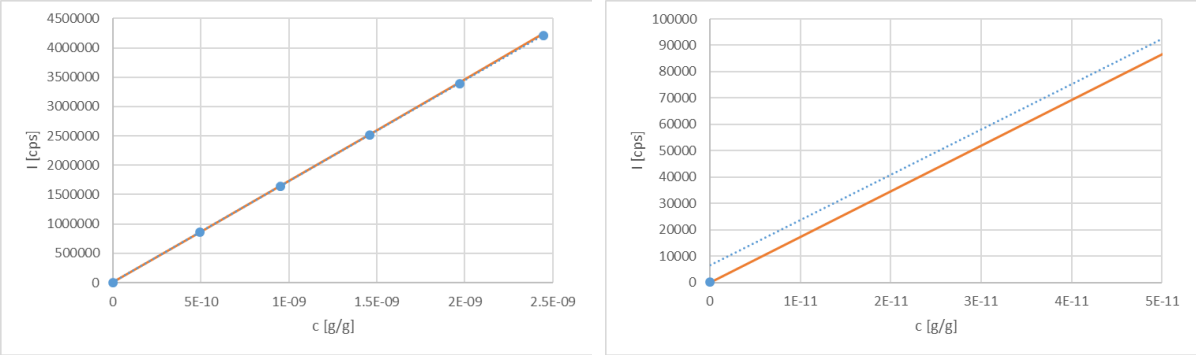

Figure 15 Left: Calibration lines based on calibration data on holmium. The blue dots are the data points used for the calibration, the dotted line is the OLS based on these data points. The orange line is the corresponding WLS regression. Right: The same calibration lines in the low concentration part of the calibration.

5.4.2 Quality control samples

The results of the measurement of the 1 ng g^{-1} QC samples and the comparison to the certified value using WLS regression can be seen in Figure 16. The figure shows that the concentration of some of the elements in Standard solution 1 deviates from the certified values. If the zeta score is larger than 2, the difference between measured and certified value is not covered by their uncertainties on an approximate 95% confidence level. The measurement results of Standard solution 2, on the other hand, agreed well with the certified values. One possibility is that the difference between the CRM is a result of differing isotopic compositions in the solutions. Therefore, all masses between 137 and 176 in one sample from each CRM was measured and compared. There were no significant differences in isotopic compositions between the materials. These results could imply that, for some elements, there is a difference in concentration between Standard solution 1 and the CRM used for calibration not covered by the uncertainty of the two solutions. Therefore, this discrepancy needs to be addressed.

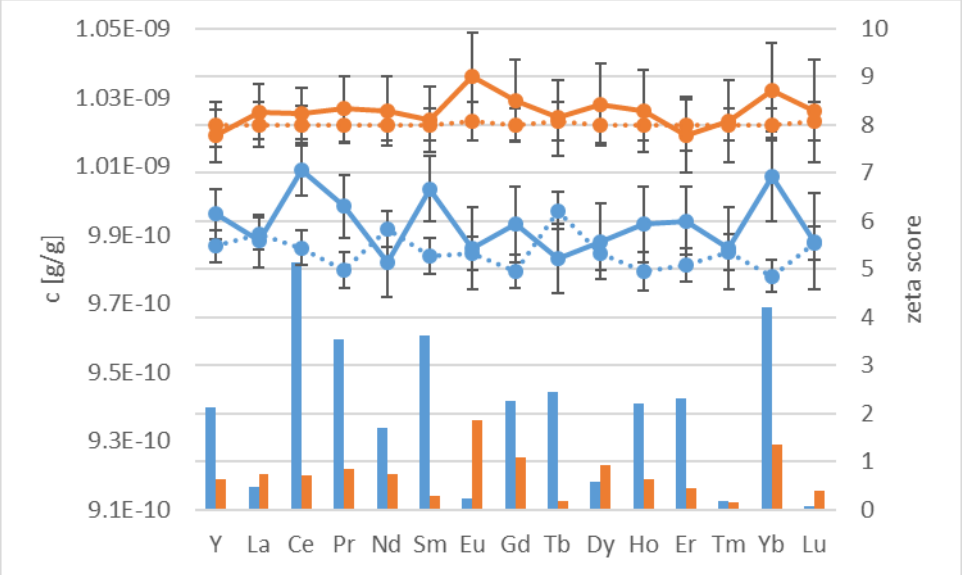

Figure 16 Measurement results and certified values of each element together with the calculated zeta score. The blue series correspond to Standard solution 1 and the orange series corresponds to Standard solution 2. The continuous lines are the measured values and the dashed lines are certified values. The bars corresponds to the calculated zeta scores.

According to ISO Guide 33:2015, any discovered bias should primarily be reduced or eliminated, secondly corrected for and the additional uncertainty added to the uncertainty budget and thirdly, if these approaches are regarded as impossible to carry through, the bias should be included in the uncertainty budget [ISO 33:2015]. Since it is difficult to determine which of the solutions that has the correct concentration, the third approach, to include the bias in the uncertainty budget was chosen. Therefore, an extra input quantity, δ, was added to the model equation for the calculation of the concentration of isotope *j* in sample *i*, $c_{i,j}$, of the measured sample where m_j is the intercept and k_j is the slope of the calibration function and $I_{corr,i,j}$ is the intensity of isotope *j* in the sample *i* corrected for dead-time and internal standard:

$$c_{i,j} = \frac{I_{corr,i,j} - m_j}{k_j} + \delta \tag{25}$$

δ has value 0 and the uncertainty of δ, $u(\delta)$, was increased until the zeta score was 2. This approach ensures that the result of the measurement of the QC sample corresponds to the certified value within uncertainties at the 95% confidence level and has previously been applied on replicate samples by Kessel et al. [2008] in a similar fashion. This δ and its uncertainty would, in other cases, be added to

samples that are measured in the same measurement sequence. It should be noted that if the choice was made to use the same CRM for the calibration as for the QC sample, this inconsistency would not have been detected and the risk of reporting analytical results containing bias or underestimated uncertainties would be considerable.

The initial uncertainties of the measurements varied between 0.7 and 1.5% depending on element. After some of the measurands had received an extra uncertainty the measurement uncertainty increased to about maximum 3%, see Figure 17. The, in most cases, low combined uncertainty is largely a result from performing the sample preparation gravimetrically. The results from volumetric sample preparation gives uncertainties around 3%. Most of the uncertainty in this case can be explained by the addition of internal standard and the uncertainty in the estimation of the slope. The uncertainty of the pipettes were evaluated according to ISO 8655-6 [2002]. For volumes less than 1 ml the combined uncertainty was evaluated to 0.8%, k=1 and 0.4% for volumes larger than 5 ml. Due to the relatively high measurement uncertainty, there was no need for the extra uncertainty, u(δ), for any element, at the 1 ng g^{-1} level for the volumetric samples.

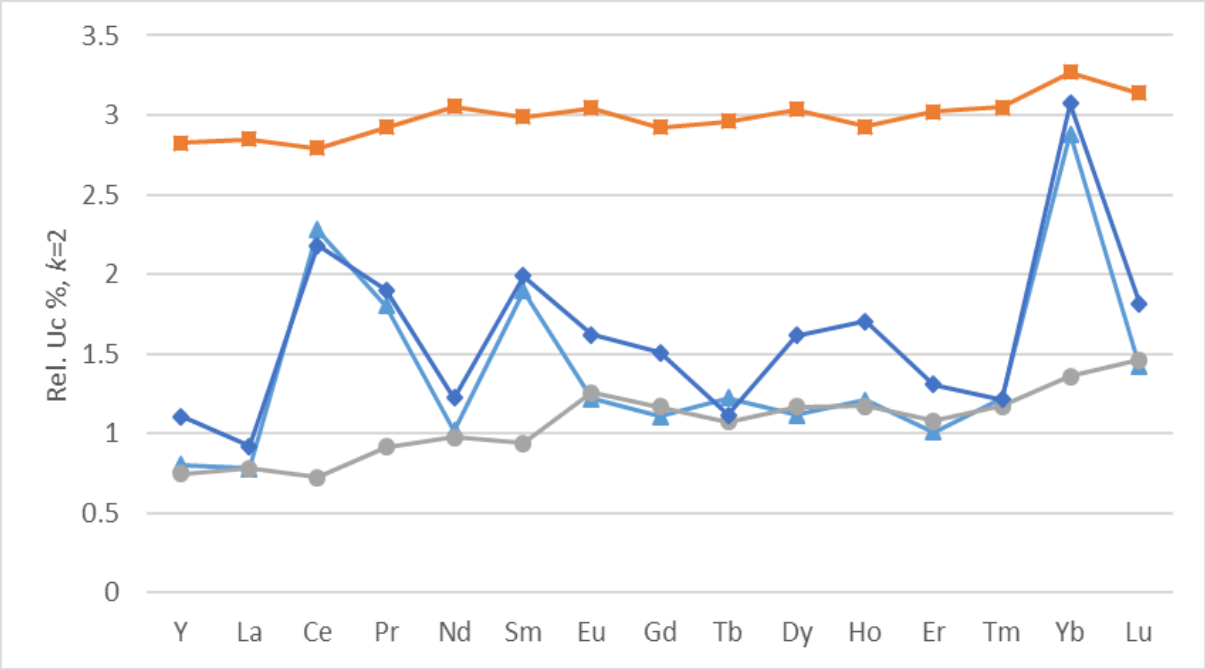

Figure 17 Relative uncertainties for the measured 1 ng g^{-1} control samples when an extra uncertainty has been added when necessary. The following data are evaluated using weighted linear regression: The triangles correspond to Standard solution 1, the circles to Standard solution 2 both with dilutions performed gravimetrically, the squares to Standard solution 1 in the case where dilutions were performed volumetrically. The diamonds correspond to the control sample from Standard solution 1 evaluated using OLS.

It can be noted that the measurement uncertainty of Standard solution 1 using either OLS or WLS results in practically the same uncertainties at the 1 ng g^{-1} level. This implicates that the OLS regression works rather well in this part of the calibration. At the 100 pg g^{-1} level, however, the measurement uncertainty is substantially higher for the results based on OLS, see Figure 18. This is mainly due to the large uncertainty in the intercept that follows from using OLS regression on heteroscedastic data [Ketkar and Bzik, 2000].

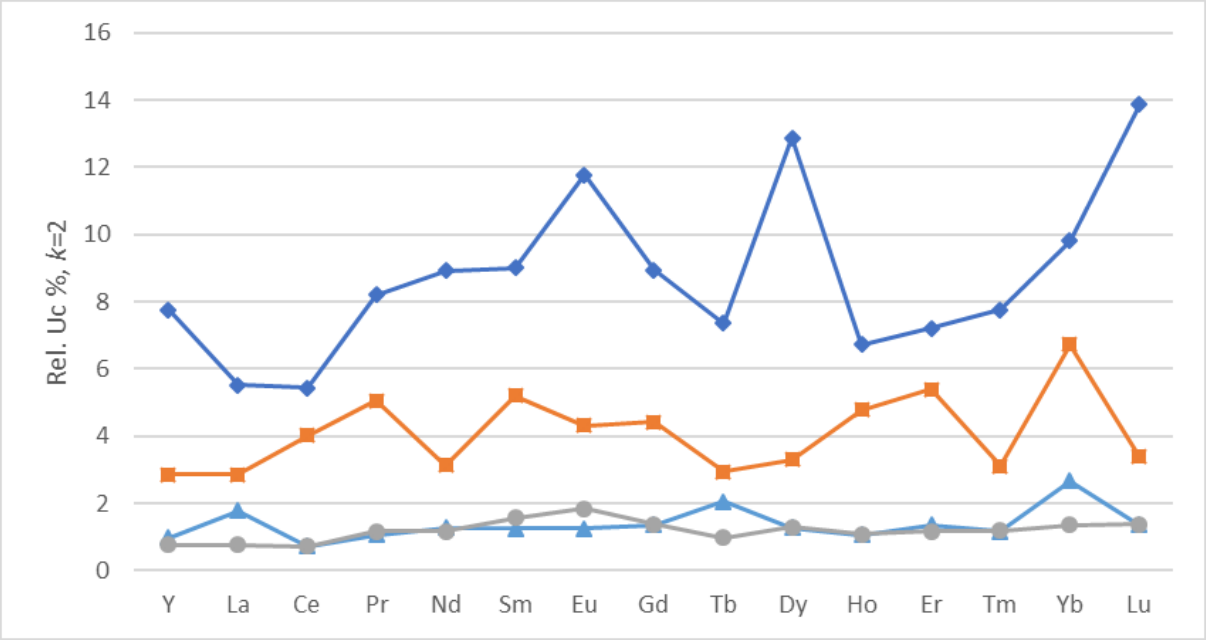

Figure 18 Relative uncertainties for the measured 100 pg g^{-1} control samples when an extra uncertainty has been added when necessary. The following data are evaluated using WLS: The triangles correspond to Standard solution 1, the circles to Standard solution 2 both with dilutions performed gravimetrically and the squares to Standard solution 1 in the case where dilutions were performed volumetrically. The diamonds correspond to the control sample from Standard solution 1 evaluated using OLS.

6 CONCLUSIONS

This work has shown the development of a series of signatures that are useful in the field of nuclear forensics. The work also highlights some problems that may be encountered in measurements of nuclear forensic signatures. One of the primary goals in nuclear forensics is to achieve accurate and precise measurements. There should be no ambiguity in the obtained analysis results. Therefore, the method development in nuclear forensics strive to reduce measurement uncertainty and to understand measurement processes to the extent that the measurement uncertainties are fully understood and accounted for.

Paper I highlights the difficulty of categorizing uranium automatically using low-resolution instruments. Even though a categorization carried out with such an instrument hardly would be the only measurement performed in a nuclear forensic investigation, the direction of the initial investigation may rely upon that measurement. The progress of the investigation could be impeded if the categorization would be incorrect. Therefore, it is important to be aware of the limitations of low-resolution measurements.

Paper II illustrates a number of possible signatures that can be used to identify ^{241}Am sources in cases where labels and serial numbers are destroyed or unreachable. Corresponding signatures should be possible to use in other types of sources with an alpha emitting nuclide. These signatures would be useful to populate an NNFL, since the combination of multiple signatures could single out or at least narrow down the identity of a source found out of regulatory control.

The work in **Paper III** investigated the prospect of maximizing accuracy and precision in measurements of lanthanides for geolocation of uranium using ICP-MS. Polyatomic interferences in measurements of the lanthanide series are well-known but have been neglected since the conclusion of geological origin is based on visual inspection of the chondrite normalized lanthanide pattern. If closer examinations need to be made, as often in the case of nuclear forensics, the interferences may start to affect conclusions drawn from the lanthanide measurement results. Since the oxide formation may vary on a daily basis, the impact of interfering species may also vary. This means that if two identical materials are measured on different occasions, the lanthanide measurements could indicate that the materials have different provenance. Therefore, by correcting for or avoiding the polyatomic interferences, the possibility to use the lanthanide series for comparison between materials in different parts of the nuclear fuel production, opens up.

Paper IV highlights the intricacy of measuring trace elements using external calibration and mass spectrometry. Since trace elements can be expected to be very low in concentration in uranium materials, the importance of providing an accurate calibration over the whole calibration range cannot be emphasized enough. The study shows that, in order to perform measurements with high confidence, a number of parameters need to be considered. The choices that are made considering type of regression and how the sample preparation has been performed, are crucial for the quality of the measurement results and at the end on the decision making process where the measurement result is an important part.

7 ACKNOWLEDGEMENTS

Along the way, I have had a lot of people to help me. Therefore, I would like to thank:

- My supervisor Henrik for the never-ending stream of ideas and passion for science. I am grateful for all the discussions we have had over the years.

- My supervisor Christian for providing feedback on my papers and guiding me through Chalmers' administration.

- Angelica and Stina, my partners in crime, my colleagues and good friends. I owe you a lot.

- My colleagues Annika, Sofia and Petra, you are all role models for female scientists. Thank you for your support.

- Micce for the help with the measurements of the ^{241}Am-sources and all the bad puns you deliver whether we like it or not.

- My remaining colleagues at the Department for Radioactive substances. Thank you for all the laughs around the coffee table, AW's and past and future hallway parties.

- Leif Persson for valuable discussions about what I thought was basic maths.

- The rest of my colleagues at FOI, CBRN Defence and Security. It is amazing how much expertise that can fit in a house in the middle of a forest.

- The Swedish Defence Research Agency for giving me the opportunity to complete my thesis.

- My fellow colleagues in the nuclear forensics community, participating in the ITWG meetings. Meeting you once in a while is a great inspiration.

- Einar for your contagious optimism and for proofreading the thesis with reluctant joy.

- My family for believing in me even though you might not always know what I work with.

- The Swedish Civil Contingencies Agency, the Swedish Radiation Safety Authority and the Ministry of Defence for funding my research.

8 ABBREVIATIONS

ANSI	American National Standards Institute
CRM	Certified Reference Material
DU	Depleted uranium
ESA	Electrostatic Analyzer
FTIR	Fourier Transform Infrared Spectrometry
GC-MS	Gas Chromatography Mass Spectrometry
GICNT	Global Initiative to Combat Nuclear Terrorism
HDEHP	Di-(2-ethylhexyl)-phosphoric acid
HEU	Highly enriched uranium
HPGe	High Purity Germanium detector
IAEA	International Atomic Energy Agency
ICP-MS	Inductively Coupled Plasma - Mass Spectrometry
ISO	International Organization for Standardization
ITDB	Incident and Trafficking Data Base
ITWG	Nuclear Forensics International Technical Working Group
LEU	Low enriched uranium
LREE	Light rare earth elements
MCNPX	Monte Carlo N-Particle eXtended
NAA	Neutron activation analysis
NNFL	National Nuclear Forensics Library
NPT	Treaty on the Non-proliferation of Nuclear Weapons
NU	Natural uranium
OLS	Ordinary least squares regression
RDD	Radiological Dispersion Device
SEM	Scanning Electron Microscope
SIMS	Secondary Ion Mass Spectrometry
SME	Subject Matter Expert
SSAMS	Single Stage Accelerator Mass Spectrometry
TEM	Transmission Electron Microscopy
TIMS	Thermal Ionisation Mass Spectrometry
UOC	Uranium ore concentrate
VGSL	Virtual Gamma Spectroscopy Laboratory
WLS	Weighted least squares regression
XRD	X-ray Diffraction
XRF	X-ray Fluorescence

9 REFERENCES

Almeida A.M., Castel-Branco M.M., Falcão A.C., Linear regression for calibration lines revisited: weighting schemes for bioanalytical methods, Journal of Chromatography B, 774 (2002) 215-222.

Alstad J., Augustson J. H., Danielssen T., Farbu L., A comparative study of the rare earth elements in extraction by HDEHP/Shell Sol T from nitric and sulfuric acid solutions, International Solvent Extraction Conference (1974) 1083-1102.

American National Standard Performance Criteria for Hand-Held Instruments for the Detection and Identification of Radionuclides, ANSI N42.34-2006 (Revision of ANSI N42.34-2003), c1-35, 2007.

Anders E., Grevesse N., Abundances of the elements: Meteoritic and solar, Geochim. Cosmochim. Acta, 53 (1989) 197-214.

Appelblad P., Baxter D., A model for calculating dead-time and mass discrimination correction factors from inductively coupled plasma mass spectrometry calibration curves, J. Anal. At. Spectrom., 15 (2000) 557-560.

Arnold L., The history of nuclear weapons: The Frisch-Peierls memorandum on the possible construction of atomic bombs of February 1940, Cold War History, 3:3 (2003) 111-126.

Balboni E., Simonetti A., Spano T., Cook N., Burns P., Rare-earth element fractionation in uranium ore and its U(VI) alteration minerals, Applied Geochemistry, 87 (2017) 84-92.

Beauchemin D., McLaren J. W., Berman S. S., Study of the effects of concomitant elements in inductively coupled plasma mass spectrometry, Spectrochim. Acta, 3 (1987) 467-490.

Becker J. S., Inorganic Mass Spectrometry, Principles and Applications, John Wiley & Sons Ltd, Chichester, West Sussex, England, 2007.

Blackadar J.M., Bounds J.A., Hypes P.A., Mercer D.J., Sullivan C.J., Evaluation of Handheld Isotope Identifiers, LA-UR-03-2742, Los Alamos National Lab., Los Alamos, NM, 2003.

Borgardt J., Canaday J., Chamberlain D., Results from the second Galaxy Serpent web-based tabletop exercise utilizing the concept of nuclear forensics libraries, J. Radioanal. Nucl. Chem., 311 (2017) 1517-1524.

Boulyga S. F., Cunningham J. A., Macsik Z., Hiess J., Peńkin M. V., Walsh S. J., Development, validation and verification of an ICP-MS procedure for a multi-element analysis of uranium ore concentrates, J. Anal. At. Spectrom., 32 (2017) 2226-2237.

Bulska E., Danko B., Dybczyński R. S., Krata A., Kulisa K., Samczyński Z., Wojciechowski M., Inductively coupled plasma mass spectrometry in comparison with neutron activation and ion chromatography with UV/VIS detection for the determination of lanthanides in plant materials, Talanta, 97 (2012) 303-311.

Catz A.L., Amiel S., Study of lifetimes of nuclear levels by Doppler broadening attenuation using a Ge(Li) gamma-ray spectrometer, Nucl. Phys. A, 92 (1967) 222-232.

Cheong C., Kim N., Yi K., Jo H.J., Jeong Y-J., Kim Y., Koh S.M., Iizuka T., Recurrent rare earth element mineralization in the northwestern Okcheon Metamorphic Belt, Korea: SHRIMP U-Th-Pb

geochronology, Nd isotope geochemistry, and tectonic implications, Ore Geology Reviews, 71 (2015) 99-115.

Code of Conduct on the Safety and Security of Radioactive Sources, IAEA/CODEOC/2004, Vienna, Austria, 2004.

Dampare S. B., Asiedu D. K., Osae S., Nyarko B. J. B., Banoeng-Yakubo B., Determination of rare earth elements by neutron activation analysis in altered ultramafic rocks from the Akwatia District of the Birim diamondiferous field, Ghana, J. Radioanal. Nucl. Chem., 265 (2005) 101-106.

Decay Data Evaluation Project (DDEP), http://www.nucleide.org/DDEP_WG/DDEPdata.htm, accessed in January 2018.

Deming W. E. Statistical Adjustment of Data, Dover, New York, 1964.

Development of a National Nuclear Forensic Library: A System for the Identification of Nuclear or Other Radioactive Material out of Regulatory Control, IAEA-TDL-009, IAEA, Vienna, 2018.

De Voigt M.J.A., Maas J.W., Veenhof D., Van Der Leun C., The reaction $^{23}Na(\alpha,\gamma)^{27}Al$ (I). Yield curve, excitation energies and branchings of ^{27}Al levels, Nucl. Phys., A170 (1971) 449-466.

Dulski P., Interferences of oxide, hydroxide and chloride analyte species in the determination of rare earth elements in geological samples by inductively coupled plasma-mass spectrometry, Fresenius J. Anal. Chem., 350 (1994) 194-203.

Eppich G. R., Williams R. W., Gaffney A. M., Schorzman K. C., ^{235}U-^{231}Pa age dating of uranium materials for nuclear forensic investigations, J. Anal. At. Spectrom., 28 (2013) 666-674.

Estep R.J., Rawool-Sullivan M., Miko D., A method for correcting NaI spectra for attenuation losses in hand-held instrument applications. IEEE Transactions on Nuclear Science, 45 (1998) 1022-1028.

Evans E. H., Giglio J. J., Interferences in Inductively Coupled Plasma Mass Spectrometry – A Review, J. Anal. At. Spectrom., 8 (1993) 1-18.

Fisher D., History of the International Atomic Energy Agency, The First Forty Years, IAEA, Austria, 1997.

Frimmel H. E., Schedel S., Brätz H., Uraninite chemistry as forensic tool for provenance analysis, Appl. Geochem., 48 (2014) 104-121.

Fryer B. J., Taylor R. P., Rare-earth element distributions in uraninites: Implications for ore genesis, Chem. Geology, 63 (1987) 101-108.

Funderberg R., Arevalo Jr R., Locmelis M., Adachi T., Improved Precision and Accuracy of Quantification of Rare Earth Element Abundances via Medium-Resolution LA-ICP-MS, J. Am. Soc. Mass. Spectrom., 28 (2017) 2344-2351.

Gehrke R.J, East L.V., Information in spectra from sources containing “aged” ^{241}Am as from TRU waste, Waste Management, 20 (2000) 555–559.

Gehrke R.J., Baker J.D., Hartwell J.K., Riddle C.L., McGrath C.A., Measurement of neutron-to-γ-ray production ratios from (α,n) reactions for their application to assay TRU waste, Nucl. Instr. Meth. Phys. Res. A, 511 (2003) 444-456.

GICNT, 2018, http://www.gicnt.org/, retrieved January 2018.

Gilmore, G.R., Practical Gamma-ray Spectrometry, 2nd Edition, John Wiley & Sons Ltd, Chippenham, United Kingdom, 2011.

Groopman E., Grabowski K., Fahey A., Kööp L., Rapid, molecule-free, in situ rare earth element abundances by SIMS-SSAMS, J. Anal. At. Spectrom.,, 32 (2017) 2153-2163.

Hahn O., Strassmann F., Nachweis der Entstehung aktiver Bariumisotope aus Uran und Thorium durch Neutronenbestrahlung; Nachweis weiterer aktiver Bruchstücke bei der Uranspaltung, Naturwiss., 37 (1939) 89-95.

Harris D. C., Quantitative Chemical Analysis, 6th edition, W. H. Freeman and Company, New York, United States, 2003.

Healey G., Button P., Change in impurities observed during the refining and conversion processes, Esarda Bulletin, 49 (2013) 57-65.

Holmgren Rondahl S., Pointurier F., Ahlinder L., Ramebäck H., Marie O., Ravat B., Delaunay F., Young E., Blagojevic N., Hester J. R., Thorogood G., Nelwamondo A. N., Ntsoane T. P., Roberts S. K., Holliday K. S., Comparing results of X-ray diffraction, μ-Raman spectroscopy and neutron diffraction when identifying chemical phases in seized nuclear material, during a comparative nuclear forensics exercise, 315 (2018) 395-408.

Hofstetter K., Beals D., Odell D., Uranium detection using small scintillators in a maritime environment. J. Radioanal. Nucl. Chem., 276 (2008) 433-439.

Hubaux A., Vos G., Decision and Detection Limits for Linear Calibration Curves, Analytical Chemistry, 42 (1970) 849-855.

Hutcheon I.D., Kristo M.J., Knight K.B., Non-proliferation Nuclear Forensics, Uranium – Cradle to Grave, Min. Assoc. of Canada, pp. 377-394, 2013.

IAEA Safeguards Glossary, 2001 Edition, International Nuclear Verification Series No. 3, Vienna, Austria, 2002.

Incident and Trafficking Database (ITDB), http://www-ns.iaea.org/security/itdb.asp, retrieved January 2019.

ISO Guide 33:2015 (2015) Reference materials – Good practice in using reference materials, the International Organization for Standardization, Geneva, Switzerland.

ISO/IEC Guide 98-3:2008 (2008) Uncertainty of measurement – Part 3: Guide to the expression of uncertainty in measurement, the International Organization for Standardization, Geneva, Switzerland.

ISO 8655-6:2002 (2002) Piston-operated volumetric apparatus – Part 6: Gravimetric methods for the determination of measurement error, the International Organization for Standardization, Geneva, Switzerland.

ISO 13528:2015 (2015) Statistical methods for use in proficiency testing by interlaboratory comparison, the International Organization for Standardization, Geneva, Switzerland.

Jakubowski N., Moens L., Vanhaecke F., Sector field mass spectrometers in ICP-MS, Spectrochim. Acta, 53B (1998) 1739-1763.

Jakubowski N., Prohaska T., Rottmann L., Vanhaecke F., Inductively coupled plasma- and glow discharge plasma-sector field mass spectrometry, 26 (2011) 693-726.

Kaminski M., Nuñez L., Separation of Uranium from Nitric- and Hydrochloric-Acid Solutions with Extractant-Coated Magnetic Microparticles, Separation Science and Technology, 35:13 (2000) 2003-2018.

Keegan E., Kristo M. J., Colella M., Robel M., Williams R., Lindwall R., Eppich G., Roberts S., Borg L., Gaffney A., Plaue J., Wong H., Davis J., Loi E., Reinhard M., Hutcheon I., Nuclear forensic analysis of an unknown uranium ore concentrate sample seized in a criminal investigation in Australia, Forensic Science International, 240 (2014) 111-121.

Kessel R., Berglund M., Wellum R., Application of consistency checking to evaluation of uncertainty in multiple replicate measurements, Accred Qual Assur, 13 (2008) 293-298.

Ketkar S. N., Bzik T. J., Calibration of Analytical Instruments. Impact of Nonconstant Variance in Calibration Data, Anal. Chem., 72 (2000) 4762-4765.

Knoll G.F., Radiation Detection and Measurement, John Wiley & Sons, New York, United States, 2000.

Kristo M. J., Keegan E., Colella M., Williams R., Lindvall R., Eppich G., Roberts S., Borg L., Gaffney A., Plaue J., Knight K., Loi E., Hotchkis M., Moody K., Singleton M., Robel M., Hutcheon I., Nuclear forensic analysis of uranium oxide powders interdicted in Victoria, Australia, Radiochim. Acta, 103 (2015) 487-500.

Kristo M.J., Tumey S.J., The state of nuclear forensics, Nucl. Inst. Meth. Phys. B, 294 (2013) 656-661.

Leggitt J., Inn K., Goldberg S., Essex R., LaMont S., Chase S., Nuclear forensics – metrological basis for legal defensibility, J. Radioanal. Nucl. Chem., 282 (2009) 997-1001.

Litwak R. S., Deterring Nuclear Terrorism, Wilson Center, Washington DC, United States, 2016, ISBN 978-1-938027-59-8.

Lobato L.M., Pimentel M.M., Cruz S.C.P., Machado N., Noce C.M., Alkmim F.F., U-Pb geochronology of the Lagoa Real uranium district, Brazil: implications for the age of the uranium mineralization, J. South Am. Earth Sci., 58 (2015) 129-140.

Longerich H., Fryer B., Strong D., Kantipuly C., Effects of operating conditions on the determination of the rare earth elements by inductively coupled plasma-mass spectrometry (ICP-MS), Spectrochimica Acta,, 42B (1987) 75-92.

Lützenkirchen K., Wallenius M., Varga Z., Wiss T., Knott A., Nicholl A., Mayer K., Nuclear forensics on uranium fuel pellets, Radiochim. Acta, 107 (2019) 635-643.

Mayer K., Glaser A., Nuclear Forensics, From: Routledge Handbook of Nuclear Proliferation and Policy, Routledge, ISBN 978-1-1360-1248-8, London, United Kingdom, 2015.

Meija J., Coplen T. B., Berglund M., Brand W. A., De Bièvre P., Gröning M., Holden N. E., Irrgeher J., Loss R. D., Walczyk T., Prohaska T., Isotopic compositions of the elements 2013 (IUPAC Technical Report) Pure Appl. Chem., 88(3) (2016) 293-306.

Meitner L., Frisch O.R., Disintegration of Uranium by Neutrons: a New Type of Nuclear Reaction, Nature, 143 (1939) 239-240.

Mercadier J., Cuney M., Lach P., Boiron M-C., Bonhoure J., Richard A., Leisen M., Kister P., Origin of uranium deposits revealed by their rare earth element signature, Terra Nova, 23 (2011) 264-269.

Miller J. N., Miller J. C., Statistics and Chemometrics for Analytical Chemistry, 6 ed, Pearson Education Limited, ISBN 978-0-273-73042-2, Harlow, Essex, England, 2010.

Morais C. A., Ciminelli V. S. T., Recovery of europium from a rare earth chloride solution, Hydrometallurgy, 49 (1998) 167-177.

Morais C. A., Ciminelli V. S. T., Selection of solvent extraction reagent for the separation of europium(III) and gadolinium(III), Minerals Engineering, 20 (2007) 747-752.

Nash K. L., Jensen M. P., Analytical Separations of the Lanthanides: Basic Chemistry and Methods, Chapter 180 in Handbook on the Physics and Chemistry of Rare Earths, Vol. 28, Elsevier Science B.V., North-Holland, 2000.

Nelms S. M., ICP Mass Spectrometry Handbook, Blackwell Publishing Ltd, ISBN 978-1-4051-0916-1, Oxford, UK, 2005.

Nelson K. E., Gosnell T. B., Knapp D. A., The effect of energy resolution on the extraction of information content from gamma-ray spectra. Nucl. Inst. Meth. Phys. A, 659 (2011) 207-214.

Nelwamondo A. N., Colletti L. P., Lindvall R. E., Vesterlund A., Xu N., Hiong Jun Tan A., Eppich G. R., Genetti V. D., Kokwane B. L., Lagerkvist P., Pong B. K., Ramebäck H., Tandon L., Rasmussen G., Varga Z., Wallenius M., Uranium assay and trace element analysis of the fourth collaborative material exercise samples by the modified Davies-Gray method and the ICP-MS/OES techniques, J Radioanal Nucl Chem, 315 (2018) 379-394.

Nguyen C.T., Zsigrai J., Basic characterization of highly enriched uranium by gamma spectrometry. Nucl. Inst. Meth. Phys. B, 246 (2006) 417-424.

NPT/CONF.2015/13, Activities of the International Atomic Energy Agency relevant to article III of the Treaty on the Non-Proliferation of Nuclear Weapons: background paper prepared by the secretariat of the International Atomic Energy Agency, Review Conference of the Parties to the Treaty on the Non-Proliferation of Nuclear Weapons, Conference paper, 2015.

Nuclear Forensics Support, IAEA Nuclear Security Series No.2: Technical Guidance, Vienna, 2006.

Nuclear Forensics in Support of Investigations: Implementing Guide, IAEA Nuclear Security Series No.2-G (rev.1), Vienna, 2015.

Nuclear Security Recommendations on Nuclear and Other Radioactive Material out of Regulatory Control, IAEA Nuclear Security Series No.15, Vienna, 2011.

NuDat 2.6 database, 2014, http://www.nndc.bnl.gov/nudat2/, National Nuclear Data Center, Brookhaven National Laboratory, USA.

Nygren U., Ramebäck H., Nilsson C., Age determination of plutonium using inductively coupled plasma mass spectrometry, J. Radioanal. Nucl. Chem., 272 (2007) 45-51.

Peppard D. F., Mason G. W., Maier J. L., Driscoll W. J., Fractional extraction of the lanthanides as their di-alkyl orthophosphates, J. Inorg. Nucl. Chem., 4 (1957) 334-343.

Pibida L., Unterweger M., Karam L.R., Evaluation of Handheld Radionuclide Identifiers. Journal of Research of the National Institute of Standards and Technology, 109 (2004) 451-456.

Pin C., Zalduegui J. F. S., Sequential separation of light rare-earth elements, thorium and uranium by miniaturized extraction chromatography: Application to isotopic analyses of silicate rocks, Anal. Chim. Acta, 339 (1997) 79-89.

Plenteda R., A Monte Carlo Based Virtual Gamma Spectrometry Laboratory. Atominstitut der Österreichischen Universitaten, 2002.

Prohaska T., Hann S., Latkoczy C., Stingeder G., Determination of rare earth elements U and Th in environmental samples by inductively coupled plasma double focusing sector field mass spectrometry (ICP-SMS), J. Anal. At. Spectrom., 14 (1999) 1-8.

Qureshi I. H., McClendon L. T., LaFleur P. D., Radiochim. Acta, 12 (1969) 107-111.

Ramebäck H., Nygren U., Lagerkvist P., Verbruggen A., Wellum R., Skarnemark G., Basic characterization of ^{233}U: Determination of age and ^{232}U content using sector field ICP-MS, gamma spectrometry and alpha spectrometry, Nucl. Inst. Meth Phys. B, 266 (2008) 807-812.

Ramebäck H., Nygren U., Tovedal A., Ekberg C., Skarnemark G., Uncertainty assessment in gamma spectrometric measurements of plutonium isotope ratios and age, Nucl. Instr. Meth. Phys. Res. B, 287 (2012) 56–59.

Ramebäck H., Lindgren P., Uncertainty evaluation in gamma spectrometric measurements: Uncertainty propagation versus Monte Carlo simulation, Appl. Rad. Isot., 142 (2018) 71-76.

Raposo F., Evaluation of analytical calibration based on least-squares linear regression for instrumental techniques: A tutorial review, Trends in Analytical Chemistry, 77 (2016) 167-185.

Raut N. M., Huang L-S., Aggarwal S. K., Lin K-C., Determination of lanthanides in rock samples by inductively coupled plasma mass spectrometry using thorium as oxide and hydroxide correction standard, Spectrochim. Acta, 58B (2003) 809-822.

Reed T. C., Stillman D. B., The Nuclear Express: A political history of the bomb and its proliferation, Zenith Press, Minneapolis, USA, 2009.

Rydberg J., Musikas C., Choppin G. R., Principles and Practices of Solvent Extraction, Marcel Dekker, New York, 1992.

Sayago A., Asuero A., Fitting Straight Lines with Replicated Observations by Linear Regression: Part II. Testing for Homogeneities of Variances, Critical Reviews in Analytical Chemistry, 34 (2004) 133-146.

Shabana R., Ruf H., Extraction and separation of uranium, thorium and cerium from different mixed media with HDEHP, J Radioanal Chem,, 36 (1977) 389-397.

Sharpey-Schafer J.F., Alderson P.R., Bailey D.C., Durell J.L., Greene M.W., James A.N., Lifetimes and decays of energy levels in ^{30}Si and ^{30}P, Nucl. Phys., A167 (1971) 602-624.

Simitchiev K., Stefanova V., Kmetov V., Andreev G., Sanchez A., Canals A., Investigation of ICP-MS spectral interferences in the determination of Rh, Pd, and Pt in road dust: Assessment of correction algorithms via uncertainty budget analysis and interference alleviation by preliminary acid leaching, Talanta, 77 (2008) 889-896.

Spano T. L., Simonetti A., Balboni E., Dorais C., Burns P. C., Trace element and U isotope analysis of uraninite and ore concentrate: Applications for nuclear forensic investigations, Appl. Geochem., 84 (2017) 277-285.

Sprinkle Jr J. K., Christiansen A., Cole R., Collins M. L., Hsue S. T., Knepper P. L., McKown T. O., Siebelist R., Low-resolution gamma-ray measurements of uranium enrichment. Appl. Radiat. Isot., 48 (1997) 1525-1528.

Sturm M., Richter S., Aregbe Y., Wellum R., Mialle S., Mayer K., Prohaska T., Evaluation of chronometers in plutonium age determination for nuclear forensics: What if the “Pu/U clocks” do not match?, J Radioanal. Nucl. Chem., 302 (2014) 399-411.

Sweet L. E., Blake T. A., Henager Jr C. H., Hu S., Johnson T. J., Meier D. E., Peper S. M., Schwantes J. M., Investigation of the polymorphs and hydrolysis of uranium trioxide, J. Radioanal. Nucl. Chem., 296 (2013) 105–110.

Tan S., Horlick G., Matrix-effect Observations in Inductively Coupled Plasma Mass Spectrometry, J. Anal. At. Spectrom., 2 (1987) 745-752.

Thompson J. J., Houk R. S., A Study of Internal Standardization in Inductively Coupled Plasma-Mass Spectrometry, 41 (1987) 801-806.

Trešel I., Quétel C. R., Taylor P. D. P, Solution to data integration problems during isotope ratio measurements by magnetic sector inductively coupled plasma mass spectrometer at medium mass resolution: application to the certification of an enriched ^{53}Cr material by isotope dilution, Spectrochimica Acta Part B, 58 (2003) 551-563.

Vanhaecke F., Vanhoe H., Dams R., The use of internal standards in ICP-MS, Talanta, 39 (1992) 737-742.

Varga Z., Wallenius M., Mayer K., Origin assessment of uranium ore concentrates based on their rare-earth elemental impurity pattern, Radiochim. Acta, 98 (2010a) 771-778.

Varga Z., Katona R., Stefánka Z., Wallenius M., Mayer K., Nicholl A., Determination of rare-earth elements in uranium-bearing materials by inductively coupled plasma mass spectrometry, Talanta, 80 (2010b) 1744-1749.

Varga Z., Wallenius M., Mayer K., Hrnecek E., Alternative method for the production date determination of impure uranium ore concentrate samples, J. Radioanal. Nucl. Chem., 290 (2011) 485-492.

Varga Z., Krajko J., Peńkin M., Novák M., Eke Z., Wallenius M., Mayer K., Identification of uranium signatures relevant for nuclear safeguards and forensics, J Radioanal Nucl Chem, 312 (2017) 639-654.

Vaughan M., Horlick G., Oxide, Hydroxide, and Doubly Charged Analyte Species in Inductively Coupled Plasma/Mass Spectrometry, Appl. Spectrosc., 40 (1986) 434-445.

Vaughan M., Horlick G., Correction Procedures for Rare Earth Element Analyses in Inductively Coupled Plasma- Mass Spectrometry, Applied Spectroscopy, 44 (1990) 587-593.

Vesterlund A., Lagerkvist P., Ramebäck H., Study of separation methods and spectral interferences for accurate measurements of lanthanides in uranium-rich samples using ICP-SFMS, 2014, FOI-R--3885--SE.

Wacker J.F., Curry M., Proposed Framework for National Nuclear Forensics Libraries and International Directories, PNNL-SA-70589, 2011.

Wallenius M., Mayer K., Ray I., Nuclear forensic investigations: Two case studies, Forensic Science International, 156 (2006) 55-62.

Wallenius M., Lützenkirchen K., Mayer K., Ray I., de las Heras L.A., Betti M., Cromboom O., Hild M., Lynch B., Nicholl A., Ottmar H., Rasmussen G., Schubert A., Tamborini G., Thiele H., Wagner W., Walker C., Zuleger E., Nuclear forensic investigations with a focus on plutonium, J. Alloys Compd., 444–445 (2007) 57–62.

Waters L.S. (Ed.), MCNPX user's manual, Version 2.3.0. Los Alamos National Laboratory Report LA-UR-02-2607, 2002.

White W., Geochemistry, Wiley-Blackwell, Chichester, UK, 2013.

Williams R. W., Hutcheon I. D., Kristo M. J., Gaffney A. M., Eppich G. R., Goldberg S., Morrison J. J., Essex R., Radiochronometry by Mass Spectrometry: Improving the Precision and Accuracy of Age-Dating for Nuclear Forensics, LLNL-CONF-655059, International Conference on Advances in Nuclear Forensics: Countering the Evolving Threat of Nuclear and Other Radioactive Material out of Regulatory Control, Vienna, Austria, 2014.

United Nations Security Council Resolution (UNSCR) 1540, S/RES/1540, 2004.

Yang Y., Zhang H., Chu Z., Xie L., Wu F., Combined chemical separation of Lu, Hf, Rb, Sr, Sm and Nd from a single rock digest and precise and accurate isotope determinations of Lu-Hf, Rb-Sr and Sm-Nd isotope systems using Multi-Collector ICP-MS and TIMS, Int. J. Mass Spectrom., 290 (2010) 120-126.

Zinn W.H., Szilard L., Emission of Neutrons by Uranium, Phys. Rev., 56 (1939) 619-624.

Zsigrai J., Nguyen C.T., Berlizov A., Gamma-spectrometric determination of ^{232}U in uranium-bearing materials, Nucl. Instrum. Meth. B, 359 (2015) 137-144.

Paper I

Applied Radiation and Isotopes 72 (2013) 54–57

Contents lists available at SciVerse ScienceDirect

Applied Radiation and Isotopes

journal homepage: www.elsevier.com/locate/apradiso

On the categorization of uranium materials using low resolution gamma ray spectrometry

A. Vesterlund [a,*], T. Ulvsand [a], K. Lidström [a], G. Skarnemark [b], C. Ekberg [b], H. Ramebäck [a,b]

[a] Swedish Defence Research Agency, FOI Division of CBRN Defence and Security, SE-901 82 Umeå, Sweden
[b] Chalmers University of Technology, Department of Chemical and Biological Engineering, Nuclear Chemistry, SE-412 96 Göteborg, Sweden

HIGHLIGHTS

- Categorization of U using Na(Tl) detectors is dependent on matrix and shielding.
- Detector response curves were simulated.
- Errors in ^{235}U abundance due to inadequate detector responses were quantified.

ARTICLE INFO

Article history:
Received 29 May 2012
Received in revised form
17 October 2012
Accepted 29 October 2012
Available online 2 November 2012

Keywords:
Low resolution gamma spectrometry
Uranium
Categorization

ABSTRACT

In order to characterize uranium materials during e.g. nuclear safeguards inspections and in initial stages of nuclear forensic investigations, hand-held low resolution gamma ray detection instruments with automatic uranium categorization capabilities may be used. In this paper, simulated response curves for a number of matrices applied on NaI(Tl) scintillation detector spectra show that the result of the categorization is strongly dependent on the physical properties of the uranium material. Recommendations on how to minimize the possibility of misclassification are discussed.

1. Introduction

Measurement of special nuclear material (SNM) is important from a nuclear safeguards and illicit trafficking perspective. In order to perform this task there is a need for reliable instruments that can detect and categorize radioactive material. Hand-held gamma spectrometers are important tools for, among others, safeguards applications, first responders and border control. Other techniques for categorization of nuclear materials are high-resolution gamma spectrometry, alpha spectrometry and mass spectrometry. These techniques might, however, not be readily available for field use by e.g. first responders. Commonly, the instruments used are low resolution gamma spectrometers with e.g. NaI(Tl) scintillation detectors. The instruments are normally equipped with libraries for different scenarios or purposes each containing a number of radionuclides for automatic identification and categorization. The advantages with these instruments are their true portability and the possibility to use them at room temperature, i.e. there is no need to cool like what the high-purity germanium semiconductor detectors (HPGe) require, as well as their lower cost compared to portable HPGe detectors. Furthermore, the measurement efficiency is high which implies that data acquisition is fast. However, the low resolution of these instruments impedes the identification capability, and a number of reports have shown that the ability of these instruments to automatically identify gamma emitting radionuclides is somewhat limited (Blackadar et al., 2003; Nelson et al., 2011; Pibida et al., 2004). Another problem concerns the ability of categorization of nuclear materials. Some instruments report categories such as SNM or naturally occurring radioactive materials (NORM) while other instruments, for uranium, report categories divided into depleted uranium (DU), natural uranium (NU), low-enriched uranium (LEU), high-enriched uranium (HEU) or weapons grade uranium (WGU). One technique that can be used for uranium categorization using gamma spectrometry is template matching where an acquired spectrum is compared to a library of reference spectra (Burr and Hamada, 2009). Another way to categorize uranium is to evaluate the content of ^{235}U and ^{238}U using e.g. the 185.7 keV ^{235}U-peak and the 1001 keV ^{234m}Pa-peak (^{234m}Pa being the progeny of ^{238}U and assuming radioactive

* Corresponding author. Tel.: +46 90 106600; fax: +46 90 106800.
E-mail address: anna.vesterlund@foi.se (A. Vesterlund).

0969-8043/$ - see front matter © 2012 Elsevier Ltd. All rights reserved.
http://dx.doi.org/10.1016/j.apradiso.2012.10.018

equilibrium between ^{234m}Pa and ^{238}U). The measurement efficiency, or the relative response at different gamma ray energies, is dependent on the physical properties of the sample such as density, chemical composition and possible shielding materials between the sample and the detector. The effect is most prominent in the low energy region where the attenuation of gamma rays will be substantial if e.g. the density of the material is high, or if the uranium is shielded with a high density material. Hence, the physical and chemical characteristics of the measured material will affect the shape of the spectrum. This infers that the instrument needs to be able to evaluate spectra depending on the physical condition of the material examined, in order to make correct categorizations. For example, if the instrument is calibrated to categorize uranium contained in a steel container, the instrument may be delivering a categorization lower than the real category if the shielding is heavier. Furthermore, the result of a misclassification of uranium material may lead to an incorrect risk assessment if only low resolution gamma spectrometry is available. Categorization of uranium using low resolution gamma spectrometry has earlier, however, been proven to be difficult (Hofstetter et al., 2008). A number of different algorithms, both off-line and on-line, have been proposed to resolve the self-attenuation problem (Estep et al., 1998; Hofstetter et al., 2008; Sprinkle Jr. et al., 1997). The problem, however, seems to remain.

In this work the problems concerning categorization of uranium performed by these instruments were investigated further by evaluating a number of uranium spectra from a NaI(Tl) detector, using calculated response curves for various matrices and shieldings. Furthermore, the possible errors in the evaluated ^{235}U abundance of a uranium material due to an inadequate instrumental setting, i.e. wrong assumptions of the physical and chemical characteristics, as well as absorber material, were quantified.

2. Material and methods

2.1. Theory

Uranium can be categorized by evaluating the fraction of ^{235}U of the total amount of uranium. This can be done by using the 185.7 keV peak for ^{235}U and the 1001 keV peak for ^{234m}Pa in the gamma spectrum, assuming radioactive equilibrium with ^{238}U, which occurs at about 4 months after separation. The abundance, f_{235}, is given by

$$f_{235} = \frac{N_{235}}{N_{235}+N_{238}} \tag{1}$$

where N_x is the number of atoms of uranium isotope x. In this case N_{234} is considered negligible. When the enrichment of ^{235}U approaches 90%, the ^{234}U abundance is around 1% depending on the history of the material (Nguyen and Zsigrai, 2006). Furthermore, the 185.7 keV peak is assumed not to be interfered by ^{226}Ra. This assumption is made on the basis that there are no significant amounts of Ra in a processed anthropogenic uranium material. Moreover, the Ra originating from the background may be subtracted from the spectrum.

The radioactivity of isotope x, A_x, evaluated from a gamma spectrometric measurement is given by

$$A_x = \frac{C_{x,\gamma}}{tI_{x,\gamma}\Psi_\gamma} \tag{2}$$

where $C_{x,\gamma}$ and $I_{x,\gamma}$ are the number of counts and photon emission probability of isotope x at energy E_γ, respectively; t is the measurement time and Ψ_γ is the measurement efficiency at energy E_γ. Using the well-known relation

$$A_x = \frac{N_x \ln(2)}{t_{½,x}} \tag{3}$$

where $t_{½,x}$ is the half-life of isotope x in seconds, combined with Eqs. (1) and (2) one acquires for the abundance of ^{235}U

$$f_{235} = \frac{C_{235,185\ \mathrm{keV}} t_{½,235}/I_{235,185\ \mathrm{keV}}\Psi_{185\ \mathrm{keV}}}{C_{235,185\ \mathrm{keV}} t_{½,235}/I_{235,185\ \mathrm{keV}}\Psi_{185\ \mathrm{keV}} + C_{238,1001\ \mathrm{keV}} t_{½,238}/I_{238,1001\ \mathrm{keV}}\Psi_{1001\ \mathrm{keV}}} \tag{4}$$

From Eq. (4) it is obvious that besides the information contained in a particular spectrum, the efficiency is also needed. In a high resolution spectrum, a relative efficiency function can easily be established (Ramebäck et al., 2010). The possibility of using the relative efficiency for isotope ratio measurements makes the absolute efficiency calibration redundant. However, this cannot be achieved using a low-resolution gamma spectrum. Due to the low resolution, not all the peaks needed to establish a relative efficiency function can be distinguished.

2.2. Simulations

The efficiencies for a number of different matrices and shieldings were simulated using the Monte Carlo based simulation software Virtual Gamma Spectroscopy Laboratory, VGSL. VGSL uses a modified version of MCNPX as particle transport simulation engine (Plenteda, 2002; Waters, 2002). The NaI(Tl) detector was defined to imitate the detector of the hand-held NaI(Tl) scintillation detector identiFINDER® (ICx, FLIR Systems, Inc., Wilsonville, USA); hence, the dimensions of the crystal were 35×51 mm^2 and the density was 3.7 g/cm^3. The matrices and shieldings used for simulations were

- water matrix, $\rho = 1.0$ g/cm^3;
- UO_2 matrix, $\rho = 11$ g/cm^3;
- uranium metal matrix, $\rho = 19$ g/cm^3;
- water matrix with a 1 mm lead shielding, $\rho = 11$ g/cm^3;
- water matrix with a 5 mm steel shielding, $\rho = 7.5$ g/cm^3.

The density of steel varies depending on alloy composition, commonly between 7.2 and 7.9 g/cm^3 (Lide, 2009). The following 5-grade polynomial was fitted to each of the sets of efficiencies from the simulations:

$$\Psi = e^{c_1 + c_2/E^2 + c_3(\ln E)^2 + c_4(\ln E)^3 + c_5/E} \tag{5}$$

which is an empirical expression used in a previous paper, where $c_1,\ldots,c_5$ are constants and E is the energy(Ramebäck et al., 2010). The enrichment of ^{235}U was calculated for each spectrum, with different response functions, from the peak areas at 185.7 keV and 1001 keV using Eq. (4).

2.3. Measurements

Spectra from the following uranium materials and matrices were collected using a NaI(Tl) identiFINDER®: NU as UO_2, LEU with approximately 4% ^{235}U as UO_2, DU as UO_2 and NU in an aqueous solution (certified reference material IRMM-184). Data was collected for 60 s at a distance of 10 cm from the source. The data for the IRMM-184 solution was acquired for 600 s close to the instrument due to its low uranium content. The instrument reported the evaluated uranium category after the measurement. Thereafter, the spectrum data were downloaded for off-line evaluation according to Eqs. (4) and (5).

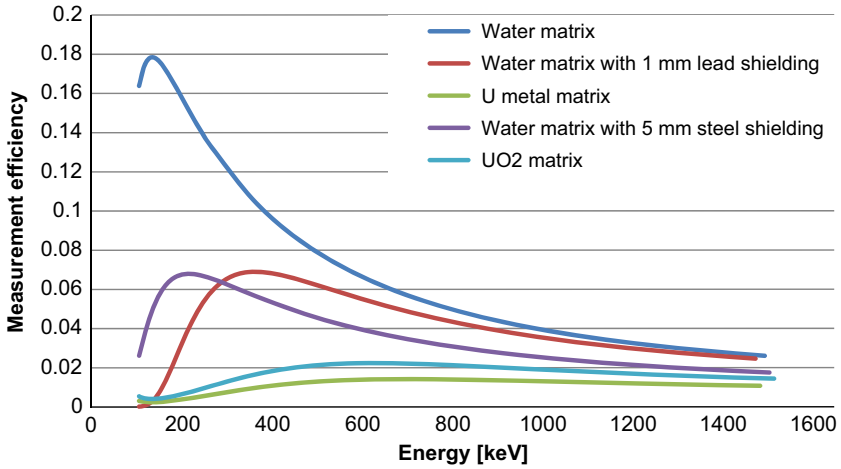

Fig. 1. Simulated response for the different matrices considered in this work. The lines correspond to the parameterization of the response curves according to Eq. (5).

Table 1
Results of the automatic categorization performed by the identiFINDER®.

Uranium type	Sample matrix	Instrument categorization
NU	UO_2	DU
LEU	UO_2	DU
DU	UO_2	DU
NU	Aqueous	LEU

3. Results and discussion

The results of the simulated responses can be seen in Fig. 1. Clearly, the response differs markedly in the low energy region depending on matrix and shielding. In the 185.7 keV region the efficiency varies between 0.16 and 0.004, i.e. a factor of 40, from the least to the most self-absorbing material. At 1001 keV the responses vary between 0.038 and 0.013, i.e. a factor of 2.9.

Both the NU and the LEU as UO_2 were categorized as DU by the automatic evaluation of the instrument. However, natural uranium in an aqueous solution (IRMM-184) was given the higher category, i.e. LEU, see Table 1.

For comparison, the calculated abundances using the different responses in Fig. 1 can be found in Table 2. For the UO_2 samples it is obvious that the evaluated abundances of ^{235}U are too low when the response curve for the aqueous solution was used. However, by evaluating the abundance using a response function for a denser matrix, the abundance increases and when the response curve for UO_2 is used, the categorization is correct, as would be expected. In the same way, when the aqueous sample is evaluated according to the unshielded water matrix response, the fraction corresponds to natural uranium. Using the other response functions, the sample would be categorized as LEU.

The performance criteria according to ANSI (American National Standards Institute) for hand-held instruments require that instruments should be able to identify a number of radionuclides without shielding as well as with a 5 mm steel shielding (ANSI N42.34-2006, 2007). Fig. 2 shows the evaluated abundance of various types of uranium using a response function that corresponds to a water matrix with a 5 mm steel shielding, as a function of density. The black line in Fig. 2 corresponds to the abundance of natural uranium. This means that an instrument with a response optimized for a 5 mm steel shielding most likely will categorize uranium as DU for materials with enrichment and density corresponding to the parts of the lines that are under this line. Furthermore, by using the responses in Fig. 1 it can be shown that, in order for an instrument with a setting corresponding to an inherent 5 mm steel response to show that a UO_2 material is low-enriched (2% enrichment), the enrichment in the material needs to be about 15%.

The expanded uncertainty presented in Table 2 includes uncertainty from counting statistics only. The uncertainties in photon emission probabilities and half-lives are considered negligible compared to the counting statistics. The uncertainty in the responses will, however, be unknown in a real measurement situation, if the analyst from a visual inspection cannot identify the matrix. A conservative approach might be to evaluate the ^{235}U abundance with response functions corresponding to the possible extremes of matrices. However, a possible drawback of using a U metal response for all samples would be that a low density sample such as a water sample with a ^{235}U abundance higher than 0.1% would be assigned to some category of enriched uranium (LEU or HEU). The opposite case, where the water response is used, would result in depleted uranium for all uranium containing samples, possibly with the exception of high enriched uranium samples. The consequence would be many false positives and false negatives, correspondingly. Another problem that may arise even though the matrix is known is that the response is dependent on the geometry of the sample. A very thin sample will have a substantially higher response at 185.7 keV compared to a thick sample. In this study, however, only bulky samples are considered.

The categorization of natural uranium is difficult due to the narrow abundance interval. In Table 2 the evaluation of natural uranium using the correct response functions for a given matrix yields an abundance of 0.0088 and 0.0106 for the UO_2 and the aqueous sample, respectively. The combined measurement uncertainty for isotope ratio measurements using high resolution gamma spectrometry was previously determined to be around 10–20% ($k=2$, about 95% confidence interval; Ramebäck et al., 2010). Thus, it is reasonable to believe that the measurement uncertainty for isotope ratio measurements using low resolution gamma spectrometry is at least not less than 10–20%. In this perspective, it is realistic to categorize the natural uranium samples as natural uranium based on the evaluated abundance.

Looking at the results it is clear that the evaluation of the uranium category is strongly dependent on the knowledge of the material that is being investigated. If the categorization algorithm is not independent of the nature of the uranium, which seems to be the case with this specific instrument, the outcome of the instrument's evaluation is not reliable. The instrument user is hereby compelled to take the spectrum off-line to evaluate the ^{235}U-enrichment in a different manner taking into consideration

Table 2
Calculated abundances of ^{235}U for different categories of uranium using different combinations of matrices and shieldings. The numbers within the brackets correspond to the expanded uncertainty in counting statistics ($k=2$, about 95% confidence interval).

Sample		Evaluated f_{235} with respective response function				
Uranium type	Real matrix	Water matrix	Water matrix+5 mm steel shielding	Water matrix+1 mm lead shielding	UO_2 matrix	U metal matrix
NU	UO_2	0.000681(51)	0.001052(79)	0.00348(26)	0.00882(66)	0.01041(78)
LEU	UO_2	0.00166(20)	0.00257(30)	0.0085(10)	0.0213(25)	0.0251(30)
DU	UO_2	0.0000449(63)	0.000069(10)	0.000230(32)	0.000587(82)	0.00069(10)
NU	Aqueous	0.0106(16)	0.0163(24)	0.0520(77)	0.123(18)	0.142(21)

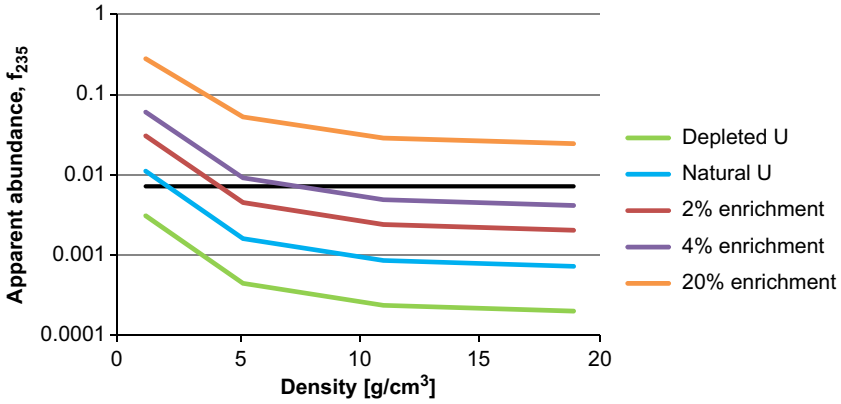

Fig. 2. Apparent abundance of ^{235}U using the response function, corresponding to a water sample with 5 mm steel shielding, as a function of density for different uranium containing matrices. The black line corresponds to the abundance of natural uranium.

the nature of the material or use another measurement method, e.g. high resolution gamma spectrometry. One way to minimize the possibility for misclassification is to equip the instrument with options corresponding to a number of different matrices and shieldings. Then the user could choose the proper option according to the composition of the material examined, if this is known, e.g. during safeguards inspections.

Another case, which might be even more problematic to evaluate, is when the matrix of the material is unknown. Then it is difficult to know whether the assumed response corresponds to the attenuation in the material. In this case the solution could be to try out a number of response curves for different matrices. The result would in this case be, as outlined above, a range of compositions, corresponding to a range of categories, depending on the matrix of the material measured. If the instrument reports correct categorization only in a fraction of all examinations, the instrument is useless in this aspect. It is necessary to modify the algorithms in these types of instruments to decrease the number of misclassifications or to give the users possibility to alter the instrumental settings depending on whether knowledge of the material composition and possible shielding exists.

4. Conclusions

In this work the significance of the knowledge of a material when low resolution gamma spectrometry is used for categorization of uranium is highlighted. It was shown how the sample matrices affect the categorization by comparing results based on evaluation of uranium spectra with different response functions. In order to make correct categorizations it is important that the sample matrix, if known, is taken into consideration. Otherwise, the spectra should be evaluated with a range of material compositions in mind, giving a range of possible uranium categories.

References

American National Standard Performance Criteria for Hand-Held Instruments for the Detection and Identification of Radionuclides, 2007. ANSI N42.34-2006 (Revision of ANSI N42.34-2003), pp. c1–c35.
Blackadar, J.M., Bounds, J.A., Hypes, P.A., Mercer, D.J., Sullivan, C.J., 2003. Evaluation of Handheld Isotope Identifiers. Los Alamos National Lab, Los Alamos, NM.
Burr, T., Hamada, M., 2009. Radio-isotope identification algorithms for NaI γ spectra. Algorithms 2, 339–360.
Estep, R.J., Rawool-Sullivan, M., Miko, D., 1998. A method for correcting NaI spectra for attenuation losses in hand-held instrument applications. IEEE Trans. Nucl. Sci. 45, 1022–1028.
Hofstetter, K., Beals, D., Odell, D., 2008. Uranium detection using small scintillators in a maritime environment. J. Radioanal. Nucl. Chem. 276, 433–439.
Lide, D.R. (Ed.), 2009. CRC Handbook of Chemistry and Physics. CRC Press, Boca Raton.
Nelson, K.E., Gosnell, T.B., Knapp, D.A., 2011. The effect of energy resolution on the extraction of information content from gamma-ray spectra. Nucl. Instrum. Methods Phys. Res. Sect. A 659, 207–214.
Nguyen, C.T., Zsigrai, J., 2006. Basic characterization of highly enriched uranium by gamma spectrometry. Nucl. Instrum. Methods Phys. Res. Sect. B 246, 417–424.
Pibida, L., Unterweger, M., Karam, L.R., 2004. Evaluation of Handheld Radionuclide Identifiers. J. Res. Natl. Inst. Stand. Technol. 109, 451–456.
Plenteda, R., 2002. A Monte Carlo Based Virtual Gamma Spectrometry Laboratory. Atominstitut der Österreichischen Universitaten.
Ramebäck, H., Vesterlund, A., Tovedal, A., Nygren, U., Wallberg, L., Holm, E., Ekberg, C., Skarnemark, G., 2010. The jackknife as an approach for uncertainty assessment in gamma spectrometric measurements of uranium isotope ratios. Nucl. Instrum. Methods Phys. Res. Sect. B 268, 2535–2538.
Sprinkle Jr., J.K., Christiansen, A., Cole, R., Collins, M.L., Hsue, S.T., Knepper, P.L., McKown, T.O., Siebelist, R., 1997. Low-resolution gamma-ray measurements of uranium enrichment. Appl. Radiat. Isot. 48, 1525–1528.
Waters, L.S. (Ed.), 2002. MCNPX User's Manual, Version 2.3.0, Los Alamos National Laboratory Report LA-UR-02-2607.

Paper II

Applied Radiation and Isotopes 99 (2015) 162–167

Contents lists available at ScienceDirect

Applied Radiation and Isotopes

journal homepage: www.elsevier.com/locate/apradiso

Characterization of strong ^{241}Am sources

Anna Vesterlund [a,d,*], Dina Chernikova [b], Petty Cartemo [b], Kåre Axell [b,c], Anders Nordlund [b], Gunnar Skarnemark [d], Christian Ekberg [d], Henrik Ramebäck [a,d]

[a] Swedish Defence Research Agency, FOI, Division of CBRN Defence and Security, 901 82 Umeå, Sweden
[b] Chalmers University of Technology, Department of Applied Physics, Nuclear Engineering, Göteborg, Sweden
[c] Swedish Radiation Safety Authority, Stockholm, Sweden
[d] Chalmers University of Technology, Department of Chemical and Biological Engineering, Nuclear Chemistry, Göteborg, Sweden

HIGHLIGHTS

- Age and impurities can be used as a signature for ^{241}Am sources.
- Nuclear reactions take place in sources with low Z impurities.
- Some sources contain ^{243}Am as an impurity.

ARTICLE INFO

Article history:
Received 23 January 2015
Accepted 2 March 2015
Available online 3 March 2015

Keywords:
^{241}Am
Nuclear forensics
Impurities
Signatures
Age
Gamma spectrometry

ABSTRACT

Gamma ray spectra of strong ^{241}Am sources may reveal information about the source composition as there may be other radioactive nuclides such as progeny and radioactive impurities present. In this work the possibility to use gamma spectrometry to identify inherent signatures in ^{241}Am sources in order to differentiate sources from each other, is investigated. The studied signatures are age, *i.e.* time passed since last chemical separation, and presence of impurities. The spectra of some sources show a number of Doppler broadened peaks in the spectrum which indicate the presence of nuclear reactions on light elements within the sources. The results show that the investigated sources can be differentiated between by age and/or presence of impurities. These spectral features would be useful information in a national nuclear forensics library (NNFL) in cases when the visual information on the source, *e.g.* the source number, is unavailable.

1. Introduction

Nuclear forensic science is an important tool for combating illicit trafficking of nuclear material as well as other criminal activities related to nuclear and other radioactive materials. Nuclear forensic investigations commonly include characterization of nuclear material and other radioactive materials such as isotope ratio measurements, age determination (*i.e.* time passed since last chemical separation), impurity measurements and physical characterization (Wallenius et al., 2006; Kristo, Tumey, 2013; Stanley et al., 2013). Traditionally, the nuclear material investigated is uranium or plutonium but there are also other nuclides, such as ^{241}Am, that are fissionable and hence regarded as an alternative nuclear material (IAEA, 2002). ^{241}Am is a radionuclide that can be used in other contexts as well, such as ionizing smoke detectors where ^{241}Am is used in small amounts (about 30 kBq in the small ones). Stronger ^{241}Am sources are used in industrial gauging applications and in combination with low Z elements such as beryllium or lithium, ^{241}Am can be used as a neutron source. However, the useful applications of ^{241}Am in society also entails that the sources may be susceptible to theft or other illegal activities. The Code of Conduct on the Safety and Security of Radioactive Sources (2004) states that every State should establish a national register of radioactive sources and further, that the State should ensure that radioactive sources are identifiable and traceable, or when this is not practicable, ensure that there are alternative processes for identifying and tracing sources. One way of keeping track of sources is by building national nuclear forensics libraries (NNFL) where information about radioactive sources and nuclear material in a State is kept in order to track the origin of a source when necessary. The information may, besides visual information

* Corresponding author at: Swedish Defence Research Agency, FOI, Division of CBRN Defence and Security, 901 82 Umeå, Sweden.
E-mail address: anna.vesterlund@foi.se (A. Vesterlund).

http://dx.doi.org/10.1016/j.apradiso.2015.03.002
0969-8043/

and serial numbers, be information inherent in the source, *i.e.* the signatures described above.

Some work has been done to gather information that can be used as signatures for ^{241}Am. Gehrke and East (2000) determined the age of an ^{241}Am source by looking at the ratio between ^{241}Am and ^{233}Pa, the progeny of ^{241}Am. Another possibility of inherent signatures in strong alpha emitting sources is to measure *e.g.* emitted gamma photons from nuclear reactions taking place within the source. A number of papers and reports have been studying the alpha induced gamma rays from nuclear reactions on light elements (Lappalainen et al., 1983; Sastri and Schelhaas, 1985; Fazzari et al., 2003; Martin, 1975). These reactions occur when a strong alpha emitter is in close contact with light elements, *e.g.* fluorine, sodium, aluminum or magnesium. The low Z elements may be present as a part of the encapsulation of the source or as impurities within the source. The alpha particles will react with a low Z nucleus which in turn may emit a neutron or a proton. The resulting nucleus de-excites or decays resulting in emission of characteristic gamma rays. Moreover, other radionuclides may also be present as impurities, which could be measured and quantified relative to the main radioactive component of the source.

The aim of this work was to investigate the possibility of using gamma spectrometry to find inherent signatures in order to discriminate between different ^{241}Am sources in cases when visual signatures may not be accessible. A number of high activity ^{241}Am sources were measured using gamma spectrometry and the spectra were compared for possible signatures. During the initial gamma measurements, instead of identifying the material as ^{241}Am, the automatic identification of the instrument indicated that the measured material was plutonium due to the presence of neutrons together with ^{241}Am. The investigated signatures were age and impurities in the form of both radioactive nuclides and stable elements. Furthermore, Monte Carlo simulations have been used to clarify and explain the origin of the impurities seen in the gamma spectra.

2. Experimental

2.1. Source description and Monte Carlo model

Five sources were studied, of which two sources were apparently similar by visual inspection. The sources and measurement conditions were as follows:

- Source 1: Nominal activity 185 GBq ^{241}Am, sealed source contained in a lead shield during gamma spectrometric measurement.
- Source 2: Nominal activity 185 GBq ^{241}Am, sealed source contained in a lead shield during gamma spectrometric measurement.
- Source 3: Nominal activity 3.7 GBq ^{241}Am, sealed source measured with 1.10 mm Cd shielding.
- Source 4: Electroplated ^{241}Am source.
- Source 5: Smoke detector.

In order to evaluate the range of de-excitation time for nuclei excited due to nuclear reactions in an ^{241}Am source for nuclei with different initial energies, MCNPX+SRIM simulations were performed (Pelowitz, 2011; Ziegler and Biersack, 2014). The model used in the Monte Carlo simulations had the same geometrical parameters and material composition as Source 1 and Source 2. The dimensions of these sources can be found in Fig. 1. The total mass of each source was 68 g assuming a gross density of approximately 6.8 g/cm^3.

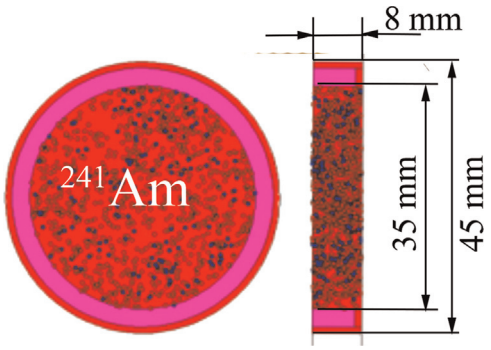

Fig. 1. Dimensions of Sources 1 and 2.

2.2. Gamma spectrometry and intrinsic efficiency calibration

Sources 1–4 were measured at a distance of about 30 cm using a p-type coaxial high purity germanium detector (Detective-EX, EG&G Ortec, Oak Ridge, TN, USA) which has a relative efficiency of about 15% and a resolution of 2.5 keV at 1332 keV. In addition, Source 5, the smoke detector, was measured for comparison. This spectrum was acquired with a p-type coaxial HPGe detector (EG&G Ortec, Oak Ridge, TN, USA) having a relative efficiency of 50% and a resolution of 2.0 keV at 1332 keV. The smoke detector was placed in a lead-shielded laboratory setup and measured for about one week. In order to characterize the response of these particular measurements, intrinsic response functions were established using a number of ^{241}Am gamma lines covering the energies from 59.5 to 801.9 keV and the response curves, *i.e.* the relative efficiency, were fitted to the following empirical polynomial previously published by Ramebäck et al. (2010):

$$\Psi = e^{c1+\frac{c2}{E^2}+c3(\ln(E))^2+c4(\ln(E))^3+\frac{c5}{E}} \quad (1)$$

Using the response curve, the activity of ^{233}Pa relative to ^{241}Am could be calculated and furthermore, the age of the source could be determined as well as the level of impurities (normalized to the activity of ^{241}Am). All spectra had the background subtracted prior to evaluation. The ^{241}Am gamma lines that were used for the intrinsic calibration and the following age determination can be found in Table 1.

2.3. Neutron measurements

As a part of evaluation, Source 1 was measured with two liquid

Table 1
Gamma energies with corresponding photon emission probabilities used for the intrinsic calibration and the age determination. Data are taken from Decay Data Evaluation Project (2013).

	E_γ [keV]	I_γ [%]
^{241}Am	59.5	35.92
^{241}Am	103.0	0.0195
^{241}Am	125.3	0.0041
^{241}Am	208.0	0.000786
^{233}Pa	300.1	6.6
^{233}Pa	311.9	38.3
^{241}Am	322.6	0.000151
^{233}Pa	340.5	4.47
^{241}Am	376.7	0.000137
^{241}Am	383.8	0.0000281
^{233}Pa	398.5	1.408
^{241}Am	619.0	0.000060
^{241}Am	662.4	0.000367
^{241}Am	722.0	0.000196
^{241}Am	801.9	0.0000012

scintillation detectors of EJ-309 type (76×76 mm^2, ELJEN TECHNOLOGY, TX 79556, USA), in order to identify the presence of neutrons. Afterwards, the neutron emission from this source was evaluated and quantified in the same setup. During the measurements, the PMTs of the liquid scintillation detectors were connected to a VX1720 CAEN digitizer (8 Channel, 12 bit, 250 MS/s Digitizer, CAEN S.p.A., Viareggio (LU), Italy).

2.4. Age determination

The time that has passed since the last chemical separation is referred to as the age of a nuclear or other radioactive material. The age can be assessed by measuring the relation between the mother nuclide and its progeny. Radioactive decay can be described according to:

$$X_1 \xrightarrow{\lambda 1} X_2 \xrightarrow{\lambda 2} X_3 \xrightarrow{\lambda 3}_{\ldots} \quad (2)$$

where λ_i is the decay constant for nuclide X_i. The age of a material, t, can be calculated according to

$$t = \frac{1}{\lambda_1 - \lambda_2} \cdot \ln\left(1 - \left(\frac{\lambda_2}{\lambda_1} - 1\right)\frac{N_2}{N_1}\right) \quad (3)$$

where N_i is the number of atoms of nuclide X_i. Therefore, by measuring the activity of the mother and daughter nuclides the number of atoms and hence the age can be calculated using the well-known relation

$$A_i = N_i \lambda_i \quad (4)$$

where A_i is the activity of nuclide X_i. ^{241}Am decays according to:

$$^{241}\mathrm{Am} \rightarrow {}^{237}\mathrm{Np} \rightarrow {}^{233}\mathrm{Pa} \rightarrow \ldots \quad (5)$$

However, the photon emission probabilities for the ^{237}Np gamma lines are too low to be used for age determination of ^{241}Am. Fortunately, the daughter of ^{237}Np, ^{233}Pa, has substantially higher photon emission probabilities and is also short-lived in comparison and will therefore reach secular equilibrium with ^{237}Np within a few months. Therefore, the activity of ^{233}Pa is the same as the activity of ^{237}Np and can be used for age determination of the material. The half-lives of ^{241}Am, ^{237}Np and ^{233}Pa are 432.6 years, 2.144 million years and 26.98 days, respectively (DDEP, 2013).

3. Results and discussion

The resulting response curve, using the gamma lines for ^{241}Am in Table 1 and Eq. (1), for one of the sources is shown in Fig. 2.

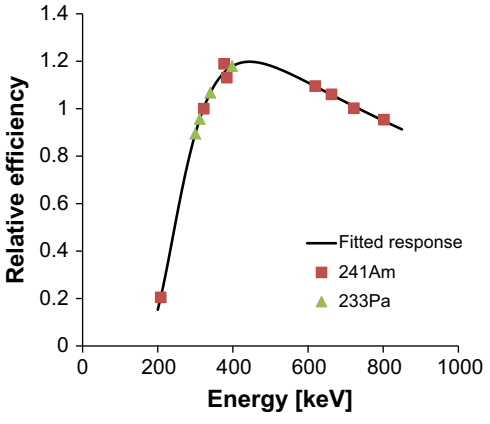

Fig. 2. Fitted response curve for Source 1. The squares are data from ^{241}Am peaks used for the fit, and the triangles are estimated responses for the peaks of ^{233}Pa.

Table 2
Results from the age determination of the different sources. The separation dates are derived from the calculated ages. Uncertainties are presented with a coverage factor $k=2$, which corresponds to an approximate 95% confidence interval.

Source	Age [y]	*Uc* [y] $k=2$	*Separation date*
Source 1	31.4	2.0	1982–01–06
Source 2	40.8	2.6	1972–07–18
Source 3	43.9	3.6	1969–07–06
Source 4	12.2	2.3	2001–06–25
Source 5	21.5	6.9	1985–07–09

The calculated ages of the sources are presented in Table 2. The 322.6 keV ^{241}Am line and the 311.9 keV gamma line of ^{233}Pa were used for the age determination. The combined uncertainty includes uncertainties in decay constants, photon emission probabilities, counting statistics and the fitted response. The uncertainty of the response function was estimated using the jackknife procedure (Ramebäck et al., 2010). All uncertainties were evaluated according to ISO: Guide to the Expression of Uncertainty in Measurement (1995) (ISO/GUM) and the results are presented with a coverage factor $k=2$, unless otherwise stated, which corresponds to an approximate 95% confidence interval. The age of Source 4 was known, the separation and the subsequent electroplating was performed in 2001, which is in good agreement with the measured age.

The gamma spectra of Sources 1–3 have a number of peaks that cannot originate from ^{241}Am. These energies together with their suggested reactions are presented in Fig. 4. Many of these peaks do not have a Gaussian shape but consist of two components, one that is narrow and one that is broadened at the base of the peak. This, so called Doppler broadening, occurs when *e.g.* an atom captures a particle and the formed atom is in motion but is slowing down in the surrounding medium and de-excites before it comes to rest. Fig. 3 shows a comparison between a normal peak and Doppler broadened peaks. This is in itself an indication that there are other, light, elements present and that there are nuclear reactions taking place within the source (Gehrke et al., 2003; Catz and Amiel, 1967). The neutron measurements confirmed the presence of neutrons in the sources even though the sources are not intended as neutron sources. The other two sources are ^{241}Am electroplated on stainless steel, and will therefore contain no significant amounts of impurities.

The deceleration time of ^{26}Mg and ^{29}Si nuclei in an ^{241}Am source was calculated to vary from approx. 400 fs to 500 fs for ^{26}Mg and from approx. 350 fs to 450 fs for ^{29}Si. The half-lives of the suggested nuclear reaction products can also be seen in Fig. 4. The de-excitation half-lives shorter than approx. 500 fs may therefore be expected to add a Doppler broadened component to the peak. The peak broadening in the examined spectra is, however, most prominent in the largest peaks, i.e. 1129 keV, 1779 keV and 1809 keV.

The analysis results of some of the peaks in the spectra, obtained by gamma spectrometric measurements led to the conclusion that ^{23}Na impurities are present in Sources 1, 2 and 3, as shown in Fig. 4. The matrix of these sources might be a fused glass which would explain the presence of sodium. There are also indications of reactions on ^{26}Mg in the gamma spectra. The ^{26}Mg may originate either from build-up due to the ^{23}Na(α,p)^{26}Mg nuclear reaction or from magnesium of natural composition embedded in the source as either an impurity or part of the encapsulation. There are some peaks in the spectra that can be derived from the other stable magnesium isotopes. These energies are, however, not exclusive to magnesium and it is therefore difficult to establish the origin of magnesium.

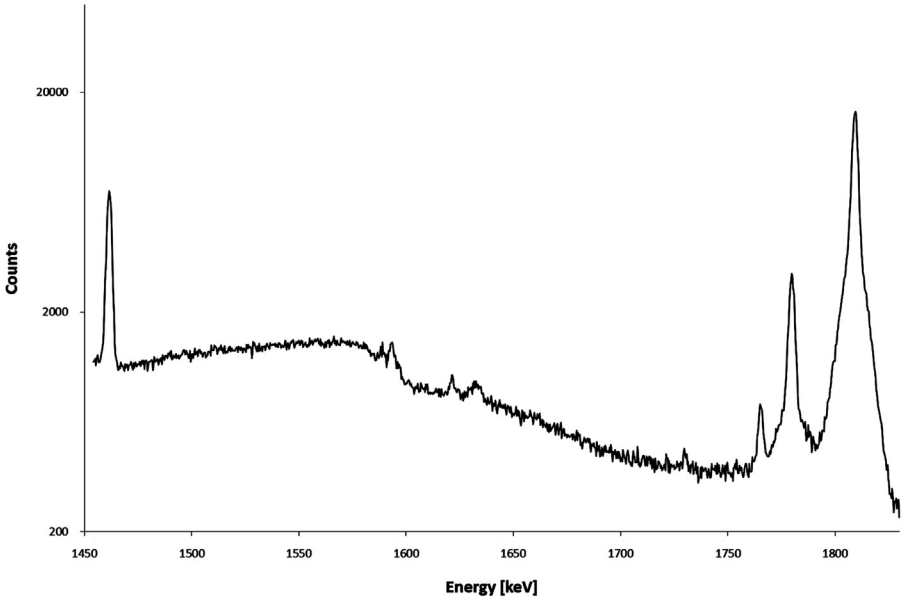

Fig. 3. Comparison of a non-Doppler broadened peak (^{40}K at 1461 keV) and the Doppler broadened peaks at 1779 and 1808 keV.

Another possible low Z element present is aluminum. The gamma lines at 709 keV, 844 and 1014 keV could point towards the existence of ^{27}Al within the source (Giles and Peisach, 1979). However, as shown in Fig. 4, the two latter lines may also indicate reactions on magnesium. The 709 keV line is also an ^{241}Am gamma line. Abdul-Hadi (1998) has published gamma lines from measurements of intense ^{241}Am sources. Some of the lines presented had never before been published. Two of these lines were 844 and 1014 keV. Later, these gamma lines were refuted with the explanation that the lines also could be the result of ^{27}Al(α,α′)^{27}Al reactions (Gehrke, 2000). There are also other explanations to these lines, see Fig. 4. It is therefore difficult to draw conclusions on whether ^{27}Al is present or not, or whether ^{27}Al is present as a part of the encapsulation or has been built up over a long period of time via the reactions ^{23}Na(α,γ)^{27}Al* and ^{26}Mg(p,γ)^{27}Al*. A further obstruction to concluding the presence of aluminum is that the largest peak from nuclear reactions on aluminum at 2235 keV, originating from the reaction ^{27}Al(α,p)^{30}Si* is too small compared to other peaks (Giles and Peisach, 1979). This investigation shows that it is rather difficult to understand the origin and composition of the low Z gamma lines. However, it is important to remember that the peaks still can be used as discriminators when the aim is to differentiate sources. It is likely that the impurity composition may vary depending on the material used to construct the source.

At 440 keV there is a peak that can be assigned to the ^{23}Na(α,α′)^{23}Na-reaction. To estimate the concentration of the sodium impurity, the ratio between the relative activities at 440 and 619 keV was calculated according to

$$R_{440/619} = \frac{S_{440}/\Psi_{440}}{S_{619}/\Psi_{619}} \quad (6)$$

where S_E is the peak area at energy E. The peak at 440 keV is interfered by two gamma lines from ^{241}Am. These areas were subtracted using the peak area at 619 keV. Table 3 shows the results of the calculations.

Source 1 and Source 2 have the same nominal activity. However, the ratios $R_{440/619}$ differ significantly. This may imply that the amount of sodium in Source 2 is higher than in Source 1 and this information could be used as a signature of the sources. Source 3 shows a higher ratio than the two other sources. One reason for this may be that the activity, *i.e.* the alpha particle flux, of source 1 and 2 are 50 times higher than source 3. This could imply that the sodium content in source 3 could be higher due to possible lower sodium depletion. Another explanation could be that the initial sodium content was significantly higher. The difference between Source 2 and 3 are, however, not statistically significant. One concern which needs to be considered is whether the $R_{440/619}$-ratio is constant or changes over time. It is possible that either the amount of sodium in the source decreases over time as ^{26}Mg is formed in the (α,p)-reaction or that the change in sodium concentration over time is minute and therefore can be considered constant. This is, however, a subject for future studies.

In the spectra for Source 1 and Source 3, peaks of ^{239}Np can be identified. This could imply that these sources contain ^{243}Am as an impurity, since ^{239}Np is the daughter of ^{243}Am. The gamma lines of ^{243}Am are too weak to be measured directly in these sources with gamma spectrometry. However, as shown in Fig. 5, the spectrum of Source 2 does not contain peaks originating from ^{239}Np. Since the half-life of ^{239}Np is 2.356 days, ^{239}Np is in secular equilibrium with ^{243}Am; the ^{243}Am/^{241}Am ratio can therefore be calculated. The ^{243}Am/^{241}Am-ratio is $1.444(48)\times10^{-6}$ and $2.09(11)\times10^{-7}$ for Source 1 and Source 3, respectively, where the numbers in parentheses, which are the numerical values of the combined uncertainty, refer to the corresponding last digits of the quoted results.

4. Conclusions

In this paper we have shown that it is possible to distinguish between the five ^{241}Am sources that were investigated using gamma spectrometry. The age of the sources was the first discriminator investigated. By age determination, three of the sources could easily be discriminated between, while two have approximately the same age. The two latter sources could, however, be separated due to the fact that one of the sources contain measurable amounts of ^{239}Np, indicating the presence of ^{243}Am within the source. Another investigated signature may be the relation between the 440 keV peak originating from the ^{23}Na(α,α′)^{23}Na* reaction and the 619 keV ^{241}Am peak. This ratio may be an

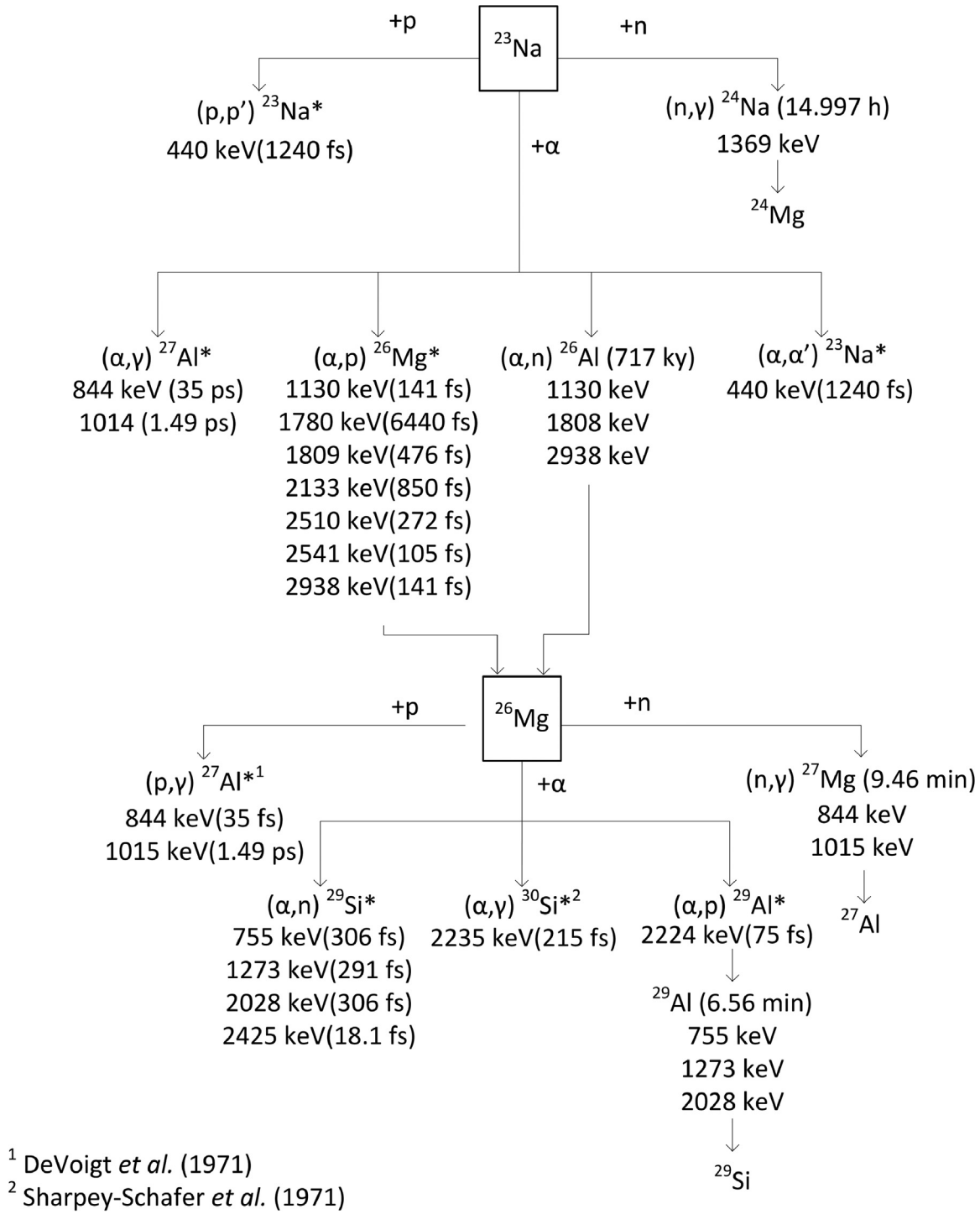

Fig. 4. Identified gamma lines from nuclides other than ^{241}Am and its progeny, and suggested reactions based on impurities. The nuclides with an asterisk are emitting gamma rays due to de-excitation. The reference to the gamma lines and corresponding half-lives are taken from the Nudat 2.6 database (2014) unless otherwise stated (De Voigt et al., 1971; Sharpey-Schafer et al., 1971).

Table 3
Ratios of efficiency corrected peak areas at 440 and 619 keV. Uncertainties are presented with a coverage factor $k=2$, which corresponds to an approximate 95% confidence interval.

	$R_{440/619}$	U_c, $k=2$
Source 1	0.1854	0.0098
Source 2	0.260	0.014
Source 3	0.286	0.056

indicator of the relative amount of sodium present in the source. Also, the lack of impurities may in itself be a signature. If these signatures were evaluated for individual ^{241}Am sources and this information was put in a library consisting of indigenous ^{241}Am sources, the information could be useful when visual information of the sources is unavailable, for example in an investigation of attribution of an orphan source, or in a nuclear forensic investigation.

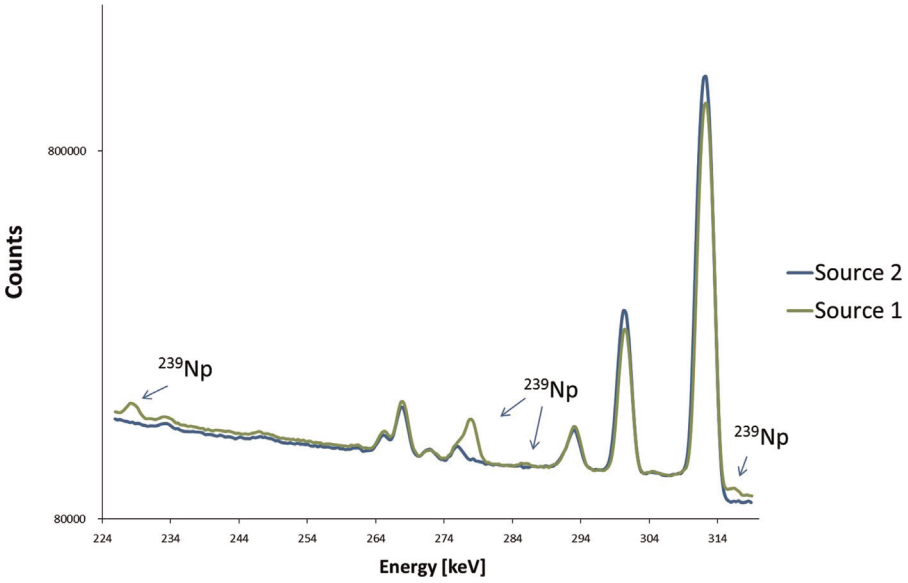

Fig. 5. Excerpt of spectra of Sources 1 and 2.

Acknowledgment

The Swedish Radiation Safety Authority, SSM (4047012-20), and the Swedish Ministry of Defence (A4043) are gratefully acknowledged for funding this work. The authors would also like to thank Stina Holmgren for valuable help with figures.

References

Abdul-Hadi, A., 1998. Gamma-spectrum of ^{241}Am. J. Radioanal. Nucl. Chem. 231, 147–152.

Code of Conduct on the Safety and Security of Radioactive Sources, 2004. IAEA/CODEOC/2004, Vienna, Austria.

Catz, A.L., Amiel, S., 1967. Study of lifetimes of nuclear levels by Doppler broadening attenuation using a Ge(Li) gamma-ray spectrometer. Nucl. Phys. A 92, 222–232.

Decay Data Evaluation Project (DDEP), 2013, ⟨http://www.nucleide.org/DDEP_WG/DDEPdata.htm⟩.

De Voigt, M.J.A., Maas, J.W., Veenhof, D., Van Der Leun, C., 1971. The reaction ^{23}Na(α,γ)^{27}Al (I). Yield curve, excitation energies and branchings of ^{27}Al levels. Nucl. Phys. A 170, 449–466.

Fazzari, D.M., Jones, S.A., Delegard, C.H., 2003. Application of Prompt Gamma-ray Analysis to Identify Electrorefining Salt-bearing Plutonium Oxide at the Plutonium Finishing Plant. PNNL-14409, Richland, Washington.

Gehrke, R.J., East, L.V., 2000. Information in spectra from sources containing "aged" ^{241}Am as from TRU waste. Waste Manag. 20, 555–559.

Gehrke, R.J., 2000. Artifact (α, x) reaction gamma-ray peaks reported as ^{241}Am decay gamma-rays; comments to the paper by Abdulrahman Abdul-Hadi. J. Radioanal. Nucl. Chem. 246, 449–450.

Gehrke, R.J., Baker, J.D., Hartwell, J.K., Riddle, C.L., McGrath, C.A., 2003. Measurement of neutron-to-γ-ray production ratios from (α,n) reactions for their application to assay TRU waste. Nucl. Instr. Meth. Phys. Res. A 511, 444–456.

Giles, I.S., Peisach, M., 1979. A survey of the analytical significance of prompt gamma-rays induced by 5 MeV alpha-particles. J Radioanal Chem 50, 307–360.

IAEA Safeguards Glossary, 2002, 2001 Edition, International Nuclear Verification Series no. 3, Vienna, Austria.

ISO: Guide to the Expression of Uncertainty in Measurement, 1995. International Organisation for Standardisation, Geneva, Switzerland.

Kristo, M.J., Tumey, S.J., 2013. The state of nuclear forensics. Nucl. Instrum. Methods Phys. Res. B 294, 656–661.

Lappalainen, R., Anttila, A., Räisänen, J., 1983. Absolute α-induced thick-target gamma-ray yields for the elemental analysis of light elements. Nucl. Instrum. Methods Phys. Res. 212, 441–444.

Martin, H.R., 1975. Reaction Gamma Rays in Plutonium Compounds, Mixtures, and Alloys, RFP-2382. DOW Chemical U.S.A, Rocky Flats Division, Golden, Colorado.

NuDat 2.6 database, 2014. National Nuclear Data Center. Brookhaven National Laboratory, Los Alamos, USA.

Pelowitz, D.B., 2011. MCNPX User's Manual, Version 2.7.0, LA-CP-11-00438. Los Alamos National Laboratory.

Ramebäck, H., Vesterlund, A., Tovedal, A., Nygren, U., Wallberg, L., Holm, E., Ekberg, C., Skarnemark, G., 2010. The jackknife as an approach for uncertainty assessment in gamma spectrometric measurements of uranium isotope ratios. Nucl. Instrum. Methods Phys. Res. B 268, 2535–2538.

Sastri, C.S., Schelhaas, K.P., 1985. Analytical use of alpha-source induced gamma-ray emission. Fresenius Z. Anal. Chem. 321, 739–747.

Sharpey-Schafer, J.F., Alderson, P.R., Bailey, D.C., Durell, J.L., Greene, M.W., James, A. N., 1971. Lifetimes and decays of energy levels in ^{30}Si and ^{30}P. Nucl. Phys. A 167, 602–624.

Stanley, F., Stalcup, A.M., Spitz, H.B., 2013. A brief introduction to analytical methods in nuclear forensics. J. Radioanal. Nucl. Chem. 295, 1385–1393.

Wallenius, M., Mayer, K., Ray, I., 2006. Nuclear forensic investigations: Two case studies. Forensic Sci. Int. 156, 55–62.

Ziegler, J.F., Biersack, J.P., 2014. SRIM: The Stopping and Range of Ions in Matter. IBM-Research, Yorktown.

Paper III

Journal of Radioanalytical and Nuclear Chemistry (2019) 321:723–731
https://doi.org/10.1007/s10967-019-06623-5

Avoiding polyatomic interferences in measurements of lanthanides in uranium material for nuclear forensic purposes

Anna Vesterlund[1,2] · **Henrik Ramebäck**[1,2]

Received: 28 April 2019 / Published online: 20 June 2019

Abstract
Measurements of the lanthanide series with ICP-SF-MS provide low detection limits but suffer from oxides of the lighter lanthanides interfering on the heavier ones. In this work, two different methods to measure the lanthanide series without interferences, were investigated and compared to measuring the lanthanides directly with a standard sample introduction system. It is shown that by using a desolvating sample introduction system during measurements, the impact of polyatomic interferences are eliminated. It is also shown that using chemical separations to separate the elements in the lanthanide series into three fractions almost eliminates polyatomic interferences, while direct measurements with a standard sample introduction system may lead to inaccurate results due to interferences.

Keywords Nuclear forensics · Uranium · Lanthanides · ICP-MS

Introduction

Nuclear forensics is a scientific discipline that aims to aid in criminal investigations concerning illicit trafficking and use of nuclear material or other radioactive substances. The ultimate goal with an investigation is to find the origin and the intended use of the seized material. Nuclear forensics combine a number of methods to establish an attribution of nuclear or other radioactive material. Lanthanide patterns have proven to be a promising signature for determination of the geographical origin of uranium for nuclear forensic purposes [1–3]. The lanthanides are a series of rare elements which share similar chemical and physical properties and therefore maintain the same relative composition compared to each other even though the material undergo various chemical processes, such as uranium ore processing [4]. Another use for lanthanide patterns is material provenance in nuclear safeguards, where the aim is to confirm that the origin of declared nuclear material is consistent with the actual material [5].

✉ Anna Vesterlund
anna.vesterlund@foi.se

[1] CBRN Defence and Security, Swedish Defence Research Agency (FOI), Cementvägen 20, 901 82 Umeå, Sweden

[2] Department of Chemistry and Chemical Engineering, Nuclear Chemistry, Chalmers University of Technology, 412 96 Göteborg, Sweden

The concentrations of the lanthanides are generally low in uranium material that has undergone various processes such as uranium ore processing to obtain nuclear fuel; therefore, a measurement technique with low detection limits, such as mass spectrometry, is needed. However, by using mass spectrometry, the concentrated uranium matrix may cause matrix effects resulting in decreased measurement sensitivity that, in turn, may increase the detection limits. The high amount of uranium introduced into the instrument may also cause memory effects, i.e. high uranium backgrounds that may be hard to eliminate. This might be an important factor if the same instrument is also used for uranium isotopic measurements. Varga et al. [6] proposed a method for group separation of the lanthanide series to remove uranium and barium from the samples using the TRU resin followed by lanthanide measurements using inductively coupled plasma-sector field-mass spectrometry (ICP-SF-MS). However, another problem with performing accurate lanthanide measurements by mass spectrometry is that some of the lanthanides, especially the lighter ones such as cerium and praseodymium, are prone to oxide formation in the plasma, causing polyatomic interferences at a higher mass [7]. This means that, for example, $^{143}Nd^{16}O^{+}$ will interfere with $^{159}Tb^{+}$, which may lead to an overestimation of the amount of terbium. The higher the concentrations of the lighter lanthanides are compared to the heavier lanthanides, the larger the overestimation.

In nuclear forensics, it is important that the accuracy and precision are maximized, in other words, it is important that the measurement uncertainties are well-understood and fit-for-purpose to make comparisons between materials useful [8, 9]. Therefore, an overestimation of certain elements may be detrimental to the use of a measurement result. Attempts have been made to correct for these interferences mathematically [10, 11] but this approach may lead to large measurement uncertainties if the correction is large compared to the analyte in question and may require extensive measurements each day of analysis [12]. Funderberg et al. [13] presented a method for measuring the lanthanide series using medium-resolution LA-ICP-MS (laser ablation ICP-MS) which allows for peak deconvolution of the polyatomic interferences from the analytes. However, the method did not resolve the interference of $^{143}Nd^{16}O^{+}$ on $^{159}Tb^{+}$. The resolution needed to resolve these peaks is approx. 7700. Another downside with using medium or high mass resolution is that the sensitivity decreases significantly compared to low resolution and therefore results in higher detection limits [14]. Groopman et al. [15] presented the secondary ion mass spectrometry-single stage accelerator mass spectrometry (SIMS-SSAMS) as an excellent instrument for providing interference-free lanthanide patterns at low concentrations. However, SIMS-SSAMS is a rare technique and therefore there is a need for other, much more available, mass spectrometric techniques for low concentration element measurements. Inductively coupled plasma-mass spectrometry (ICP-MS) is a widespread, multi-elemental technique that is suitable for the purpose due to low detection limits for these elements. Even though many of the lanthanides have many isotopes, there is at least one isotope for each lanthanide free of isobaric interferences, but still the oxides, hydroxides and hydrides resulting in polyatomic interferences pose a problem.

The aim of this work was to examine the possibilities to measure the lanthanide series using ICP-SF-MS without interferences of oxides, hydroxides and hydrides. Two methods for minimizing the impact of oxides during measurements have been compared to conventional measurements without attempts to minimize the oxide impact on the results. The first method was to use a desolvating sample introduction system that dries the sample before it enters the plasma and therefore the oxide and hydride formation is kept at a minimum. The second method was to chemically separate the elements in the lanthanide series in such a way that the lighter elements are separated from the heavier elements during the measurement. A chemical separation method was developed for this purpose. The separation method also removes most of the uranium from the samples, making it possible to investigate the lanthanide pattern in materials with very low lanthanide concentrations, without risking contamination of the instrument with high amounts of uranium.

Experimental

All plasticware was acid-washed prior to use and all nitric acid used was in-house sub-boiled.

Reference materials REE-2 and CUP-2 (both Canmet-MINING, Ottawa, Canada) were used for the study. REE-2 is a reference material certified for concentration of most lanthanides. CUP-2 is a uranium ore concentrate, which contains low, but uncertified amounts of lanthanides.

Dissolution of reference materials

CUP-2 was dissolved by microwave digestion (Mars 5, CEM Corporation, Matthews, US). 0.2 g was put in a Teflon tube. 9 mL concentrated HNO_3 + 0.09 mol L^{-1} HF (Suprapur, Merck KGaA, Darmstadt, Germany) was added together with 1 mL ultrapure water with 18.2 MΩ cm resistivity at 25 °C (Milli-Q, Merck KGaA, Darmstadt, Germany). The sample was digested by ramping the temperature to 180 °C for 20 min and holding at that temperature for 15 min. After digestion, the sample was transferred to a bottle and the sample was diluted to a concentration of about 10 mg U g^{-1} solution.

REE-2 was dissolved by lithium borate fusion due to incomplete dissolution using microwave digestion. 1 g of REE-2 was put in a carbon crucible together with 3 g $LiBO_2$ (Ultrapure, Claisse, Quebec, Canada). The sample was pre-oxidised for 2 h at 650 °C before fusing at 1050 °C for 15 min. The fused sample was dissolved in 100 mL 10% HNO_3 while heating. After the sample had been dissolved, 0.4 g of polyethylene glycol (PEG-2000, Alfa Aesar, Karlsruhe, Germany) was added to flocculate silica and the solution was evaporated to approximately 50 mL. The solution was left over night to let the slow silica flocculation progress. The solution was thereafter filtered through a filter paper with pore size 8–10 µm (Munktell OOM, Alstrom Munksjö, Helsinki, Finland) and diluted in 1 mol L^{-1} HNO_3. Blanks were prepared in the same way as CUP-2 and REE-2, respectively.

Chemical separations

For the separated samples, an aliquot was taken from the working solution. The sample was either diluted with Milli-Q water to a concentration of 0.05 mol L^{-1} HNO_3 or evaporated and dissolved in 2 mL 0.05 mol L^{-1} HNO_3. For yield determination, a second sample was prepared for each sample by adding a known amount of a lanthanide multi-element solution. For the REE-2 reference material, containing only low amounts of uranium, 1 mg of uranium was added to each sample prior to the separation in order to mimic a uranium-rich material. Method blanks were prepared in the same manner.

Two milliliter of Ln resin (di(2-ethylhexyl) orthophosphoric acid, HDEHP) was added to a 2 mL separation column (resin and separation column both from Triskem International, Bruz, France). The column was rinsed with 2×2.5 mL 10 mol L^{-1} HNO_3 to remove possible lanthanides in the resin, followed by 2.5 mL Milli-Q water and 3×2 mL 0.05 mol L^{-1} HNO_3. Another 2 mL 0.05 mol L^{-1} HNO_3 was added to the resin and the columns were sealed.

Prior to the separation, the columns were opened and allowed to drain. 1 mL 0.05 mol L^{-1} HNO_3 was added to the columns to condition the columns further. Thereafter the samples were added to the columns. The sample tubes were rinsed with 2×0.5 mL 0.05 mol L^{-1} HNO_3 that were added to the columns. Lanthanum to neodymium were eluted with 6 mL 0.4 mol L^{-1} HCl, samarium to gadolinium were eluted with 10 mL 0.75 mol L^{-1} HCl and terbium to lutetium were eluted with 20 mL 10 mol L^{-1} HNO_3 into Teflon beakers. All solutions were evaporated to near dryness and dissolved in 2% HNO_3 to change the solution to a more suitable matrix for ICP-MS measurements. The samples were, if needed, diluted to lanthanide concentrations less than approx. 2 ng g^{-1}.

Sample preparation

For the direct measurements, the samples were diluted so that the concentration of the lanthanides in the measurement solution was kept between 6 pg g^{-1} and 2 ng g^{-1}. An internal standard (indium, rhodium and rhenium) was added to all samples to a concentration of 1 ng g^{-1} of each element. In literature, all three elements have been chosen as internal standard for lanthanide measurements [6, 16, 17]. Initial experiments showed that the signal variation of each of the internal standards corresponded better with the signal variation of some of the lanthanides. Therefore, indium was used as internal standard for thulium, ytterbium and lutetium; rhenium was used as internal standard for terbium and dysprosium; and rhodium was used as internal standard for the rest of the lanthanide series.

Measurements

The measurements were performed on an Element2 (Thermo Fischer Scientific, Bremen, Germany). For the standard sample introduction a cyclonic spray chamber and concentric nebulizer were used (both GlassExpansion, Port Melbourne, Australia). For the measurements with a desolvating sample introduction system, a Cetac Aridus II (Teledyne Cetac Technologies, Omaha, Nebraska, US) together with a 100 µL min^{-1} C-flow nebulizer was used. The instrumental settings and measurement parameters can be found in Tables 1 and 2. The instrument was tuned with a

Table 1 Instrumental settings for the two sample introduction systems

Instrumental settings	Standard sample introduction	Desolvating sample introduction
	Twister spray chamber	Aridus II
Nebulizer	Conikal	C-flow PFA
Forward power [W]	1250	1200
Cool gas flow [L min^{-1}]	16	16
Auxiliary gas flow [L min^{-1}]	0.7	0.7
Nebulizer gas flow [L min^{-1}]	1.1	0.9
Ar Sweep gas [L min^{-1}]	N/A	3.2
Nitrogen [mL min^{-1}]	N/A	10

Table 2 Measurement parameters

Measurement parameters	
Resolution	300
Mass window	5%
Samples per peak	100
Runs and passes	100×1
Scan type	E-scan
Measured analyte isotopes	^{137}Ba, ^{139}La, ^{140}Ce, ^{141}Pr, ^{146}Nd, ^{147}Sm, ^{153}Eu, ^{157}Gd, ^{159}Tb, ^{163}Dy, ^{165}Ho, ^{167}Er, ^{169}Tm, ^{174}Yb, ^{175}Lu
Measured internal standard isotopes	^{103}Rh, ^{115}In, ^{185}Re

1 ng g^{-1} cerium standard solution to minimize the oxide formation level of cerium while maintaining high sensitivity.

For the 5-point external calibration for the measurements of the unseparated samples, a multi-element standard (Sigma Aldrich, Buchs, Switzerland) was used. For the measurements of the separated samples, three different certified standard solutions were used, containing La–Nd, Sm–Gd and Tb–Lu, respectively (Spectrascan, Inorganic Ventures, Christiansburg, USA). For quality assurance, control samples were diluted from multi-element standards of another brand (CPAchem Ltd, Stara Zagora, Bulgaria). The multi-element standards used for quality control had the same composition as the solutions used for calibration. All standard solutions used for calibration and quality assurance were certified by mass and traceable to NIST.

The dead-time was evaluated with the method proposed by Appelblad and Baxter [18] using a Lu standard solution. All data reduction and calculations were performed off-line. The external calibrations, using weighted linear regression, were carried out according to Sayago and Asuero [19] and the calculations as well as the measurement uncertainties were evaluated using a Monte Carlo method in the same manner as Ramebäck and Lindgren [20].

The uncertainties were evaluated in accordance with ISO GUM [21]. All uncertainties are, unless stated otherwise, presented with a coverage factor $k = 2$, corresponding to an approximate 95% confidence level. The measurement results were normalized using Chondrite values, see Figs. 1, 2, 3 and 4 [22].

Results and discussion

Direct measurements

The acquired pattern of the REE-2 reference material from direct measurement using a standard sample introduction system can be seen in Fig. 1. For most elements, the results agree well with the certified values. The exceptions in this case are gadolinium and terbium, which are overestimated by approx. 60% and 40%, respectively, see Table 3. The highest amount of oxide formation can be seen in lanthanum,

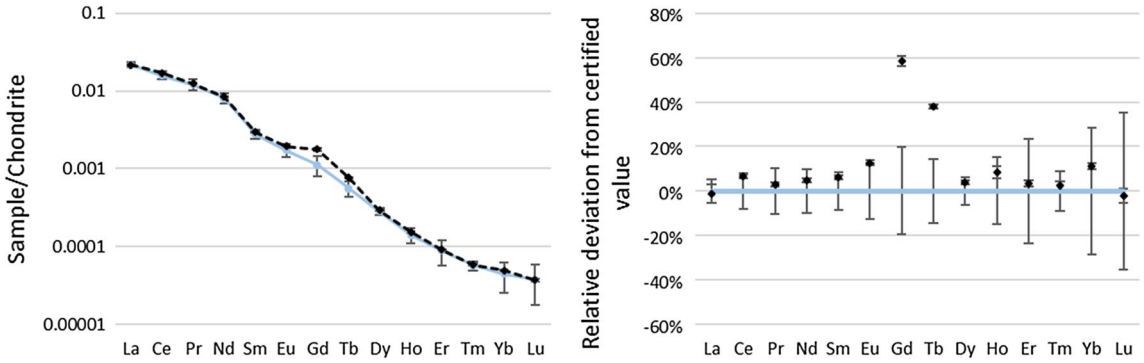

Fig. 1 Left: Comparison of the lanthanide pattern for REE-2 between certified values and results from direct measurement using a standard sample introduction system. Right: Relative deviation from the certified value. Diamonds are measured values. The continuous lines are the certified values. The uncertainty bars are, in some cases, smaller than the bullets

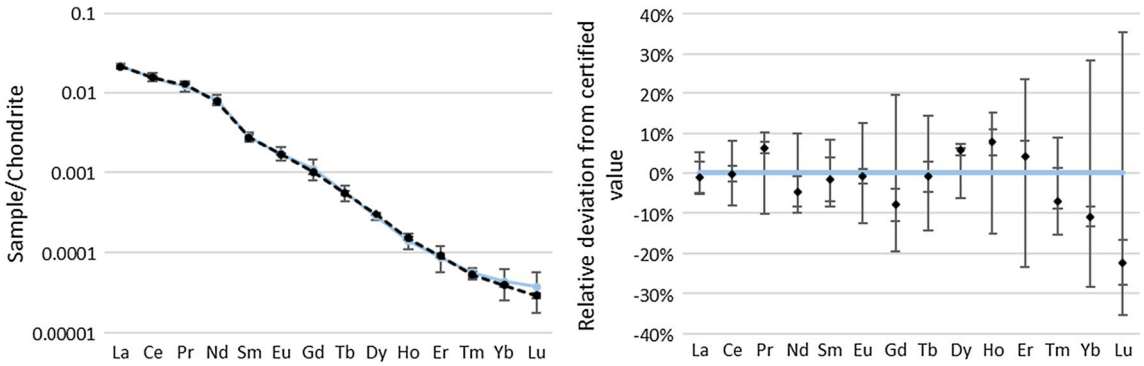

Fig. 2 Left: Comparison of the lanthanide pattern for REE-2 between certified values and measured results using a desolvating sample introduction system. Right: Relative deviation from the certified value. Diamonds are measured values. The continuous lines are the certified values. The uncertainty bars are, in some cases, smaller than the bullets

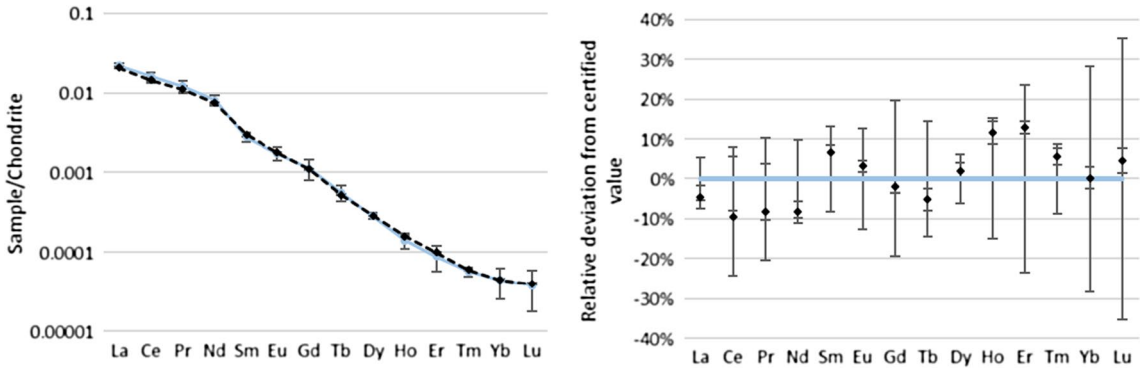

Fig. 3 Left: Comparison of the lanthanide pattern for REE-2 between certified values and measured values using a standard sample introduction system after a chemical separation. Right: Relative deviation from the certified value. Diamonds are measured values. The continuous lines are the certified values. The uncertainty bars are smaller than the bullets in some cases

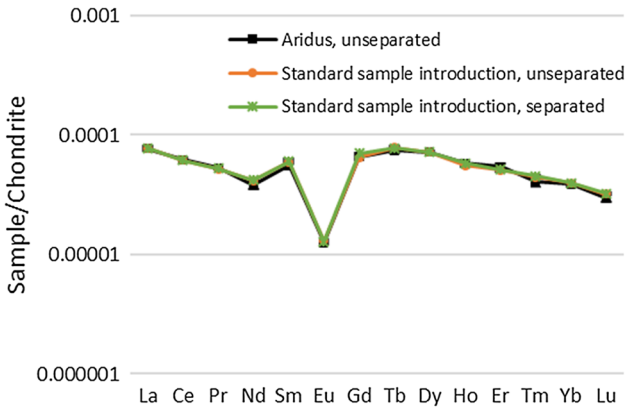

Fig. 4 Comparison of the lanthanide pattern for CUP-2 between measurements using all three methods. The uncertainty bars are smaller than the bullets in most cases

cerium, praseodymium and neodymium. Oxides of praseodymium and neodymium will therefore interfere with masses 157 and 159, for example. The CeO/Ce-ratio was approximately 2.5% at the time of measurement with the current measurement setup. The oxides of praseodymium and neodymium are expected to be lower but within the same order of magnitude [7, 23]. If the amounts of praseodymium and neodymium present in the sample are high enough compared to the amount of gadolinium and terbium, the oxides will start to interfere with the measurements of gadolinium and terbium.

Figure 2 shows the results of the direct measurements of REE-2 using a desolvating sample introduction system, compared to the certified values. At the time of measurement, the CeO-formation was approx. 0.08%. In this figure, it is clear that the interferences on gadolinium and terbium are removed; the results correspond well with the certified values.

Chemical separations

The results of the measurements of REE-2 after the chemical separation can be seen in Fig. 3. In this figure, it is evident that the interferences seen in Fig. 1 are absent. Since oxides of lighter lanthanides interfere with the heavier ones, e.g. $^{141}Pr^{16}O^{+}$ on $^{157}Gd^{+}$, it is preferable that La–Eu and Gd–Lu are measured in separate fractions. However, it has previously been shown that complete separation between Eu(III) and Gd(III) is difficult to perform in one single step using HDEHP [24–26]. Instead, a separation method including three fractions rather than two, was developed with the middle fraction containing Sm–Gd, which is more easily achieved. The separation method was developed from methods proposed previously using HDEHP as the extractant [27, 28]. By increasing the hydrochloric acid concentration, the lanthanides elute in groups. For the last elution, the acid was changed to nitric acid to avoid the elution of uranium, which will co-elute with the heavy lanthanides when high concentrations of hydrochloric acid are used [29, 30]. The mean chemical yield was (100 ± 2)% (1 sd), which is similar to the yield achieved by Varga et al. [6] using TRU resin for lanthanide group separation. The range of the chemical yield was 95% to 107%.

Other possible interferences are the oxides and hydrides from barium [7]. Performing a chemical separation of the lanthanide series using HDEHP as the extractant will also solve this problem since the Ba^{2+} ions are not extracted by HDEHP at the acid concentrations used in this work [31]. Using the desolvating sample introduction will also remove the barium hydrides and oxides in the same manner as for the lanthanides.

In Tables 3 and 4 it can be seen that the amount of the heavier elements are slightly lower when the results originate from the desolvating system compared to the standard sample introduction. This is due to interferences from the

Table 3 Results and corresponding uncertainties from mass fraction measurements of REE-2

	Certified values		Desolvating sample introduction		Standard sample introduction			
					Direct measurement		Separated samples	
	c [μg g^{-1}]	U_c $k=2$	c [μg g^{-1}]	U_c $k=2$	c [μg g^{-1}]	U_c $k=2$	c [μg g^{-1}]	U_c $k=2$
La	5130	270	5080	200	5060	210	4890	140
Ce	9610	770	9590	190	10,234	99	8700	1300
Pr	1080	110	1148	17	1111	12	990	120
Nd	3660	360	3490	130	3830	36	3356	92
Sm	410	34	404	22	435.1	4.0	438	28
Eu	97	12	95.8	1.7	108.7	1.3	99.6	1.4
Gd	219[1]	43	201.7	8.1	346.9	8.1	214.6	3.4
Tb	20.3	2.9	20.13	0.76	28.01	0.29	19.25	0.52
Dy	69.2	4.3	73.2	1.1	71.69	0.64	70.5	1.6
Ho	7.9	1.2	8.47	0.28	8.53	0.23	8.78	0.25
Er	14.0	3.3	14.60	0.56	14.46	0.22	15.81	0.25
Tm	1.38	0.12	1.29	0.11	1.415	0.026	1.461	0.030
Yb	7.2[1]	2.0	6.41	0.16	8.00	0.12	7.21	0.20
Lu	0.92[1]	0.33	0.715	0.040	0.899	0.030	0.962	0.030

[1]Provisional value

Table 4 Results and corresponding uncertainties from the mass fraction measurements of CUP-2

	Desolvating sample introduction		Standard sample introduction			
			Direct measurement		Separated samples	
	c [μg g^{-1}]	U_c $k=2$	c [μg g^{-1}]	U_c $k=2$	c [μg g^{-1}]	U_c $k=2$
La	17.87	0.57	18.02	0.59	18.13	0.24
Ce	37.27	0.63	36.81	0.41	36.80	0.72
Pr	4.674	0.069	4.579	0.032	4.629	0.069
Nd	16.97	0.91	18.56	0.21	18.67	0.35
Sm	8.11	0.40	8.66	0.10	8.78	0.43
Eu	0.701	0.014	0.723	0.014	0.711	0.016
Gd	12.73	0.51	12.61	0.25	13.66	0.20
Tb	2.68	0.10	2.832	0.035	2.80	0.11
Dy	17.17	0.24	17.35	0.18	17.29	0.33
Ho	3.20	0.11	3.066	0.076	3.177	0.080
Er	8.52	0.31	8.02	0.10	8.05	0.31
Tm	0.976	0.064	1.062	0.013	1.081	0.030
Yb	6.20	0.15	6.376	0.078	6.41	0.12
Lu	0.713	0.036	0.773	0.012	0.780	0.013

middle part of the lanthanide series. For example, $^{175}Lu^+$ is interfered by $^{159}Tb^{16}O^+$ and $^{174}Yb^+$ is interfered by $^{158}Dy^{16}O^+$ and $^{173}YbH^+$ when using the standard sample introduction system. However, the difference between measurement methods is not statistically significant, unless the concentrations of the middle lanthanides are very large in comparison to the heavier lanthanides. In this case, the oxide interference will be significant even at a low relative oxide formation level.

Figure 4 shows the results of the measurements of CUP-2 using all three methods. The pattern show close resemblance to previously published results [16]. In the figure, all results are superimposed meaning that direct measurements with a standard introduction system are good enough to achieve the same results as with separated samples or the desolvating system. The reason for this is that the difference in concentrations between elements in the lanthanide series, in this material, are too small to result in amounts of oxides that would significantly alter the measured concentrations of the heavier lanthanides. However, direct measurements of uranium rich materials will cause memory effects in the instrument, which might be a problem if the same instrument has

to be used for measuring uranium isotopics as well. Therefore, chemical separations might still be justified. In Table 4 it can be seen that the concentrations vary between approx. 40 µg g^{-1} (cerium) and 0.7 µg g^{-1} (europium and lutetium) in the CUP-2 material. For the REE-2 material, the concentrations vary between 10,000 µg g^{-1} (cerium) and 0.9 µg g^{-1} (lutetium), see Table 3.

Measurement uncertainties

In some cases, the results from the quality control samples did not correspond to the certified value. This discrepancy could not be explained in any other way than that there is a difference in concentration or underestimated uncertainty in the certified solutions used for calibration and quality control. Since it is difficult to determine which of the solutions that have the correct concentration this anomaly was addressed by adding an extra uncertainty component to the measurement model, corresponding to the uncertainty needed to force the control sample to correspond to the certified concentration of the control standard within their uncertainties:

$$c_{\mathrm{a.s}} = \left(\left(I_{\mathrm{a}} - a\right)/b\right) + \delta$$

where $c_{\mathrm{a.s}}$ is the calculated concentration of the analyte in the sample, a and b are intercept and slope, respectively, from the linear regression and I_{a} is the measured intensity of the analyte in the sample and δ is a constant with value 0 but with an uncertainty $u_{\mathrm{c}}(\delta)$. This approach ensures that the result of the measurement of the QC sample corresponds to the certified value within uncertainties at the 95% confidence level and has previously been applied on replicate samples by Kessel et al. [32] in a similar fashion.

The lowest uncertainties were achieved using direct measurement and the standard sample introduction system, since the signal stability was higher with the standard system than with the desolvating system. The highest uncertainties are calculated for the separated samples even though they are measured with the standard sample introduction system. The measurement uncertainty of the separated samples are on average around 3% ($k = 2$) with a few exceptions where the uncertainty is somewhat higher. This is mainly due to the estimation of the uncertainty in the yield determination. This estimation was done by looking at the variation of the yields for each element and adding the t-factor corresponding to the degrees of freedom, to the calculated standard deviations. Since the number of yield determinations were small, this uncertainty contribution became significant. This explains, for example, the high uncertainty of cerium in Table 3. Other important uncertainty contributions are related to the calibration and/or the addition of the uncertainty of δ to account for discrepancies in the certified reference solutions. At very low concentrations, the uncertainty of the analyte signal contributes significantly to the combined uncertainty. The level of uncertainty, however, is, in general, at the same level or even below results presented by Varga et al. [6] and Asai and Limbeck [33].

The desolvating system also suffers more from matrix effects than the standard sample introduction. In the direct measurements, the concentration of uranium was 10 µg g^{-1}. This concentration did not affect the sensitivity of the standard sample introduction to any extent, while the desolvating system suffered from an almost 50% signal suppression. This was, however, to some extent, compensated by the higher sensitivity that can be achieved with a desolvating system.

It should be mentioned that the measurements in this study does not account for inhomogeneity in the CUP-2 material. The homogeneity of REE-2 is granted when more than 0.05 g of the material is used but in the case of CUP-2 there is no such information. In case of inhomogeneous material, multiple aliquots should be dissolved and measured and the variation between lanthanide mass fractions should be included in the uncertainty budget. This, of course, means that the measurement uncertainty would increase. It should also be noted that the combined uncertainties calculated from the certificate of the REE-2 reference material are high. In some cases, the uncertainties are around 50%. This reference material is also missing certified values for gadolinium, ytterbium and lutetium. The values used in those cases are provisional values. Therefore, this reference material may be unsuitable as a reference material for nuclear forensic purposes if these elements have to be measured, but is a good example of when direct measurements with a standard sample introduction system are inappropriate.

Conclusions

This work has shown that it is possible to measure the lanthanide series with good precision and accuracy independent of the lanthanide pattern profile. Two methods have been tested with satisfying results: direct measurement of a uranium solution using a desolvating sample introduction system and measurement of separated samples using standard sample introduction. This was compared with direct measurement of a uranium solution and a standard sample introduction system. The results show that direct measurements using the standard method may result in a substantial bias in the concentration for certain elements due to oxide formation in the plasma. This means that if a laboratory has access to a desolvating sample introduction system there is a quick and easy way to obtain, essentially, interference-free lanthanide measurement data. Another advantage of the

desolvating sample introduction system is that the relative sensitivity, in general, increases compared to the normal sample introduction system.

If there is no access to a desolvating system, the other possibility to achieve interference-free measurements of the lanthanide series is to perform a chemical separation on the material to separate interfering from interfered elements and in that way avoid the oxide interferences. Another approach is to combine the desolvating sample introduction with chemical separation to remove the concentrated uranium matrix which otherwise may cause severe signal suppression in the dry plasma. This combination could provide interference-free, high sensitivity measurements of materials containing very low amounts of lanthanides.

Acknowledgements The Swedish Civil Contingencies Agency, Project No. B40095, is gratefully acknowledged for funding this work.

References

1. Mercadier J, Cuney M, Lach P, Boiron M-C, Bonhoure J, Richard A, Leisen M, Kister P (2011) Origin of uranium deposits revealed by their rare earth element signature. Terra Nova 23:264–269
2. Spano TL, Simonetti A, Balboni E, Dorais C, Burns PC (2017) Trace element and U isotope analysis of uraninite and ore concentrate: applications for nuclear forensic investigations. Appl Geochem 84:277–285
3. Varga Z, Wallenius M, Mayer K (2010) Origin assessment of uranium ore concentrates based on their rare-earth elemental impurity pattern. Radiochim Acta 98:771–778
4. Varga Z, Krajko J, Peńkin M, Novák M, Eke Z, Wallenius M, Mayer K (2017) Identification of uranium signatures relevant for nuclear safeguards and forensics. J Radioanal Nucl Chem 312:639–654
5. Peńkin M, Boulyga S, Fischer D (2016) Application of uranium impurity data for material characterization in nuclear safeguards. J Radioanal Nucl Chem 307:1995–1999
6. Varga Z, Katona R, Stefánka Z, Wallenius M, Mayer K, Nicholl A (2010) Determination of rare-earth elements in uranium-bearing materials by inductively coupled plasma mass spectrometry. Talanta 80:1744–1749
7. Dulski P (1994) Interferences of oxide, hydroxide and chloride analyte species in the determination of rare earth elements in geological samples by inductively coupled plasma-mass spectrometry. Fresenius J Anal Chem 350:194–203
8. Leggitt J, Inn K, Goldberg S, Essex R, LaMont S, Chase S (2009) Nuclear forensics—metrological basis for legal defensibility. J Radioanal Nucl Chem 282:997–1001
9. Nuclear Forensics Support (2006) IAEA Nuclear Security Series No. 2: Technical Guidance, Vienna
10. Raut NM, Huang L-S, Aggarwal SK, Lin K-C (2003) Determination of lanthanides in rock samples by inductively coupled plasma mass spectrometry using thorium as oxide and hydroxide correction standard. Spectrochim Acta 58B:809–822
11. Vaughan M, Horlick G (1990) Correction procedures for rare earth element analyses in inductively coupled plasma-mass spectrometry. Appl Spectrosc 44:587–593
12. Simitchiev K, Stefanova V, Kmetov V, Andreev G, Sanchez A, Canals A (2008) Investigation of ICP-MS spectral interferences in the determination of Rh, Pd, and Pt in road dust: assessment of correction algorithms via uncertainty budget analysis and interference alleviation by preliminary acid leaching. Talanta 77:889–896
13. Funderberg R, Arevalo Jr R, Locmelis M, Adachi T (2017) Improved precision and accuracy of quantification of rare earth element abundances via medium-resolution LA-ICP-MS. J Am Soc Mass Spectrom 28:2344–2351
14. Nelms S (2005) ICP mass spectrometry handbook. Blackwell publishing Ltd, Oxford
15. Groopman E, Grabowski K, Fahey A, Kööp L (2017) Rapid, molecule-free, in situ rare earth element abundances by SIMS-SSAMS. J Anal At Spectrom 32:2153–2163
16. Balboni E, Simonetti A, Spano T, Cook N, Burns P (2017) Rare-earth element fractionation in uranium ore and its U(VI) alteration minerals. Appl Geochem 87:84–92
17. Lawrence MG, Greig A, Collerson KD, Kamber BS (2006) Direct quantification of rare earth element concentrations in natural waters by ICP-MS. Appl Geochem 21:839–848
18. Appelblad P, Baxter D (2000) A model for calculating dead-time and mass discrimination correction factors from inductively coupled plasma mass spectrometry calibration curves. J Anal At Spectrom 15:557–560
19. Sayago A, Asuero A (2004) Fitting straight lines with replicated observations by linear regression: part II. Testing for Homogeneities of Variances. Crit Rev Anal Chem 34:133–146
20. Ramebäck H, Lindgren P (2018) Uncertainty evaluation in gamma spectrometric measurements: uncertainty propagation versus Monte Carlo simulation. Appl Radiat Isot 142:71–76
21. ISO: Guide to the Expression of Uncertainty in Measurement (1995) International Organisation for Standardisation, Geneva, Switzerland
22. Anders E, Grevesse N (1989) Abundances of the elements: meteoritic and solar. Geochim Cosmochim Acta 53:197–214
23. Longerich H, Fryer B, Strong D, Kantipuly C (1987) Effects of operating conditions on the determination of the rare earth elements by inductively coupled plasma-mass spectrometry (ICP-MS). Spectrochim Acta 42B:75–92
24. Nash KL, Jensen MP (2000) Analytical separations of the lanthanides: basic chemistry and methods. In: Gschneidner KA, Eyring L (eds) Handbook on the physics and chemistry of rare earths, vol 28. Elsevier Science B.V., North-Holland
25. Morais CA, Ciminelli VST (1998) Recovery of europium from a rare earth chloride solution. Hydrometallurgy 49:167–177
26. Morais CA, Ciminelli VST (2007) Selection of solvent extraction reagent for the separation of europium(III) and gadolinium(III). Miner Eng 20:747–752
27. Pin C, Zalduegui JFS (1997) Sequential separation of light rare-earth elements, thorium and uranium by miniaturized extraction chromatography: application to isotopic analyses of silicate rocks. Anal Chim Acta 339:79–89
28. Yang Y, Zhang H, Chu Z, Xie L, Wu F (2010) Combined chemical separation of Lu, Hf, Rb, Sr, Sm and Nd from a single rock digest and precise and accurate isotope determinations of Lu–Hf, Rb–Sr and Sm–Nd isotope systems using multi-collector ICP-MS and TIMS. Int J Mass Spectrom 290:120–126

29. Shabana R, Ruf H (1977) Extraction and separation of uranium, thorium and cerium from different mixed media with HDEHP. J Radioanal Chem 36:389–397
30. Kaminski M, Nuñez L (2000) Separation of uranium from nitric- and hydrochloric-acid solutions with extractant-coated magnetic microparticles. Sep Sci Technol 35:2003–2018
31. Horwitz E, Bloomquist C (1975) Chemical separations for super-heavy element searches in irradiated uranium targets. J Inorg Nucl Chem 37:425–434
32. Kessel R, Berglund M, Wellum R (2008) Application of consistency checking to evaluation of uncertainty in multiple replicate measurements. Accred Qual Assur 13:293–298
33. Asai S, Limbeck A (2015) LA-ICP-MS of rare earth elements concentrated in cation-exchange resin particles for origin attribution of uranium ore concentrate. Talanta 135:41–49

Paper IV

Journal of Radioanalytical and Nuclear Chemistry
https://doi.org/10.1007/s10967-019-06795-0

Achieving confidence in trace element analysis for nuclear forensic purposes: ICP-MS measurements using external calibration

Anna Vesterlund[1,2] · **Henrik Ramebäck**[1,2]

Received: 4 July 2019

Abstract
In this work, problems arising from performing trace element analysis using inductively coupled plasma—mass spectrometry with low measurement uncertainties are addressed. It is shown that some reference materials certified for massic concentration of lanthanides may have either deviating concentrations or underestimated measurement uncertainties. It is also shown that the choice of methods for sample preparation and linear regression to perform external calibration is affecting the outcome of the measurement results and their uncertainties. The results show that, from the selection of methods investigated in this work, the lowest measurement uncertainties can be achieved by using weighted linear regression to evaluate the calibration function and gravimetric dilutions of samples.

Keywords External calibration · Quality control · Nuclear forensics · Trace element analysis

Introduction

Nuclear forensic science is a discipline that deals with providing information regarding chemical and physical characteristics of material connected to criminal investigations concerning e.g. illicit use of nuclear- and other radioactive material. In nuclear forensics, it is very important that the results from measurements, used for the interpretation of the materials in an investigation, are precise and accurate to stand up in court. Incorrectly estimated measurement uncertainties may lead a comparison between different materials or a comparison between a material and a nuclear forensic library to false conclusions, which at the end may result in wrong decisions. If the measurement uncertainties are underestimated, the comparison may give the result that an investigated material is different from another material or an entry in a nuclear forensic library even though they are similar. On the other hand, a measured material with an overestimated measurement uncertainty may not be possible to distinguish from another material even though they, in fact, are different. Therefore, it is imperative in nuclear forensics that the evaluated measurement uncertainty is as low as possible for a given measurement technique, but still accurate, to sharpen comparisons when materials are similar. For example, isotopic composition of uranium may be performed at an uncertainty level of 1–2% using gamma spectrometry [1] while mass spectrometric measurements using thermal ionization mass spectrometry (TIMS) may reach uncertainty levels as low as 0.1% [2] Even so, the uncertainty of the gamma spectrometric measurement may be adequate if compared materials are different enough.

One important characteristic in nuclear material are trace elements either as contamination from the production process or from the ore [3, 4]. This signature may be used, together with other characteristics such as isotopic and molecular composition [5, 6] to identify the origin of the material or what type of processes the material has undergone. [7, 8]. For example, rare earth elements have previously been used to determine the origin of uranium [3, 9]. Another application is to use trace elements to compare different materials in order to establish a possible common origin or history.

A suitable technique for quantification of trace elements is inductively coupled plasma mass spectrometry (ICP-MS). Depending on the analyte, the quantification can be performed in different ways. In general, isotope dilution

✉ Anna Vesterlund
anna.vesterlund@foi.se

[1] Swedish Defence Research Agency (FOI), CBRN Defence and Security, Cementvägen 20, 901 82 Umeå, Sweden

[2] Department of Chemistry and Chemical Engineering, Nuclear Chemistry, Chalmers University of Technology, 412 96 Göteborg, Sweden

Published online: 25 September 2019

is known to provide the lowest measurement uncertainties [10]. However, for many elements, isotopically enriched reference materials are rare and for elements with single isotopes, isotope dilution is not possible. Standard addition is another technique that can be used, but require tedious measurements as each sample requires many measurements in order to obtain a result. Therefore, the most widely used technique for quantification is external calibration.

To achieve confidence in measurement results, quality assurance is essential. Quality control (QC) during measurement assures the instrumental status and the laboratory proficiency. In quantification of elements, a common QC is the use of a QC sample consisting of a certified reference material with a known and certified concentration. Preferably, this material should be of different supplier than the reference material used for the calibration. If the measured concentration of the control sample deviates from the certified concentration this deviation needs to be handled. The most common way of handling deviating results from QC samples is to discard the measurement sequence due to some identified instrumental or sample preparation problem. However, if the deviation remains during multiple measurements and no cause of the deviation can be identified, the anomaly may need to be treated differently. Kessel et al. [11] approached this problem in a similar context by increasing the measurement uncertainty when replicates of the same sample deviated in measured concentration. Another important aspect in performing accurate measurements is the evaluation of the measurement data. It is important that the choice of evaluation method provides accurate results and measurement uncertainties.

In this study, three certified reference materials of different origins have been measured using sector field ICP-MS (ICP-SF-MS) to show that, when attempting to minimize the measurement uncertainties, there are indications that the certified reference materials may not be, within the stated uncertainty, accurate in terms of concentrations. The study showed that the choice of linear regression method and method of sample preparation affects the quality of the measurement results at this level of uncertainty. The study was performed on the lanthanide series but the discussion would be transferable to any element measurable using e.g. ICP-MS.

Experimental

Instrumentation

The measurements were performed using an Element 2 (Thermo Scientific, Bremen, Germany) with a concentric nebulizer and a cyclonic spray chamber (both GlassExpansion, Melbourne, Australia). The conditions for the measurement setup can be found in Table 1. The instrument was tuned with a 1 ng g^{-1} cerium solution to maximize the signal of cerium while keeping the formation of CeO low, as cerium typically is one of the strongest oxide-formers of the lanthanide series [12, 13]. The magnitude of the CeO formation was 2.5% during the measurements.

Standard solutions

Three different certified reference materials (CRM) were measured. The standard solutions were Periodic Table Mix 3 for ICP (Sigma Aldrich, Buchs, Switzerland), Spectrascan (Spectrascan, Inorganic Ventures, Christiansburg, USA) and CPAchem (CPAchem Ltd, Stara Zagora, Bulgaria), all certified by mass and traceable to NIST. The measurement uncertainties varied between 0.2 and 0.8%, $k=2$, depending on analytes and brands. One of the standard solutions was used as the calibration standard and the other two standard solutions were used as QC samples. The standard solutions were diluted using MQ-water and in-house sub-boiled nitric acid to suitable concentrations. The calibration standard was diluted and measured at concentrations 0 pg g^{-1}, 500 pg g^{-1}, 1000 pg g^{-1}, 1500 pg g^{-1}, 2000 pg g^{-1} and 2500 pg g^{-1}. The standard solutions used as QC samples were diluted to 100 pg g^{-1} and 1000 pg g^{-1}. Rhodium was used as internal

Table 1 Instrumental and measurement settings

Forward power (W)	1250
Cool gas flow (L min^{-1})	16
Auxiliary gas flow (L min^{-1})	0.7
Nebulizer gas flow (L min^{-1})	1.1
Resolution	300
Detection mode	Counting
Runs and passes	100 × 1
Mass window	5%
Samples per peak	100
Measured isotopes	^{103}Rh, ^{139}La, ^{140}Ce, ^{141}Pr, ^{146}Nd, ^{147}Sm, ^{153}Eu, ^{157}Gd, ^{159}Tb, ^{163}Dy, ^{165}Ho, ^{167}Er, ^{169}Tm, ^{174}Yb, ^{175}Lu

standard according to [3], and was added to all measured samples to a concentration of 1 ng g^{-1}. All sample preparations were performed gravimetrically in order to reduce uncertainties compared to volumetric additions. However, uncertainty modelling was also done in order to compare volumetric and gravimetric additions from an uncertainty perspective. The analytical balance used in this work was a Mettler Toledo AX204 (Columbus, Ohio, US) with an uncertainty of 0.3 mg. It should be noted that in the case of measuring real samples, the calibration solutions as well as the QC samples should be matched to have the same matrix as the samples to be quantified. Preferentially, the QC samples should originate from a certified reference material of the same composition as the unknown samples.

Data evaluation

To achieve the lowest measurement uncertainties and to account for all uncertainty contributions, all data evaluation was performed offline. The raw intensity for each sample and isotope was extracted from the Element ICP-MS software (ver. 3.1.2.242). The mean value and standard deviation of the mean were calculated from the 500 data points from each sample and isotope resulting from 5 samples per peak and 100 runs. The intensities were corrected for dead-time using the method presented by Appelblad and Baxter [14]. Thereafter, the intensities were corrected for internal standard. To provide accurate internal standard corrections, the internal standard intensities were corrected for the added amount of internal standard, see Eq. 1.

$$I_{corr,i,j} = \frac{I_{i,j}}{I_{IS,i}/m_{IS,i}} \cdot \frac{I_{IS,blk}}{m_{IS,blk}} \tag{1}$$

$I_{corr,i,j}$ is the intensity for isotope j in sample i corrected for internal standard, $I_{i,j}$ is the dead-time corrected intensity of isotope j in sample i, $I_{IS,i}$ and $I_{IS,blk}$ are the dead-time corrected intensities of the internal standard in sample i and the blank sample and $m_{IS,i}$ and $m_{IS,blk}$ are the masses of the added internal standard in sample i and the blank sample.

To obtain a calibration curve, the measurement data from the calibration standards were used. Ordinary least squares regression (OLS) was performed using the Microsoft Excel 2016 function LINEST(). Additionally, linear regression was performed on the same data set using weighted least squares regression (WLS), weighted with the reciprocal variance of $I_{corr,i,j}$ according to Sayago and Asuero [15], to fit the line

$$I_{corr,i,j} = k_j \cdot c_{i,j} + m_j \tag{2}$$

where $c_{i,j}$ and $I_{corr,I,j}$ is the concentration and the measured intensity of isotope j in sample i, respectively. Using WLS regression, two calibration functions were calculated where uncertainties from the sample preparations performed gravimetrically and volumetrically, respectively, were included. For each method of linear regression, the slope, k_j, and intercept, m_j, and their corresponding uncertainties were evaluated. In the Excel OLS regression, the additional regression statistics was retrieved and used as uncertainties. For the WLS regression the uncertainties were evaluated according to Sayago and Asuero [15]. This was followed by the calculation of the limit of detection according to Miller and Miller [16]:

$$L_D = m + 3u_m \tag{3}$$

The results from the measurements of Standard solution 1 and 2 were used as quality control samples. The corrected intensities were used to calculate the concentrations using the calibration function. The calculated concentrations were compared to the certified values using the zeta score (ζ) [17]:

$$\zeta = \frac{c_{measured} - c_{reference}}{\sqrt{u^2(c_{measured}) + u^2(c_{reference})}} \tag{4}$$

where $c_{measured}$ is the measured and calculated concentration and $c_{reference}$ is the certified concentration and $u(c_{measured})$ and $u(c_{reference})$ are their respective uncertainties. If $|\zeta| \leq 2$ the measured value is consistent with the certified value within their respective uncertainties at 95% confidence level.

All uncertainties were evaluated according to ISO GUM [18] using the software GUM Workbench Pro (Metrodata GmbH, Weil am Rhein, Germany). All uncertainties are, unless stated otherwise, presented with a coverage factor $k = 2$, corresponding to an approximate 95% confidence level.

Results and discussion

Considerations for linear regression

Performing different linear regressions on the same calibration data provides the opportunity to evaluate the adequacy of the methods. For OLS to be valid there are a number of conditions that need to be fulfilled. Two important conditions for using OLS in calibration is homoscedasticity in the variance of the dependant variable (in this case $I_{corr,i,j}$) and that the variance in the independent variable ($c_{i,j}$) is zero or very small compared to the variance in the dependant variable. The homoscedasticity condition implies that the absolute standard deviation of each point $I_{corr,i,j}$ is constant throughout the calibration interval. Even though this is rarely true in many analytical methods, OLS is commonly used for constructing calibration curves [19]. In ICP-MS, the expected signal variance is similar in relative measures with the exception that the uncertainty is relatively higher close to zero. Since OLS gives each point in the calibration

equal importance in the regression, the calibration points closer to zero will be given less weight than they should be given, even though these points are more certain in absolute measures. Whereas OLS might work well on heteroscedastic data in the high end of the calibration, since the equal weight gives the points in the high end of the calibration unreasonably high importance to the calibration model, the lower part of the calibration tends to be badly estimated which in turn will result in severely overestimated limits of detection [20–22].

It can be discussed what weight to use in the regression. Weighting with the reciprocal variance of the y data has been the classical method for WLS [15, 23]. This is also the weight that has been used throughout this work. However, using the variance for weighting may be difficult in cases where there is only one measurement for each x. In these cases, another weight has to be used. There are a number of suggestions of different weights such as $1/y$, $1/x$, $1/y^2$ [24, 25]. However, there may be very little statistical difference between using $1/y$ and $1/x$ for a linear model [24] and, moreover, using a weight such as $1/x$ may be impossible if the measurement of the blank, $x=0$, is included in the calibration [26]. Therefore, the choice of weight is an important consideration for the evaluation of the calibration function.

Detection limits

The detection limits, calculated using Eq. 3, for each element and evaluated calibration functions based on OLS and WLS using gravimetric dilutions, can be seen in Fig. 1.

The detection limits calculated from the OLS method are orders of magnitude larger than the corresponding results using the WLS methods. This is the result from giving too little weight to calibration points close to the y axis in comparison to calibration points high up in concentration. This results in very high uncertainties in the intercept and also, in many cases, an intercept deviating immensely from the blank measurement. One consequence of this is that if for example a sample containing trace elements at 1 pg g^{-1}, the question whether this concentration is detectable or not is dependent on the type of regression applied. If the sample was evaluated using OLS the concentration would be clearly below detection limit while if the sample was evaluated using WLS there would be quantifiable amounts present even though the same sample is measured, and the same measurement data is used to evaluate the calibration curve.

Quality control samples

The results from the evaluated concentrations and uncertainties of the 1 ng g^{-1} QC samples using WLS and uncertainties from gravimetric sample preparation, together with corresponding certified values are shown in Fig. 2. The figure also displays the zeta score from the comparison between measured and certified values. The figure shows that there are large deviations in concentrations between the measured and certified values for some elements in Standard solution 1. When the zeta score is larger than 2, the difference between measured and certified values is not covered by their uncertainties on an approximate 95% confidence level. The difference cannot not be explained by polyatomic interferences since possible interferences should be cancelled out if the composition of the element standards are the same. To make sure that the isotopic composition of the rare earth elements were not fundamentally different or that no other interferences were present in the three solutions, all masses from 137 to 176 in a sample from each CRM were measured and compared. The examination showed no large differences in composition between the materials.

The results from Standard solution 2 do not show any significant differences in concentration between measured and certified values. This means that this CRM correlates well with the CRM used for calibration. The conclusion that can be drawn is that the stated concentrations of certain elements

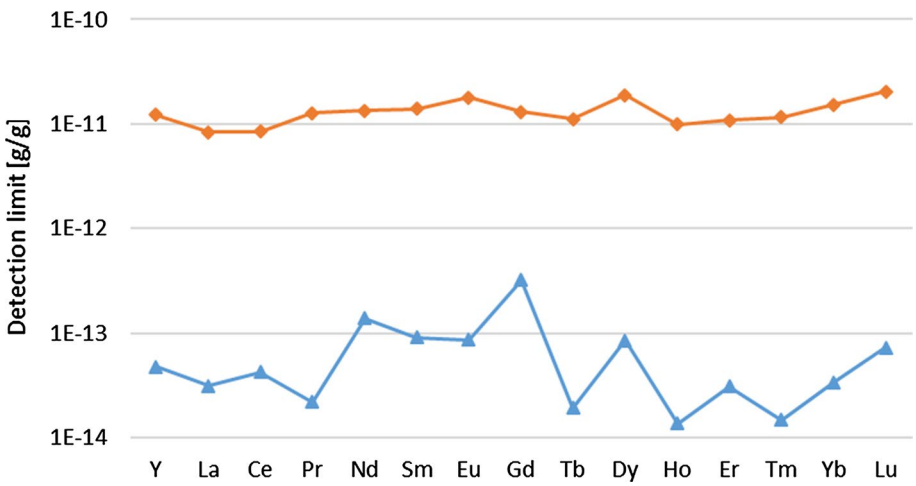

Fig. 1 Detection limits for regression models using gravimetric OLS (diamonds) and gravimetric WLS (triangles), respectively

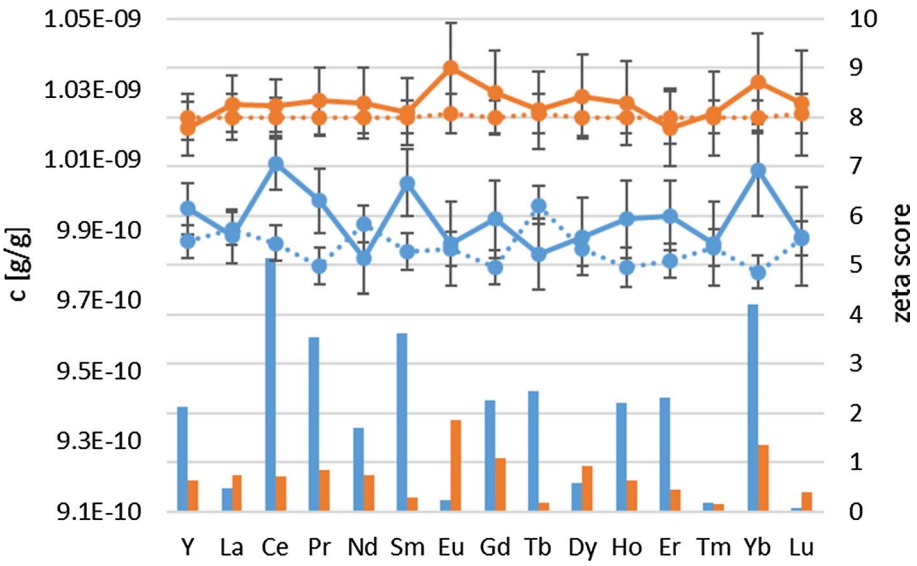

Fig. 2 Measurement results and certified values of each element together with the calculated zeta score. The blue series correspond to Standard solution 1 and the orange series corresponds to Standard solution 2. The continuous lines are the measured values and the dashed lines are certified values. The bars corresponds to the calculated zeta scores

in Standard solution 1 are significantly different from those in the calibration solution, or that the uncertainty in one, or both, CRMs are underestimated.

The discrepancy between measured and certified concentrations in QC samples can be handled in different ways. According to ISO Guide 33:2015 [27], any discovered bias should primarily be reduced or eliminated, secondly corrected for and the additional uncertainty added to the uncertainty budget and thirdly, if these approaches are regarded as impossible to carry through, the bias should be included in the uncertainty budget [27]. Since it is difficult to determine which of the solutions that has the correct concentration, this bias was regarded as an additional uncertainty component. Therefore, an extra input quantity, δ, was added to the model equation for the calculation of the concentration of isotope j in sample i, $c_{i,j}$, of the measured sample where m_j is the intercept and k_j is the slope of the calibration function and $I_{corr,i,j}$ is the intensity of isotope j in the sample i corrected for dead-time and internal standard:

$$c_{i,j} = \frac{I_{corr,i,j} - m_j}{k_j} + \delta \tag{5}$$

δ has value 0. In the measurement uncertainty software GUM Workbench, the uncertainty of δ, $u(\delta)$, was increased until the relative expanded uncertainty ($k = 2$) of the difference between measured concentration and certified concentration was 100%. This is equivalent to a zeta score of 2 (see Eq. 4).

This approach ensures that the result of the measurement of the QC sample corresponds to the certified value within uncertainties at the 95% confidence level. This methodology has previously been applied on replicate samples by Kessel et al. [11] in a similar fashion. It should be noted that if the choice was made to use the same CRM for the calibration as for the QC sample, this anomaly would not have been detected and the risk of reporting analytical results containing bias or underestimated uncertainties would be considerable.

The initial combined uncertainty when $u(\delta) = 0$ varied between 0.7 and 1.5% depending on the measured isotope. The main part of the initial uncertainty originates from the uncertainty in the slope, k, of the calibration function. In cases where an extra uncertainty, $u(\delta)$, had to be added, the contribution to the total measurement uncertainty was, in most cases, dominated by this extra uncertainty. However, even though the extra uncertainty $u(\delta)$ was added, the combined expanded measurement uncertainties were rarely higher than 2%. The relative combined uncertainty for the final measurement uncertainty calculations can be seen in Fig. 3. The elements in Standard solution 1 that have obviously deviating uncertainties do all have an extra uncertainty, $u(\delta)$, added to the measurement uncertainty budget.

The, in most cases, low measurement uncertainty is the result of diluting all the samples gravimetrically rather than volumetrically and using a CRM certified for mass. If the dilutions were performed volumetrically instead, assuming a combined uncertainty of 0.8%, $k = 1$, for volumes less than 1 ml and 0.4% for volumes greater than 5 ml, the combined uncertainty would increase to approximately 3%, see Fig. 3. The uncertainty was evaluated according to ISO 8655-6 [28] In this case, most of the uncertainty originates from the uncertainty in the addition of the internal standard and the uncertainty of the slope of the calibration function. In the case of volumetric sample preparation, there was no need for the extra uncertainty, $u(\delta)$, for any element at the 1 ng g^{-1} level.

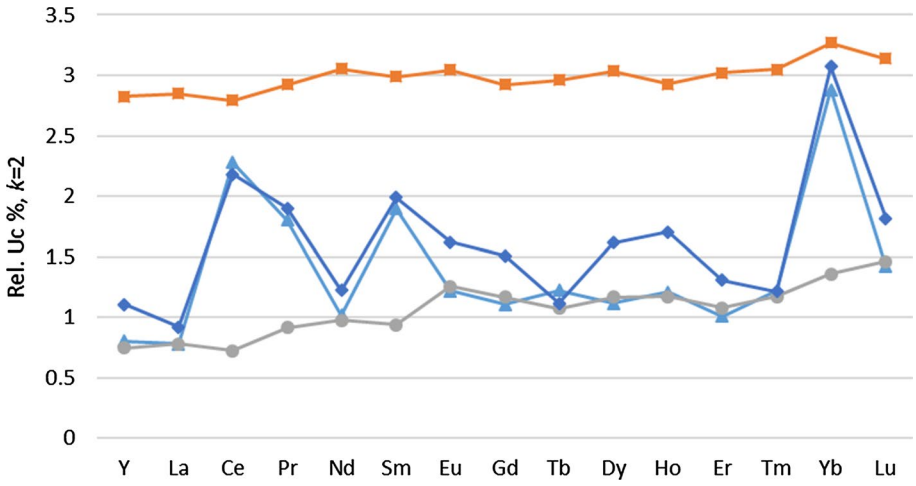

Fig. 3 Relative uncertainties for the measured 1 ng g^{-1} control samples when an extra uncertainty has been added when necessary. The following data are evaluated using weighted linear regression: The triangles correspond to Standard solution 1, the circles to Standard solution 2 both with dilutions performed gravimetrically, the squares to Standard solution 1 in the case where dilutions were performed volumetrically. The diamonds correspond to the control sample from Standard solution 1 evaluated using OLS

The relative uncertainties in the data evaluated using OLS is, in general, following the relative uncertainties of the WLS evaluated data, see Fig. 3. This implies that at the 1 ng g^{-1} level, the ordinary least regression provides as accurate calibration as the weighted linear regression. The large difference can be seen in the evaluation of a 100 pg g^{-1} sample, see Fig. 4. The relative uncertainties for the results based on WLS are at the same level as for the 1 ng g^{-1} samples but for the results based on OLS the relative uncertainties are substantially higher than for the 1 ng g^{-1} sample. This is a result of the large uncertainty in the intercept that follows when performing an OLS on heteroscedastic data [29].

Of course, the easy option to evaluate the measurement results is to use the software of the ICP-MS instrument. This method, however, does not provide the full picture of the uncertainty estimation, i.e. it is not fully transparent to the analyst. The software does not ask for any uncertainty of the dead-time, which, even though it may be small, may affect the overall uncertainty at high count rates. Further, the software does not include any uncertainty from the linear regression into the calculations of the sample concentration and does not give any room for corrections due to addition of the internal standard, which, at least for volumetric additions, is a substantial part of the uncertainty. The uncertainty provided by the software is based on the standard deviation (not the standard deviation of the mean) of the calculated concentrations for each sweep, which basically is the uncertainty of the blank subtracted measured intensity. These uncertainties are, in general, larger than the uncertainties from the volumetrically prepared samples and the uncertainties are, in fact, evaluated on the wrong assumptions, including uncertainties that can be made smaller and leaving out uncertainties that may be significant.

An example of when this methodology has been applied to measurements of trace elements in a uranium matrix can be found in another published paper [30].

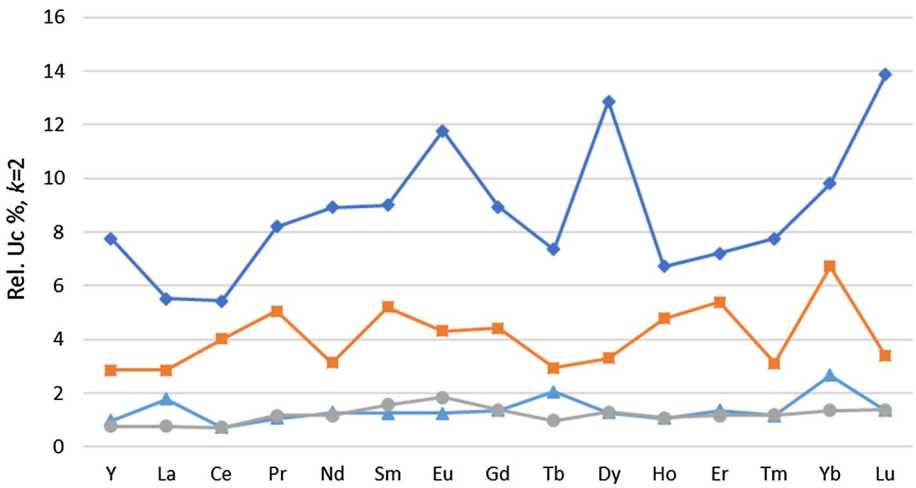

Fig. 4 Relative uncertainties for the measured 100 pg g^{-1} control samples when an extra uncertainty has been added when necessary. The following data are evaluated using WLS: The triangles correspond to Standard solution 1, the circles to Standard solution 2 both with dilutions performed gravimetrically and the squares to Standard solution 1 in the case where dilutions were performed volumetrically. The diamonds correspond to the control sample from Standard solution 1 evaluated using OLS

Conclusions

Since nuclear forensic evidence, like all evidence presented in a court of law, need to be defensible, it is important that the results and the attached uncertainties are correctly evaluated. This work shows that to perform accurate and precise measurements of elements using ICP-MS, the data evaluation should be made manually with careful considerations regarding sample preparation and choice of regression method prior to performing the measurements, to be able to retrieve correct information from the measurements.

In this paper, it is shown that gravimetric sample preparation is preferred over volumetric sample preparation to achieve the lowest measurement uncertainties and that OLS provides large measurement uncertainties at low concentrations and unrealistically high detection limits. However, depending on the purpose and thus the requirements of the measurement, work effort might be saved if volumetric sample preparations are done but then on the cost of higher measurement uncertainties.

The study also shows that careful quality control is imperative to measurements at this uncertainty level. The risk of biases due to inconsistencies in the certified reference materials needs to be carefully monitored and attended. In this study, the bias was addressed by adding an extra uncertainty to the calculated concentration since it was not possible to know which of the certified reference materials that was deviating either in the value of the certified concentration or in its uncertainty. The discrepancy between the deviating CRMs would not have been observed if volumetric sample preparation had been done.

Acknowledgements Open access funding provided by Swedish Defence Research Agency. The Swedish Civil Contingencies Agency, Project No. B40095, is gratefully acknowledged for funding this work. Thanks to Leif Persson, Department of Mathematics and Mathematical Statistics, Umeå University, for valuable comments.

References

1. Abousahl S, Michiels A, Bickel M, Gunnink R, Verplancke J (1996) Applicability and limits of the MGAU code for the determination of the enrichment of uranium samples. Nucl Instrum Methods Phys Res A 368:443–448
2. Bürger S, Essex RM, Mathew KJ, Richter S, Thomas RB (2010) Implementation of guide to the expression of uncertainty in measurement (GUM) to multi-collector TIMS uranium isotope ratio metrology. Int J Mass Spectrom 294:65–76
3. Varga Z, Wallenius M, Mayer K (2010) Origin assessment of uranium ore concentrates based on their rare-earth elemental impurity pattern. Radiochim Acta 98:771–778
4. Spano TL, Simonetti A, Corcoran L, Smith PH, Lewis SR, Burns PC (2018) Comparative chemical and structural analyses of two uranium dioxide fuel pellets. J Nucl Mater 518:149–161
5. Mayer K, Wallenius M, Varga Z (2015) Interviewing a silent (Radioactive) witness through nuclear forensic analysis. Anal Chem 87:11605–11610
6. Kristo MJ, Gaffney AM, Marks N, Knight K, Cassata WS, Hutcheon ID (2016) Nuclear forensic science: analysis of nuclear material out of regulatory control. Annu Rev Earth Planet Sci 44:555–579
7. Varga Z, Krajko J, Peńkin M, Novák M, Eke Z, Wallenius M, Mayer K (2017) Identification of uranium signatures relevant for nuclear safeguards and forensics. J Radioanal Nucl Chem 312:639–654
8. Healey G, Button P (2013) Change in impurities observed during the refining and conversion processes. Esarda Bull 49:57–65
9. Mercadier J, Cuney M, Lach P, Boiron M-C, Bonhoure J, Richard A, Leisen M, Kister P (2011) Origin of uranium deposits revealed by their rare earth element signature. Terra Nova 23:264–269
10. Vogl J, Pritzkow W (2010) Isotope dilution mass spectrometry—a primary method of measurement and its role for RM certification. J Meter Soc India 25:135–164
11. Kessel R, Berglund M, Wellum R (2008) Application of consistency checking to evaluation of uncertainty in multiple replicate measurements. Accred Qual Assur 13:293–298
12. Dulski P (1994) Interferences of oxide, hydroxide and chloride analyte species in the determination of rare earth elements in geological samples by inductively coupled plasma-mass spectrometry. Fresenius J Anal Chem 350:194–203
13. Longerich H, Fryer B, Strong D, Kantipuly C (1987) Effects of operating conditions on the determination of the rare earth elements by inductively coupled plasma-mass spectrometry (ICP-MS). Spectrochim Acta 42B:75–92
14. Appelblad P, Baxter D (2000) A model for calculating dead-time and mass discrimination correction factors from inductively coupled plasma mass spectrometry calibration curves. J Anal At Spectrom 15:557–560
15. Sayago A, Asuero A (2004) Fitting straight lines with replicated observations by linear regression: part II. Test Homog Var Crit Rev Anal Chem 34:133–146
16. Miller JN, Miller JC (2010) Statistics and chemometrics for analytical chemistry, 6th edn. Pearson Education Limited, Harlow. ISBN 978-0-273-73042-2
17. ISO 13528:2015 (2015) Statistical methods for use in proficiency testing by interlaboratory comparison. The International Organization for Standardization, Geneva
18. ISO/IEC Guide 98-3:2008 (2008) Uncertainty of measurement—Part 3: guide to the expression of uncertainty in measurement. The International Organization for Standardization, Geneva
19. Raposo F (2016) Evaluation of analytical calibration based on least-squares linear regression for instrumental techniques: a tutorial review. Trends Anal Chem 77:167–185
20. Zorn ME, Gibbons RD, Sonzogni WC (1997) Weighted least-squares approach to calculating limits of detection and quantification by modeling variability as a function of concentration. Anal Chem 69:3069–3075
21. Rajaković LV, Marković DD, Rajaković-Ognjanović VN, Antanasijević DZ (2012) Review: the approaches for estimation of limit of detection for ICP-MS trace analysis of arsenic. Talanta 102:79–87

22. del Río Bocio F J, Riu J, Boqué R, Rius FX (2003) Limits of detection in linear regression with errors in the concentration. J Chemom 17:413–421
23. Deming WE (1964) Statistical adjustment of data. Dover, New York
24. Almeida AM, Castel-Branco MM, Falcão AC (2002) Linear regression for calibration lines revisited: weighting schemes for bioanalytical methods. J Chromatogr B 774:215–222
25. Asuero AG, González G (2007) Fitting straight lines with replicated observations by linear regression. III. Weight Data Crit Rev Anal Chem 37:143–172
26. Tellinghuisen J (2008) Weighted least squares in calibration: the problem with using "quality coefficients" to select weighting formulas. J Chromatogr B 872:162–166
27. ISO Guide 33:2015 (2015) Reference materials—good practice in using reference materials. The International Organization for Standardization, Geneva
28. ISO 8655–6:2002 (2002) Piston-operated volumetric apparatus—Part 6: gravimetric methods for the determination of measurement error, the International Organization for Standardization. Switzerland, Geneva
29. Ketkar SN, Bzik TJ (2000) Calibration of analytical instruments. Impact of nonconstant variance in calibration data. Anal Chem 72:4762–4765
30. Vesterlund A, Ramebäck H (2019) Avoiding polyatomic interferences in measurements of lanthanides in uranium material for nuclear forensic purposes. J Radioanal Nucl Chem 321:723–731